AQRP Project 17-039

Use of Satellite Data to Improve Specifications of Land Surface Parameters

Final Report

Prepared for:
Texas Air Quality Research Program (AQRP)

By
Richard T. McNider, Kevin Doty, Yuling Wu, and Arastoo Pour Biazar
ESSC
University of Alabama in Huntsville

To

Elena McDonald-Buller
AQRP Project Manager

Bright Dornblaser
TCEQ Liason

December 12, 2017

QA Requirements: Audits of Data Quality: 10% Required

Executive Summary

It is the purpose of this project to evaluate and improve the performance of the land surface models used in the Weather Research and Forecasting model (WRF) by the use of satellite skin temperatures to better specify physical parameters associated with land use classes. This is a continuation of a previous AQRP project (project # 14-022). Some of the introductory material in this report and initial results are the same as in the 14-022 final report. For simplicity in this report that project 14-022 will be referred to as the last biennium project.

Improved temperature performance impacts boundary layer heights, biogenic emissions, thermal decomposition (chemical chain lengths and slopes of ozone/NOy curves) and thermally driven winds such as sea breezes. Also, land surface parameters control surface deposition which impacts the efficacy of long-range transport.

While considerable work has been done by the national community and especially in Texas to develop improved land use classifications, land use classes themselves are not directly used in models. Rather, physical parameters such as heat capacity, thermal resistance, roughness, surface moisture availability, albedo, etc. associated with a land use class are actually used in the land surface model. Many of the land use class associated parameters such as surface moisture availability are dynamic and ill-observed depending on antecedent precipitation and evaporation, soil moisture diffusion, the phenological state of the vegetation, irrigation applications, etc. Other parameters such as heat capacity, thermal resistance or deep soil temperature are not only difficult to observe, they are often unknowable *a priori*. In some sense they are model heuristics with different land surface models having several orders of magnitude difference in parameters such as vegetative thermal resistance. The specification of these physical parameters across grids having mixed land use types is even more problematic. Despite the difficulty in specifying these parameters they are incredibly important to model predictions of turbulence, temperature, boundary layer heights and winds.

Insolation is one of the largest components in the daytime surface energy budget. Insolation largely depends on average solar zenith angle. However, clouds can dramatically alter the solar energy received at the surface. This produces a potential source of error in air quality simulations since model clouds may be in the incorrect place or time. Thus, on certain days when clouds are present in the model but not in reality the energy difference at the surface can be large. The Weather Research Forecast (WRF) model is run using both the default model insolation and satellite insolation.

The Pleim-Xiu (hereafter referred to as P-X) land use model in WRF has used a surface moisture and deep soil nudging technique based on differences between model 2-m air temperatures at National Weather Service (NWS) observational sites. However, land use, vegetation coverage and convective precipitation can all have variations on spatial scales much smaller than the spatial scale of NWS observations. The major activity under this project was to determine whether satellite observed skin temperature, which has much finer resolution (10 km) than NWS observations (~40 km), can be used to nudge soil moisture and thermal resistance and provide improved model performance.

Under the last biennium project using skin temperatures as the performance metric, the results showed that over most of the domain that the bias was improved but there was a slight negative increase in the overall bias. This means that the few areas that had an increase in bias were larger causing a slight increase in absolute bias for the domain. An examination of time series from the nudging runs compared to the control showed that the adjustments in moisture appeared to be working as formulated. In some places part of the error may have been due to bad skin temperature data. The root-mean square statistics were also improved over the domain.

In the last biennium project comparisons with NWS observations were more mixed in regards to bias for 2-m specific humidity and 2-m temperature. Root-mean square error (RMSE) was unchanged for humidity and decreased slightly for 2-m temperature. For 10-m wind speed and wind direction there was a slight decrease in bias and RMSE for all regions.

Under this year's project several new approaches are tested. These are described under the task descriptions for this year in Chapter 4. These tasks are:

Task 1- Focus on Small Scale Performance and Other Metrics Such as Wind Performance
Task 2- Use of Skin Temperature Tendencies
Task 3- Heat Capacity Assimilation
Task 4- Vegetative Fraction
Task 5- Tool for Investigating Sensitivity of Land Surface Model Components
Task 6- Satellite Derived Insolation and Albedo
Task 7- Additional Model Evaluation Period

Model runs were made for the 2013 Discover AQ period (September 1-30, 2013). The first task was to make a model control run with which to compare successive levels of satellite assimilation. However, in making the control run several changes in model physics and nudging strategies were made that were slightly different that the last biennium runs. Additionally, the newest WRF version 3.8.1 was employed compared to version 3.6.1 used in the last biennium project. In making the control run it was found that bias and root-mean-square error statistics in the control run were significantly worse than in the last biennium control run. The source of the degradation was exhaustively investigated. This is described in Chapter 3 below. While removal of the differences in model set-ups did bring the control closer to the last biennium control, it was concluded that the remaining differences were due to the new version of WRF.

Previous model set-ups had been patterned after TCEQ inputs. However, in talking to TCEQ it was found that these are fluid and have not been firmly specified for the P-X scheme. It was thus decided that the appropriate control case would be one most likely to be used within the WRF/Air Quality Community. UAH thus contacted the EPA NERL group and obtained their model name list and set up. Since this project is trying to show that satellite data can improve model performance in the P-X scheme it seems reasonable to use what the Pleim group at EPA would use for their control model set-up. If UAH picked a different control set-up and showed improvement there might be concern that a control set-up with a larger error was chosen making the use of satellite data appear better. Thus, all of the runs for this report in Chapters 5 - 7 were based on this configuration.

The satellite assimilation runs for 2013 are described in Chapter 5. The satellite assimilation worked much as expected. Model comparisons to NWS observations showed improvement in most areas especially for 2-m temperatures. Texas showed even greater improvement than for the whole domain. Wind speed statistics were slightly improved. Comparisons against profiler data showed that the assimilations improved nighttime wind speeds aloft substantially. Daytime winds aloft were either unchanged or in some cases slightly deteriorated.

Skin temperatures were also improved compared to the control case. However, examination of the spatial plots showed that a large gradient in model performance existed across the whole domain and the Texas domain. A sharp gradient in model performance east and west of a north-south longitude approximately through Amarillo was found. Model performance with the satellite assimilations was greatly improved east of this line but model performance especially for skin temperatures was degraded west of this line. The analysis discussed in Chapter 5 suggests that the issue may be with satellite skin temperatures in the West. In the last biennium project a switch was made from the NOAA operational GSIP skin temperature product to another NOAA product produced by John Hain which did not seem to suffer from excessive warm temperatures in the West. However, this year's analysis suggest there may also be a problem with this product.

Model satellite assimilation was carried out for the new August 2012 period. The general performance results from the satellite assimilation were largely similar to the 2013 period. In fact, performance against NWS sites showed much better consistent agreement across the whole domain and Texas. However, it turned out that the largest impact of the assimilation for 2012 came from the satellite insolation product with skin temperature nudging producing less impact.

In summary the project shows that satellite assimilation can greatly improve model performance especially in the Eastern U.S. and East Texas.

Table of Contents

1 Background and Overview

1.1 Introduction and Rationale

The land surface is a critical component in local, regional and global modeling. Heat, momentum and scalar fluxes at the surface control temperature, turbulent mixing, winds and dry deposition of chemical species. Because of the importance of the characteristics of the land surface, there has been tremendous investment by the climate, weather forecasting and air quality communities in land surface research. Much of this investment has gone into developing complex land surface models, which include many intricate parameterizations that attempt to capture processes such as plant transpiration rates, leaf water interception, soil moisture and run-off, and parameterizations which control thermal and water transfer through canopies and soils (Sellers 1997, Pitman 2003). Thus, these models require additional parameter specifications to close the model systems.

A second major area of investment has been the development of land-use classification data sets that attempt to define areas which are forested, croplands, urban areas, etc. that can be used with the land surface models. The uses of satellite data (with its observables such as greenness and albedo) have greatly improved the characterization of the surface into classes. However, land surface models such as WRF National Centers for Environmental Prediction (NCEP)–Oregon State University–Air Force–Hydrologic Research Laboratory (Noah) (Chen and Dudhia 2001) do not use land use classifications directly. Rather, they use the physical parameters such as roughness, heat capacity, canopy thermal and water resistances, soil conductivity for water and heat, etc. that are associated with the land use classes. Thus, in the models, such as the WRF – Noah land use model, there are lookup tables that define these land-use associated parameters (Niu et al. 2011).

Unfortunately, the specification of some of these physical parameters is difficult even in homogeneous land use classes (Rosero et al.2009). For example, the rate of temperature change in vegetation is controlled by plant transpiration and evaporation through water resistance parameters and by the canopy thermal resistance. Thermal resistance depends on the heat capacity of the canopy and the thermal conductivity through the canopy (Noilhan and Planton 1989). The water resistance depends on root zone moisture, the phenological state of the plant, leaf area, shaded leaf area, etc. Field campaigns using tower measurements are usually conducted to try to establish these parameters. But, in effect, many of the parameters or processes have to be deduced as residuals in local canopy models, which are tied to specific turbulence and radiative models (Yang and Friedl 2003, Pleim and Gilliam 2009). Thus, the parameters are often model heuristics as opposed to fundamental observables (Wegner and Gupta 2005), which is the reason a parameter such as canopy thermal resistance can vary by three orders of magnitude in different models (Pleim and Gilliam 2009). In inhomogeneous grid boxes, which make up the real world, the situation is even worse (McNider et al 2005). Here, dominant land-use classes are often used in models such as Noah, but they may not well represent the actual mix of urban, crop and forestland uses.

Figure 1-1 illustrates the problem that is faced but also a potential solution. It shows land use classifications and also the satellite observed skin temperature for the Southeast. As can be seen, there is a correlation between land use classes and the skin temperature with urban areas and crop lands warmer than forested areas. The question facing modelers is - can physical parameters be prescribed in a land surface model impacting the skin temperature so that the model will reproduce the skin temperature variation seen in Figure 1-1 ? In the present project, the assumption is made that two of the most uncertain parameters are surface moisture and thermal resistance. The satellite observed skin temperature is used to improve the specification of these parameters. With these adjusted parameters, will model prediction of skin temperature be closer to that observed by the satellite and will comparison against other observations such as National Weather Service 2-m temperatures, humidity and winds be improved? That is the goal of the present project.

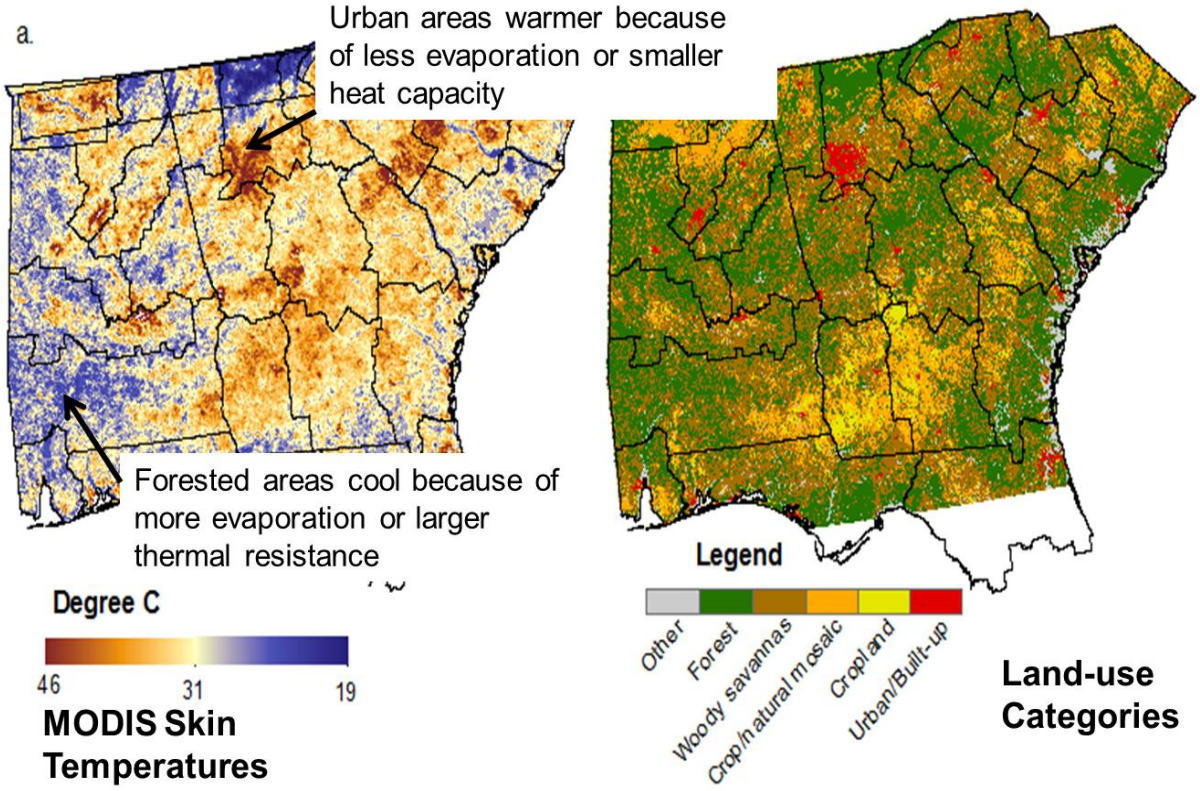

Figure 1-1 *Illustration of relation of satellite skin temperature to land use. Left is the MODIS average afternoon temperature for July 2012. The question is can the proper physical parameters be prescribed in the land use classifications so that a model reproduces the observed skin temperature distribution. From Ellenburg et al. (2015).*

In this project, two paths are described for evaluating and improving the land surface model. The first is to use satellite skin temperatures as a model evaluation metric. Satellite skin temperatures have much finer resolution than National Weather Service (NWS) observations and therefore are better able to capture variations in land use and moisture variations. Second, an approach is taken that simpler land surface models with fewer unknown parameters but constrained by

observations may provide better model performance - especially in the retroactive fashion in which SIP models are utilized.

The development of complex land surface models mentioned above was consistent with the need in the climate modeling community for surface models that could be run for years without being influenced by observed data. Thus, they needed vegetative surface interaction, water balance models, etc. However, Diak (1990), McNider et al. (1994), Anderson et al. (1997) and others argued that for short-term weather forecasting and for retrospective air quality simulations (McNider et al. 1998, Pleim and Xiu 2003) simpler models that could be constrained by observations might be preferred. The simple models avoid setting many uncertain parameters in the complex models. This is the path pursued here, with observational constraints provided by satellite skin temperature data. The P-X assimilation model (Pleim and Xiu 1995, Xiu and Pleim 2001, and Pleim and Xiu 2003) is modified to use satellite skin temperature rather than NWS observed 2-m temperatures to adjust soil moisture and to recover the surface thermal resistance following McNider et al. (2005).

Pleim and Xiu (2003) noted that since surface moisture is not a direct observation that use of auxiliary information is needed. They have used observed NWS surface temperatures to nudge moisture. Here they adjust surface layer moisture w_G using the difference between model daytime temperatures (T^F) and analyses of observed temperatures (T^A) and model and observed relative humidity(RH).

$$\Delta w_G = \alpha_1\left(T^A - T^F\right) + \alpha_2\left(RH^A - RH^F\right)_{\text{Daytime}} \quad (1\text{-}1)$$

A similar equation is also used by Pleim and Xiu (2003) to nudge the deep layer soil moisture. The P-X approach has been widely used and in recent California inter-comparisons performed better than the Noah complex land surface model (Fovell 2013). Because observed NWS observations are coarse the NWS observed temperatures are replaced with satellite skin temperatures, i.e.

$$\Delta w_G = \beta_1(T_s^{Sat} - T_s^{Mod})_{Morning} \quad (1\text{-}2)$$

It is noted that the use of skin temperatures is consistent with the P-X assumption that moisture is related to 2-m temperatures and make the same assumption for skin temperature. The technique proposed by McNider et al. (2005) is employed within the P-X model to nudge thermal resistance, C_T, using afternoon/evening skin temperatures (as opposed to the Pleim and Gilliam 2009 of using afternoon/evening temperatures to nudge deep soil temperature) as illustrated by equation (1-3). Here T_S^{SAT} is the satellite observed skin temperature and T_S^{MOD} is the modeled skin temperature.

$$C_T^{NEW} = C_T^{OLD} \frac{\frac{\partial T_S^{SAT}}{\partial t}}{\frac{\partial T_S^{MOD}}{\partial t}} \quad \text{.....(1-3)}$$

See Mackaro et al. (2011) and McNider et al. (2005) for further details.

1.2 Road Map of the Report

Chapter 2 provides an overview of the results from last year's project. It provides an evaluation of the improvement in the model performance when satellite skin temperatures are used to adjust moisture and thermal resistance. A statistical evaluation is provided against satellite observed skin temperatures. It also provides a comparison of the model results with moisture nudging against standard NWS observations of temperature, winds and humidity.

Chapter 3 provides a description and discussion on model performance for the new control runs carried out for the Discovery AQ period under this year's project and comparison to last year's runs.

Chapters 4 provides a description of the progress on specific tasks under this year's project. It also provides a path for completing the tasks.

Chapter 5 provides a description and discussion on model performance for new runs carried out for the new 2013 model evaluation period (September 2013). A statistical evaluation is provided against satellite observed skin temperatures for various levels of satellite assimilation described in Chapter 4. It also provides a comparison of the model results against standard NWS observations of temperature, winds and humidity. Statistics emphasize performance in the Texas domain.

Chapter 6 provides a description and discussion on model performance for new runs carried out for the new 2012 model evaluation period (August 2012). A statistical evaluation is provided against satellite observed skin temperatures for various levels of satellite assimilation described in Chapter 4. It also provides a comparison of the model results against standard NWS observations of temperature, winds and humidity. Statistics emphasize performance in the Texas domain.

Chapter 7 provides a discussion of the model runs in which differences in model satellite skin tendencies and model skin temperature tendencies are used rather than absolute differences between skin temperatures. This is applied to the 2013 Discover AQ Period.

Chapter 8 describes the quality assurance (QA) procedures used to remove erroneous skin temperature data that is used in the skin temperature nudging and model evaluation using skin temperatures. Cloud contamination is a major concern for the quality of the skin temperature from satellite observations. QA procedures are used to minimize erroneous data.

Chapter 9 describes a multiple regression approach to investigate model errors.

Chapter 10 gives a summary and conclusions.

Chapter 12 is a list of acknowledgements.

Chapter 13 contains an appendix of all the acronyms used in this project.

Chapter 14 provides a description of the WRF model configuration.

1.3 References

Anderson, M.C., Norman, J.M., Diak, G.R., Kustas, W.P., and Mecikalski, J.R., 1997. "A two-source time-integrated model for estimating surface fluxes using thermal infrared remote sensing", Remote Sensing Environ., 60, 195-216.

Chen, F., and J. Dudhia (2001), Coupling an advanced land surface-hydrology model with the Penn State-NCAR MM5 modeling system. Part I: Model implementation and sensitivity, *Mon. Wea. Rev.*, 129, 569-585, doi:10.1175/1520-0493(2001)129<0569:CAALSH>2.0.CO;2

Diak, G. R. ,1990: Evaluation of heat flux, moisture flux and aerodynamic roughness at the land surface from knowledge of the PBL height and satellite-derived skin temperatures, J. Agric. For. Meteorol. 52:181-198.

Ellenburg, W.L., McNider, R.T., Cruise, J.F., 2015: , Towards an Understanding of the 20th Century Cooling Trend in the Southeastern US: Biogeophysical Impacts of Land Use Change" submitted to *Earth Interactions*.

Fovell, R. 2013: WRF Performance Issues in the San Joaquin Valley and Southern California. Traversing New Terrain in Meteorological Modeling for Air Quality and Dispersion. U.California Davis. Sept 9-11, 2013.

Mackaro, S., R.T. McNider and A. Pour-Biazar, 2011: Some physical and computational issues in land surface data assimilation of satellite skin temperatures. *Pure Appl. Geophys*. Springer Basel AG DOI 10.1007/s00024-011-0377-0

McNider, R. T., W.M. Lapenta, A. Biazar, G. Jedlovec, R. Suggs, and J. Pleim, 2005: Retrieval of grid scale heat capacity using geostationary satellite products: Part I: Case-study application, *J. Appl. Meteor.*, ***88***, 1342-1360

McNider, R. T., W. B. Norris, D. M. Casey, J. E. Pleim, S. J. Roselle, and W. M. Lapenta: Assimilation of satellite data in regional air quality models XII. Edited by Gryning, Chaumerliac, and Plenum Press, pp. 25-35. 1998.

McNider, R.T., A.J. Song, D.M. Casey, P.J. Wetzel, W.L. Crosson, and R.M. Rabin, 1994: Toward a dynamic-thermodynamic assimilation of satellite surface temperature in numerical atmospheric models. *Mon. Wea. Rev.*, **122,** 2784-2803.

Niu, G.-Y., et al. 2011, The community Noah land surface model with multiparameterization options (Noah-MP): 1. Model description and evaluation with local-scale measurements, J. Geophys. Res., 116, D12109

Noilhan, J., S. Planton, 1989: A Simple Parameterization of Land Surface Processes for Meteorological Models. Mon. Wea. Rev., 117, 536–549

Pitman, A. J. 2003, The evolution of, and revolution in, land surface schemes designed for climate models, Int. J. Climatol., 23, 479–510

Pleim, J. E. and A. Xiu, 1995: Development and testing of a surface flux and planetary boundary layer model for application in mesoscale models. *J. Appl. Meteor.*, **34**, 12-32.

Pleim, J. E. and A. Xiu, 2003: Development of a land surface model. Part II: Data assimilation. *J. Appl. Meteor*., **42**, 1811-1812.

Pleim, Jonathan E., Robert Gilliam, 2009: An Indirect Data Assimilation Scheme for Deep Soil Temperature in the Pleim–Xiu Land Surface Model. J. Appl. Meteor. Climatol., 48, 1362–1376

Rosero, E., Z.-L. Yang, L. E. Gulden, G.-Y. Niu, and D. J. Gochis (2009), Evaluating enhanced hydrological representations in Noah-LSM over transition zones: Implications for model development, J. Hydrometeorol., 10, 600–62

Sellers, P. J., et al. (1997), Modeling the exchanges of energy, water, and carbon between continents and the atmosphere, Science, 275(5299), 502–509

Wagener, T., and H. V. Gupta (2005), Model identification for hydrological forecasting under uncertainty, Stochastic Environ. Res. Risk Assess., 19, 378–387.

Xiu, A. and J. E. Pleim, 2001: Development of a land surface model. Part I: Application in a mesoscale meteorological model. *J. Appl. Meteor*., **40**, 192-209.

Yang, R., and M. A. Friedl (2003), Modeling the effects of three-dimensional vegetation structure on surface radiation and energy balance in boreal forests, J. Geophys. Res., 108, 8615

2 Satellite Assimilation-Initial Results

2.1 Introduction

In this project, it was first proposed that satellite skin temperatures might be a better metric for model performance than standard NWS data in large part because of their ability to capture land use variations at fine resolution. Second, that satellite skin temperatures might be used to improve the specification of land surface parameters in land surface models. This Chapter describes the second aspect of the project, which is the use of satellite skin temperatures to adjust soil moisture in a new version of the P-X model in a similar way that observed surface air temperatures are used to adjust moisture in the current P-X model.

2.2 Description of Skin Temperature Nudging Within The Pleim-Xiu Model

The last biennium project AQRP 14-022 final report described the skin temperature products in Chapter 3. As noted in that chapter, an alternative skin temperature which is a single channel retrieval by NOAA NESDIS that supports the ALEXI suite of products will be used in the land surface adjustment process. Xiu and Pleim (2001) noted that since surface moisture is not a direct observable that use of auxiliary information is needed. They have used analyses of observed NWS surface temperatures and relative humidity to nudge moisture. They adjusted surface layer moisture w_G using the difference between model daytime temperatures (T^F) and analyses of observed temperatures (T^A) and model and observed relative humidity as in equation (2-1).

$$\Delta w_G = \alpha_1\left(T^A - T^F\right) + \alpha_2\left(RH^A - RH^F\right)_{Daytime} \quad (2\text{-}1)$$

The P-X approach has been widely used and in recent California inter-comparisons performed better than the Noah complex land surface model (Fovell 2013). Because observed NWS observations are coarse it is proposed to replace the observed temperatures with satellite skin temperatures, i.e.

$$\Delta w_G = \beta_1(T_s^{Sat} - T_s^{Mod})_{Morning} \quad (2\text{-}2)$$

where the nudging will be applied in the morning time frame. While the nudging in the original assimilation in equation (2-2) was applied throughout the day, here it is believed it best to only nudge moisture during the morning hours for two reasons. The first is that skin temperature response is most sensitive to moisture in the morning hours (Carlson 1986). Second, because of afternoon cumulus clouds there is also a greater chance that undetected clouds may contaminate the surface skin temperature satellite retrieval.

The observed satellite skin temperatures used in this investigation were described in Chapter 3 of the last biennium project AQRP 14-022 and are based on a single channel retrieval used by the NOAA/USDA ALEXI group (Anderson et al. 2007a and Anderson et al. 2007b).

2.3 Differences Between Satellite and Model Skin Temperatures

The assumption in the skin temperature assimilation process in equation (2-2) is that where model temperatures are cooler than observed temperatures then moisture will be reduced so that

more energy will be partitioned into sensible heating rather than evaporation. On the other hand, where model skin temperatures are warmer than observed skin temperatures, then moisture will be increased. This is similar to the original P-X moisture nudging by air temperatures.

Figure 2-1 provides the difference between the WRF control simulation and the observed satellite skin temperature where the USGS vegetation fraction has been used instead of the Pleim seasonal-adjusted value. It is noted that in personal communication with Jon Pleim that they also are looking at changing their vegetation fraction calculation and perhaps moving to a MODIS vegetation fraction (Ran et al 2015).

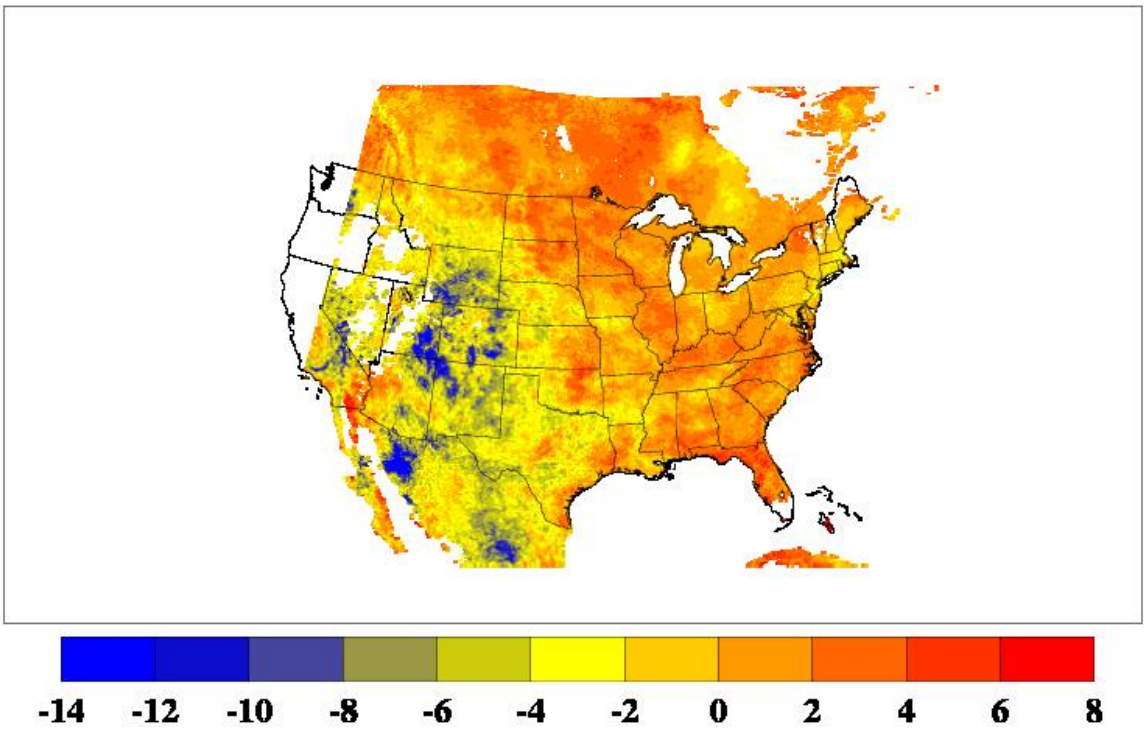

Figure 2-1 *Average daytime difference of the WRF diagnosed skin temperature minus the NOAA ALEXI observed skin temperature for the period 0000 UTC 1 September 2013 through 0000 UTC 6 September 2013. The NOAA ALEXI observed skin temperatures are the most recent version with aggressive cloud screening. Simulation is the insolation replacement run with the new (USGS) vegetation fraction and without any nudging. Values truncated between -14 and +8 degrees K. White areas indicate no satellite data.*

2.4 Defining Statistical Measures for Assessing Impact of Skin Temperature Nudging

After the first set of runs using the skin temperature it was decided to make some changes in the model and protocols. The nudging coefficient, β_1, was set to a time scale of a few minutes which provides for a fairly fast assimilation. First, it was felt that with the short time available in the morning for assimilation that a stronger nudging coefficient be used than was employed in the original P-X form which continuously assimilated the NWS observations.

Second, because in the P-X model ET from vegetation is only impacted by deep layer moisture (W_2) it was decided to nudge the deep soil moisture in a similar fashion to the first layer moisture given in (2-2), i.e.

$$\Delta W_2(x,y,t) = \beta_1(T_{SO}\ (x,y,t) - T_{SM}\ (x,y,t))_{morning} \quad . \quad (2\text{-}3)$$

In order to make comparisons of the impact of the assimilation it was felt that the control run that did not include the 2-m NWS nudging was a more appropriate control. With this WRF control run a pure comparison of the impact of the skin temperature can be seen. In the end a comparison with the P-X 2-m nudging will be made but to understand the impact of the satellite skin temperature nudging this is a better control. The control run included the satellite insolation forcing. The WRF control will be referred to as WRF-CONTR.

The WRF skin temperature nudging run (hereafter referred to as WRF-TS) was run in the same configuration.

Three statistics are used to evaluate whether the case with skin temperature nudging (WRF-TS) was providing an improvement over the control case (WRF-CONTR). These are defined below.

$$B_I = \left| \frac{1}{n} \sum_{t=1}^{n} \left(T_{WI} - T_{OBS} \right) \right| \quad (2\text{-}4)$$

$$B_N = \left| \frac{1}{n} \sum_{t=1}^{n} \left(T_{WN} - T_{OBS} \right) \right| \quad (2\text{-}5)$$

$$P = \left(B_N - B_I \right) \quad (2\text{-}6)$$

B_I is the magnitude of the skin temperature bias for the insolation replacement run as in equation (2-4), where n is the total number of comparisons pairs, T_{WI} is the WRF diagnosed skin temperature for the WRF-CONTR, and T_{OBS} is the NOAA-Alexi GOES-derived skin temperature. In a similar manner B_N is the magnitude of the skin temperature bias for the insolation replacement plus soil nudging run as in equation (2-5), where T_{WN} is the WRF-TS diagnosed skin temperature for the run. The comparison statistic is then provided by equation (2-6) which gives the change in the magnitude of the bias between the insolation and nudging runs.

2.5 Full Month Results for Moisture Nudging

The WRF model was run in the WRF-CONTR mode and WRF-TS for the period of 1-30 September 2013. For these runs it was decided to use the SPoRT insolation rather than the GSIP insolation product. This was based on the first five day simulation which appeared to show the insolation product deteriorated the statistical performance despite the GSIP product performing better than the WRF model in comparison to pyranometer data in Chapter 2 of the last

biennium's report . Also, the SPoRT insolation product performed better against pyranometer data than the GSIP product.

Figure 2-2 shows the spatial depictions of bias of the WRF-CONTR (with satellite insolation but without moisture nudging). Figure 2-3 shows the bias (with moisture nudging) and Figure 2-4 show the difference in the magnitude of the bias between the WRF-TS and WRF-CONTR. As can be seen in Figure 2-5 which shows the sign of the change in bias the moisture nudging improves the magnitude of the bias over most areas in the domain.

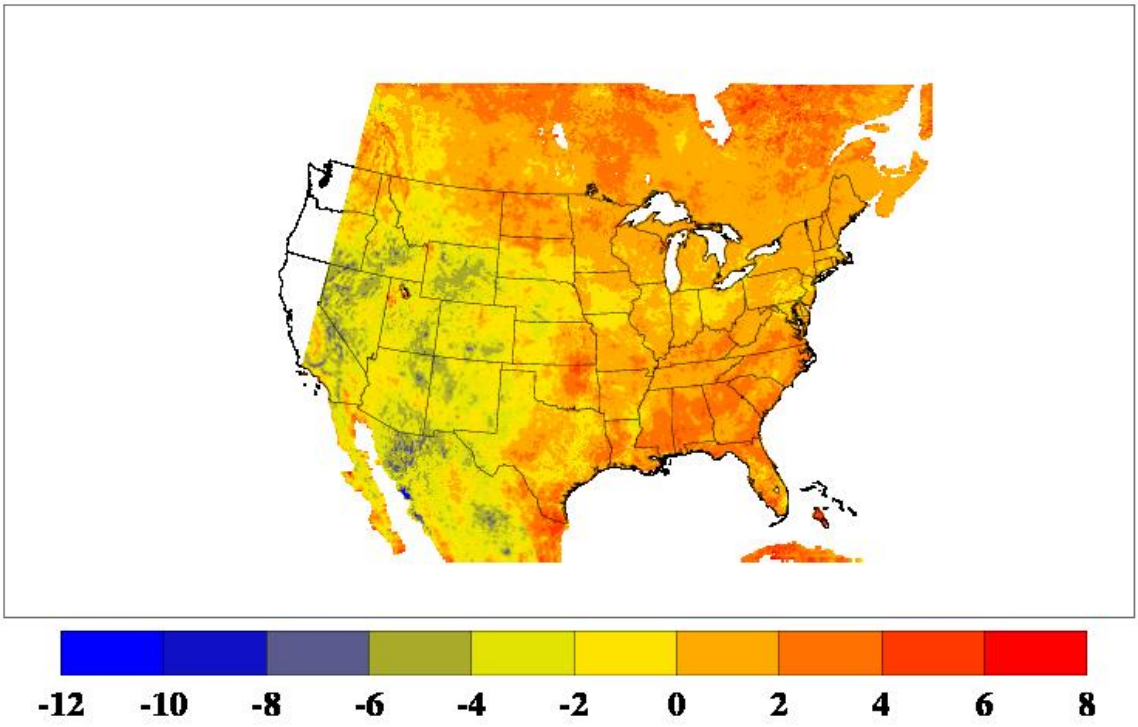

Figure 2-2 *Average bias (units of degrees K) (WRF-CONTR minus observed) of skin temperatures for the period 0000 UTC 1 September 2013 through 2300 UTC 30 September 2013 for daytime conditions.*

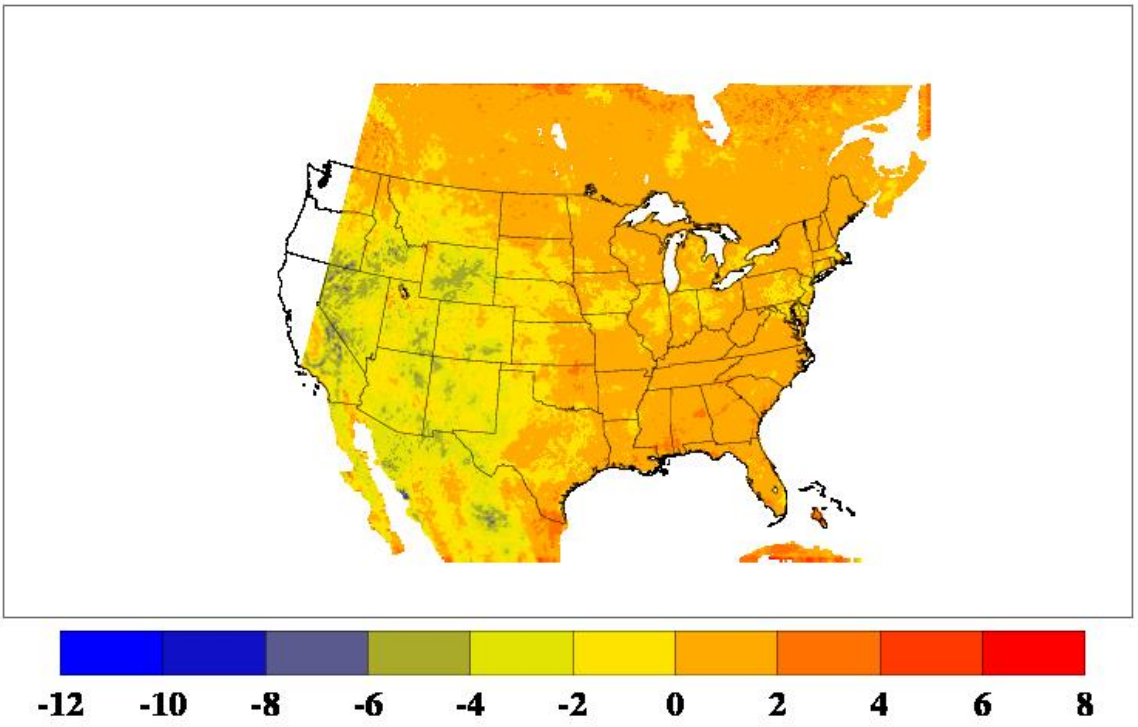

Figure 2-3 *Average bias (units of degrees K) (soil moisture nudging (WRF-TS) run minus observed) of skin temperatures for the period 0000 UTC 1 September 2013 through 2300 UTC 30 September 2013 for daytime conditions.*

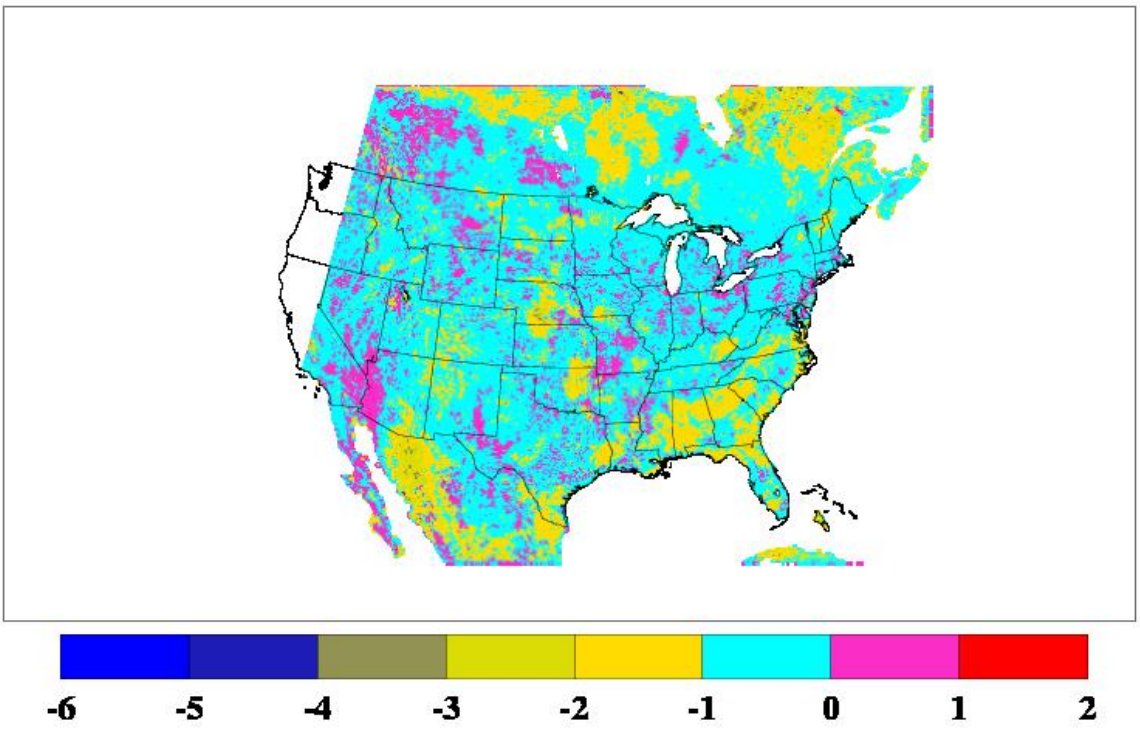

Figure 2-4 *Difference in the magnitude of the respective bias values (units of degrees K) soil moisture nudging run (WRF-TS) minus WRF-CONTR) of skin temperatures for the period 0000 UTC 1 September 2013 through 2300 UTC September 30 2013 for daytime conditions. Negative values indicate a decrease in the magnitude of the bias, and vice versa.*

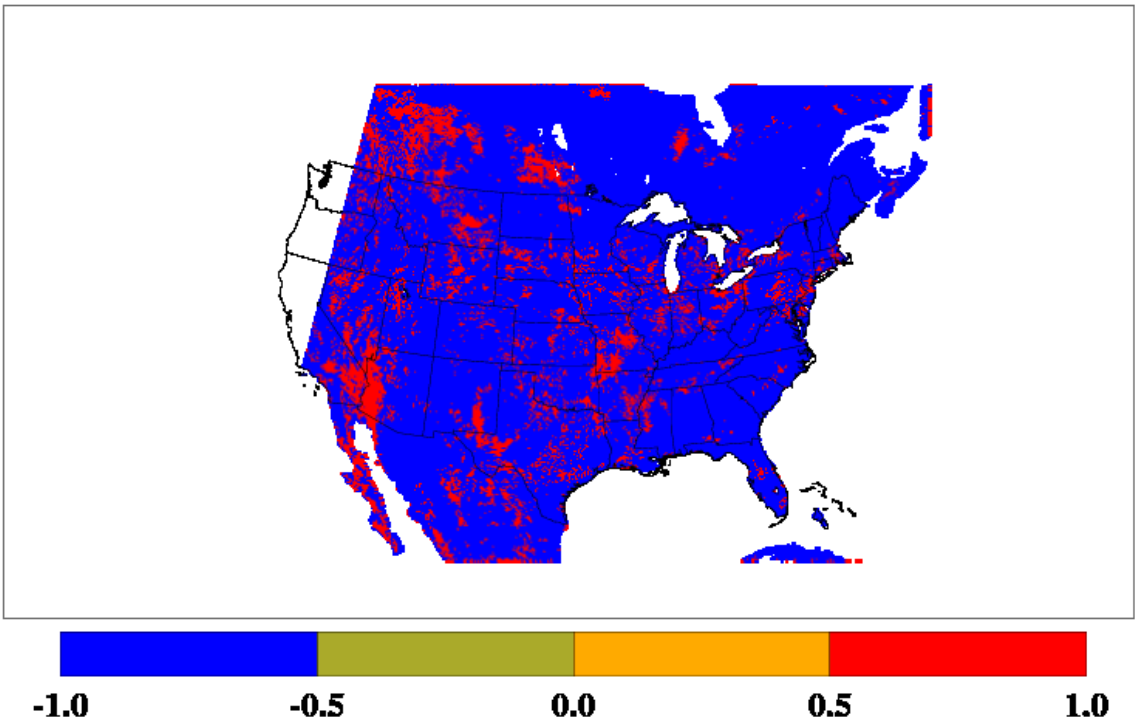

Figure 2-5 *Same as Figure* 2-4*, except only the sign is plotted. Blue areas denote a decrease in the magnitude of the bias, and red areas denote an increase in the magnitude of the bias in degrees K.*

The root mean square error (RMSE) is another measure of model performance. Figure 2-6 and Figure 2-7 show the spatial depiction of the RMSE for the domain. As can be seen in Figure 2-8 and Figure 2-9 the RMSE is improved over most of the domain.

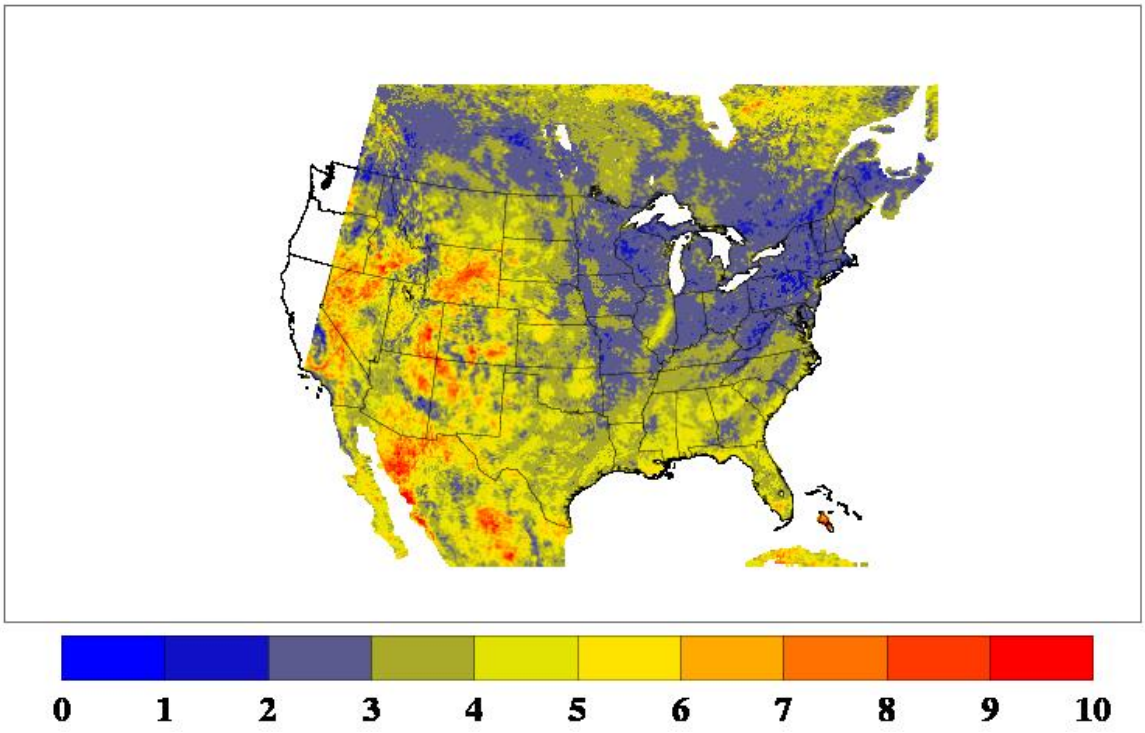

Figure 2-6 *Root mean square error (units of degrees K) (WRF-CONTR minus observed) of skin temperatures for the period 0000 UTC 1 September 2013 through 2300 UTC September 30 2013 for daytime conditions. Values truncated to 10 K.*

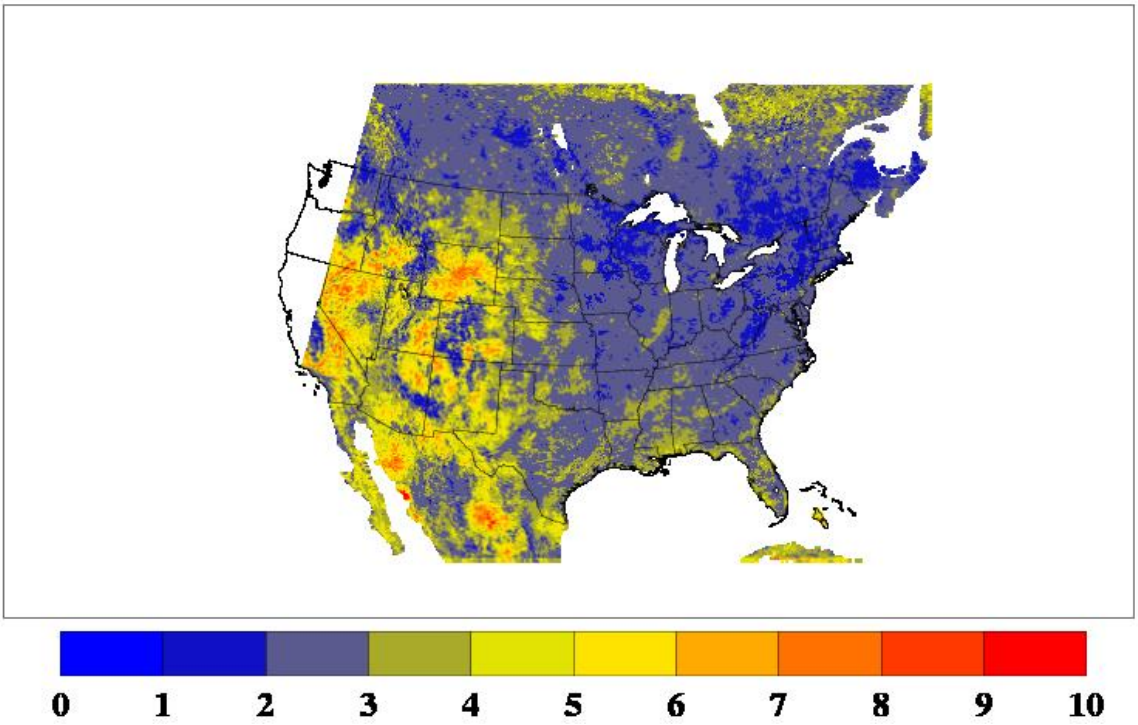

Figure 2-7 *Root mean square error (RMSE, units of degrees K) (WRF-TS minus observed) of skin temperatures for the period 0000 UTC 1 September 2013 through 2300 UTC 30 September 2013 for daytime conditions. Values truncated to 10 K.*

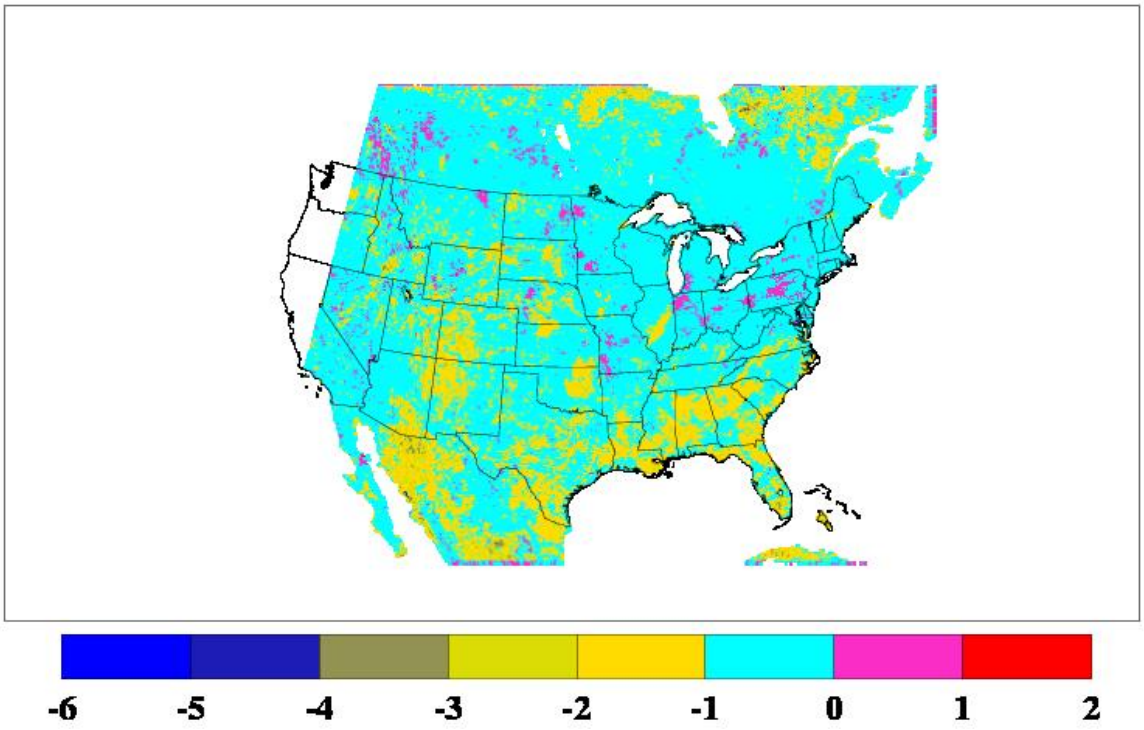

Figure 2-8 *Difference in the respective RMSE values (units of degrees K) (WRF-TS minus WRF-CONTR) of skin temperatures for the period 0000 UTC 1 September 2013 through 2300 UTC September 2013 for daytime conditions. Negative values indicate a decrease in the magnitude of the RMSE, and vice versa.*

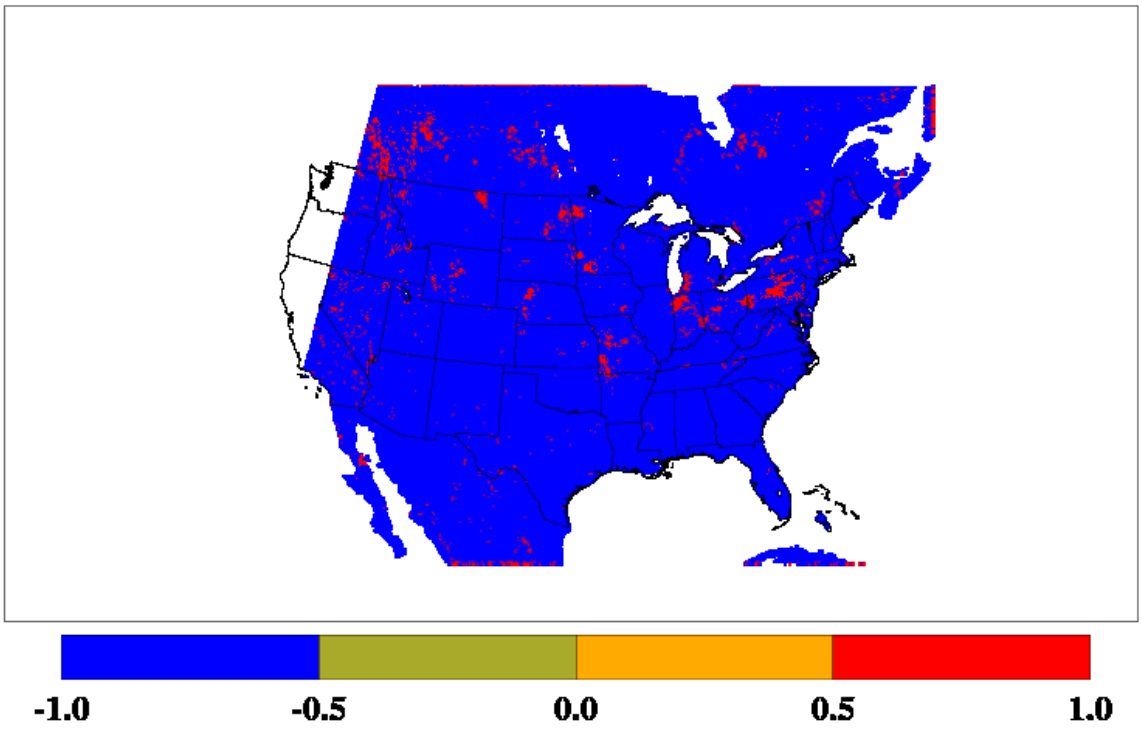

Figure 2-9 *Same as* Figure 2-8 *except only the sign is plotted. Blue areas denote a decrease in the RMSE, and red areas denote an increase in the RMSE (unitless).*

Table 2-1 below gives the total statistics for the entire domain relative to skin temperatures for various WRF simulations.

SIMULATION	BIAS ALL	BIAS WEST	BIAS EAST	RMSE ALL	RMSE WEST	RMSE EAST
WRF-BASE	**0.06**	**-1.08**	**1.31**	**3.68**	**4.11**	**3.21**
WRF-PLEIM	**0.08**	**-1.08**	**1.35**	**3.64**	**4.05**	**3.18**
WRF-CONTR	**0.09**	**-1.13**	**1.42**	**3.70**	**4.17**	**3.18**
WRF-TS	**-0.13**	**-0.95**	**0.78**	**3.00**	**3.43**	**2.53**

Table 2-1 *Overall bias and RMSE statistics for the 1-30 September, 2013. WRF-BASE is the simulation with no Pleim nudging, no satellite insolation, and no skin temperature moisture nudging. WRF-PLEIM is the same as WRF-BASE except the Pleim nudging is activated. WRF-CONTR is the simulation with no Pleim nudging, with satellite insolation, and no skin temperature moisture nudging. WRF-TS is the simulation with no Pleim nudging, with satellite insolation, and with skin temperature moisture nudging.*

2.6 Evaluation against NWS observations

While the previous section discussed the evaluation of the WRF model in comparison to satellite skin temperature, the more standard model evaluation is against National Weather Service (NWS) observations. In this section, comparisons are made to NWS surface observations such as 2-m temperature, 2-m specific humidity and 10-m wind. However, interpretation is difficult

since the NWS observations are point observations while model results are a 12-km average for the grid. Land use and cloud scale impacts in the model may not be representative of the point measure.

The following Table 2-2 through Table 2-5 provide bias and RMSE for model runs compared to NWS observations for specific humidity, temperature, wind speed and wind direction. In these tables the runs are identified in the following manner. WRF-BASE is the simulation with no Pleim nudging, no satellite insolation, and no skin temperature moisture nudging. WRF-PLEIM is the same as WRF-BASE except the Pleim nudging is activated. WRF-CONTR is the simulation with no Pleim nudging, with satellite insolation, and no skin temperature moisture nudging. WRF-TS is the simulation with no Pleim nudging, with satellite insolation, and with skin temperature moisture nudging. The WRF-TS simulation can be summarized by the following. For specific humidity there was a slight increase in absolute bias but little change in RMSE. For 2-m temperature there was also a slight increase in absolute bias but a slight reduction in RMSE. For 10-m wind direction there was a slight decrease in bias and decrease in RMSE for all regions. This was the same for wind speed which showed a slight decrease in bias and RSME.

SIMULATION	BIAS ALL	BIAS WEST	BIAS EAST	RMSE ALL	RMSE WEST	RMSE EAST
WRF-BASE	**0.0**	**-0.2**	**0.0**	**1.8**	**1.9**	**1.8**
WRF-PLEIM	**-0.1**	**-0.1**	**0.0**	**1.8**	**1.9**	**1.7**
WRF-CONTR	**0.0**	**-0.1**	**0.0**	**1.8**	**1.9**	**1.7**
WRF-TS	**0.20**	**0.0**	**0.4**	**1.8**	**1.9**	**1.8**

Table 2-2 *Bias and Root Mean Square Error (RMSE) statistics for 2-m specific humidity (g kg^{-1}) from WRF simulations for the period 1-30 September 2013 for daytime conditions. The west and east domains are divided by – 97^{o} West Longitude meridian.*

SIMULATION	BIAS ALL	BIAS WEST	BIAS EAST	RMSE ALL	RMSE WEST	RMSE EAST
WRF-BASE	**0.0**	**0.3**	**-0.2**	**2.1**	**2.4**	**2.0**
WRF-PLEIM	**0.0**	**0.2**	**-0.2**	**2.0**	**2.3**	**1.8**
WRF-CONTR	**-0.4**	**-0.1**	**-0.5**	**1.9**	**2.2**	**1.8**
WRF-TS	**-0.5**	**-0.2**	**-0.8**	**2.0**	**2.2**	**1.9**

Table 2-3 *Bias and Root Mean Square Error (RMSE) statistics for 2-m temperature (K) from WRF simulations for the period 1-30 September 2013 for daytime conditions. The west and east domains are divided by – 97^{o} West Longitude meridian.*

SIMULATION	BIAS ALL	BIAS WEST	BIAS EAST	RMSE ALL	RMSE WEST	RMSE EAST
WRF-BASE	**2.3**	**1.5**	**2.9**	**60.9**	**65.3**	**58.0**
WRF-PLEIM	**2.4**	**1.6**	**2.9**	**60.7**	**65.2**	**57.8**
WRF-CONTR	**2.0**	**1.1**	**2.6**	**60.5**	**65.0**	**57.6**
WRF-TS	**1.8**	**1.0**	**2.3**	**60.6**	**64.8**	**57.8**

Table 2-4 *Bias and Root Mean Square Error (RMSE) statistics for 10-m wind direction*

(degrees) from WRF simulations for the period 1-30 September 2013 for daytime conditions. The west and east domains are divided by – 97^{o} West Longitude meridian.

SIMULATION	BIAS ALL	BIAS WEST	BIAS EAST	RMSE ALL	RMSE WEST	RMSE EAST
WRF-BASE	**0.2**	**0.1**	**0.3**	**2.6**	**2.9**	**2.4**
WRF-PLEIM	**0.2**	**0.1**	**0.3**	**2.6**	**2.9**	**2.4**
WRF-CONTR	**0.1**	**0.0**	**0.2**	**2.5**	**2.9**	**2.3**
WRF-TS	**0.1**	**0.0**	**0.2**	**2.5**	**2.9**	**2.3**

Table 2-5 *Bias and Root Mean Square Error (RMSE) statistics for 10-m wind speed (m s^{-1}) from WRF simulations for the period 1-30 September 2013 for daytime conditions. The west and east domains are divided by – 97^{o} West Longitude meridian.*

2.7 Summary and Conclusions

Under this activity a technique was developed which diagnoses a skin temperature consistent with the surface fluxes in the P-X model. This skin temperature is then used in a technique to nudge soil moisture (see equations 2-2 and 2-3). Fundamentally, if the model temperatures are lower than the observed temperature then soil moisture is decreased. If the model temperatures are greater than the observed temperature then soil moisture is increased. This is consistent with that of Pleim and Xiu in that they argued that soil moisture is ill observed and thus needs an indirect observational adjustment. Techniques have been implemented within the WRF framework which allow the nudging of soil moisture using satellite skin temperatures as opposed to the NWS soil moisture nudging in the original P-X model.

A control simulation was carried out (WRF-CONTR) which did not include the skin temperature nudging. Bias statistics were developed for this control. Second, a new WRF run was made using the skin temperature nudging technique. The results showed that over most of the domain that the bias was improved but there was a slight negative increase in the overall bias. This means that the few areas that had an increase in bias were larger causing a slight increase in absolute bias for the domain. Results for a smaller Texas domain showed even better improvements than the statistics for the full domain.

Comparisons with NWS observations were more mixed in regards to bias for humidity and 2-m temperature. RMSE was unchanged for humidity and decreased slightly for 2-m temperature. For wind speed and wind direction there was a slight decrease in bias and RMSE for all regions. Similar results were found for the Texas domain.

Chapter 5 provides new simulations based on task descriptions under this year's project.

2.8 References

Anderson, M.C., Norman, J.M., Mecikalski, J.R., Otkin, J.A. and Kustas, W.P., 2007a. A climatological study of evapotranspiration and moisture stress across the continental United States based on thermal remote sensing: 1. Model formulation. J. Geophys. Res., 112(D10): D10117.

Anderson, M.C., Norman, J.M., Mecikalski, J.R., Otkin, J.A. and Kustas, W.P., 2007b. A climatological study of evapotranspiration and moisture stress across the continental United States based on thermal remote sensing: 2. Surface moisture climatology. J. Geophys. Res., 112(D11): D11112.

Carlson, T. N., 1986: Regional scale estimates of surface moisture availability and thermal inertia using remote thermal measurements. *Remote Sensing Rev.*, **1,** 197-246

Fovell, R. 2013: WRF Performance Issues in the San Joaquin Valley and Southern California. Traversing New Terrain in Meteorological Modeling for Air Quality and Dispersion. U.California Davis. Sept 9-11,2013

Ran, L., R. Gilliam, F. S. Binkowski, A. Xiu, J. Pleim, and L. Band, 2015: Sensitivity of the Weather Research and Forecast/Community Multiscale Air Quality modeling system to MODIS LAI, FPAR, and albedo, *J. Geophys. Res. Atmos*., **120**, 8491–8511, doi:10.1002/2015JD023424.

Xiu,A. and J. Pleim, 2001: Development of a land surface model. Part II: Data assimilation. *J. Appl. Meteor.*, **42**, 1811-1822.

3 New Model Results for Control Simulations

3.1 New Model Runs and Initial Evaluation

Chapter 2 outlines the background and model results from last year's project. Since the end of the last biennium project the UAH team considered the model results and potential improvements in the improvements in the techniques. The task descriptions in Chapter 4 outline these potential improvements. However as part of this year's project several updates were made to the model set-ups not related to the model improvement tasks including updated land-use data sets, initial and nudging analyses and nudging strategies. Below are some of these changes.

a. WRF 3.8.1 versus 3.6.1 – it is especially noted that there were several changes in the P-X scheme and in other microphysics and radiation schemes
b. Updated USGS land use data sets
c. New Short-wave/Long Wave Radiation Package
d. Different Layer where Nudging is not performed.

This chapter provides new work and comparison to last year's project.

3.2 Model Performance Statistics Compared to Last Year's Project

The following gives a summary of the initial model performance as of July during this year's project. Figure 3-1 shows the difference in the bias statistics between this year and the last biennium control simulation. As can be seen there is a dramatic deterioration in the control performance for this year's simulation. This must be due to changes in model set up. Similar errors in this year's control simulations were found in the new 2012 modeling period. It is noted that the control errors in this year's simulations for 2013 and 2012 are appear larger than errors in other simulations made in the past for Texas work and in other work undertaken by our team.

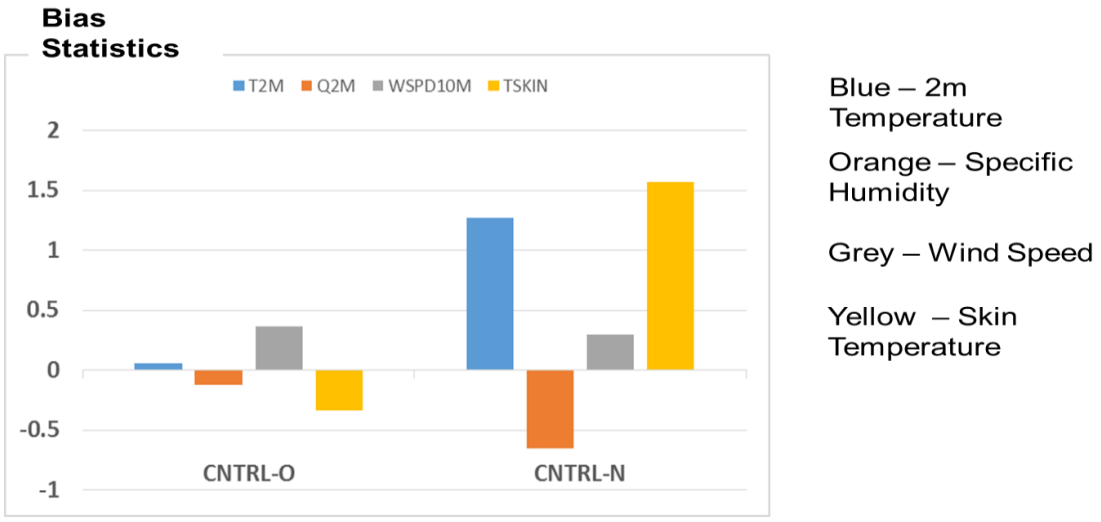

Figure 3-1 *Comparison of bias statistics for this year's simulations (CNTRL-N) and last biennium simulations (CNTRL-O).*

The possible reasons for the differences were listed above. These changes from the previous runs were investigated in a methodical fashion by making runs with and without the changes. Figure 3-2 shows the results of changing model inputs that were different in the previous runs. It shows that model input selections can greatly alter the bias statistics.

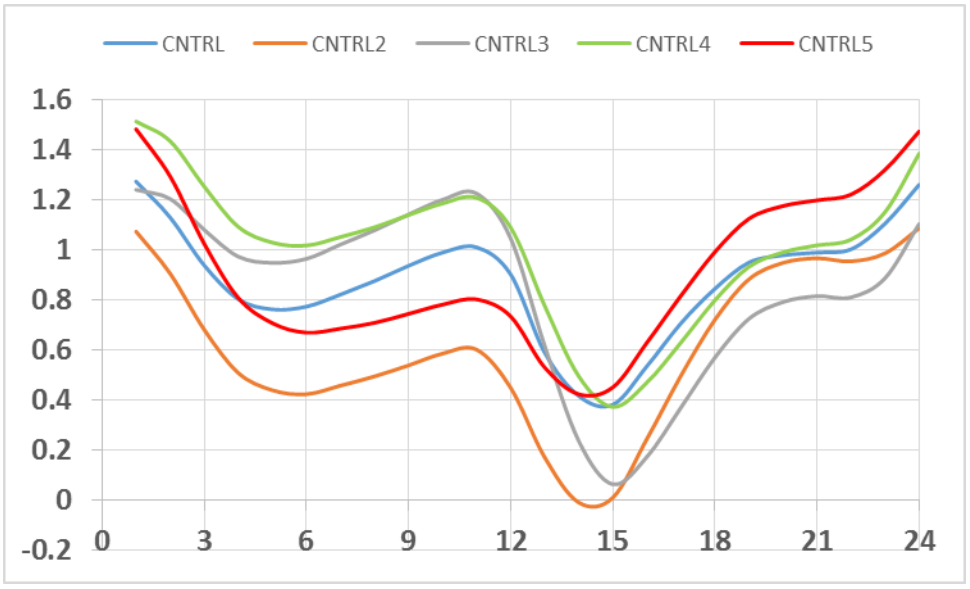

Figure 3-2 *Bias statistics for model control cases for temperature at 2-m for September 2013.*

RUN CODE	FG	STEP	DZBOT	MP_PHY	LW	SW	SFC-INP	PBL NDG
CNTRL	NAM	60	10m	10 (Morrison)	4 (RRTMG)	4 (RRTMG)	3	no
CNTRL2	NARR	30	5m	2 (Lin)	1 (RRTM)	1 (RRTM)	1	no
CNTRL3	NARR	30	5m	2 (Lin)	1 (RRTM)	1 (RRTM)	1	no
CNTRL4	NARR	30	5m	8 (Thompson)	4 (RRTMG)	4 (RRTMG)	1	yes
CNTRL5	NARR	30	5m	8 (Thompson)	4 (RRTMG)	4 (RRTMG)	1	yes

Table 3-1 *Configuration of the control simulations in Figure* 3-2. *"RUN CODE" are the labels used for each simulation as shown in Figure 3-2. "FG" is the type of first-guess data. "STEP" is the model time step in seconds. "DZBOT" is the thickness of the bottom half-sigma layer in m. "MP"PHY" is the WRF microphysics package. "LW" and "SW" are the longwave and shortwave radiation parameterization choices, respectively. "SFC-INP" is the choice for the WRF namelist.input variable "surface_input_source". "PBL NDG" indicates whether nudging was allowed within the planetary boundary layer (PBL).*

3.3 Defining Control Case Inputs

Giving the issues encountered that showed that different model versions, physics choices and input data can drastically change model performance, UAH reconsidered carefully what the control case should be. Should it be a case that has minimal error or the case that is likely to be used by the larger WRF community? Previous model set-ups had been patterned after TCEQ inputs. However, in talking to TCEQ it was found that these are fluid and have not been firmly specified for the P-X scheme.

It was thus decided in the absence of a definitive TCEQ model set-up for the P-X scheme that the appropriate control case would be one most likely to be used within the WRF/Air Quality Community. UAH thus contacted the EPA NERL group and obtained their model name list and set up. Since this project is trying to show that satellite data can improve model performance in the P-X scheme it seems reasonable to use what the Pleim group at EPA would use for their control model set-up. If UAH picked a different control set-up and showed improvement there might be concern that a control set-up with a larger error was chosen making the use of satellite data appear better. This consistency may also help Texas in any future SIP work that might use the satellite assimilation which will be eventually reviewed by EPA.

The EPA Namelist and set-ups are defined in the Appendix in Chapter 14. Using the EPA set-ups the control runs for 2013 were made. These are the control runs used in Chapter 5.

4 Progress on Project Tasks

This chapter provides a discussion of the specific tasks under this year's project (#17-039). Progress on tasks and plans for completion are provided.

4.1 Task 1: Focus on Texas and Small Scale Performance Around Houston and Dallas and Other Metrics Such as Wind Performance

Under last biennium project, in concentrating on implementing the skin temperature assimilation, attention was given to performance statistics over the entire domain. Because of limited time only cursory examination was given to fine scale performance, although the work did show that statistical improvements were even greater in the Texas domain than in the national domain. Under this year's activities a focus will be on wind performance and fine scale temperature performance in the Texas domain especially around Dallas and Houston where SIP development may be a priority. This was done for the 2013 DISCOVER-AQ period with a special emphasis on wind performance around Houston. Texas performance for the new 2012 evaluation period was also carried out. Data sources for the 2013 and 2012 cases included satellite skin temperature and standard NWS surface data as well as where appropriate special data such as aircraft skin temperature and PBL winds from the DISCOVER-AQ program. (See the DISCOVER-AQ web site for links to data http://www-air.larc.nasa.gov/missions/discover-aq/discover-aq.html.

Chapter 5 provides separate sections for evaluation statistics for Texas alone as well as small domains around Houston and Dallas. A special data mask was created such that the NWS and satellite skin temperature model evaluations were made for only NWS stations and model grid points in these domains. A section is provided on extensive evaluation of model wind performance compared to the profiler network around Houston.

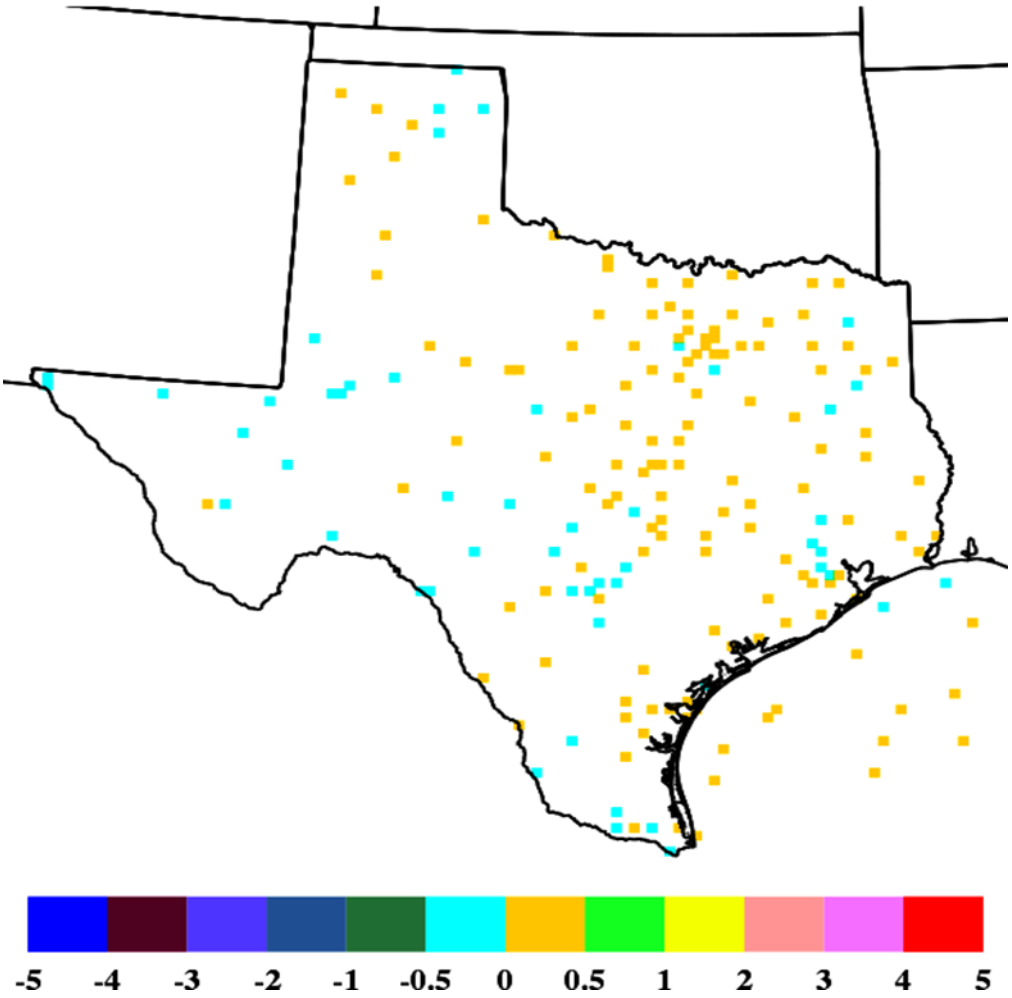

Figure 4-1 *Example of mask to provide NWS comparison for the State of Texas alone*. The blue and gold points indicate a bias value for any field.

4.2 Task 2: Use of Skin Temperature Tendencies

In previous applications of adjustments in surface parameters using satellite skin temperatures (McNider et a. 1994, Mackaro et al. 2011) greater improvement in model performance was found especially compared to NWS observations than in the previous AQRP project. Part of the differences in application was that in these earlier investigations differences in skin temperature tendencies were used to adjust surface moisture. As mentioned above in the P-X scheme absolute differences between skin temperatures are used. However, satellite skin temperatures can sometimes have absolute errors due to atmospheric corrections or emissivity assumptions. Use of skin temperature tendencies avoids issues with such absolute offsets. As an example in the prior AQRP project (14-022) , moisture was adjusted based on the difference in model skin temperatures in the morning time frame. The task will investigate whether differences in tendencies perform better. That is the difference in rate of change in the model over a three – five hour period (the temperature tendency) will be compared to the temperature change in the satellite data used to adjust moisture

Code has been developed to use tendencies in the P-X scheme to adjust moisture. That is

$$\Delta w_G = \eta_1 (\partial T_s^{sat} / \partial t - \partial T_s^F / \partial t)_{Morning}$$

has been implemented. Here Δw_G represents the adjustment in soil moisture, $\partial T_s^{sat} / \partial t$ is the satellite skin temperature tendency, $\partial T_s^F / \partial t$ is the model skin temperature tendency, and η_1 represents a nudging time scale.

Chapter 7 describes these tendency experiments.

4.3 Task 3: Heat Capacity Assimilation

Under this task it is tested whether skin temperature adjustments to surface bulk heat capacity using evening skin temperature might also improve model performance. As shown by Carlson (1986) the afternoon and evening drop in temperatures is most sensitive to thermal resistance/heat capacity. The technique proposed by McNider et al. (2005) is employed within the Pleim-Xiu model to nudge thermal resistance, C_T, using afternoon/evening skin temperatures (as opposed to the Pleim and Gilliam 2009 of using afternoon/evening temperatures to nudge deep soil temperature) as illustrated by equation (3). Here T_S^{SAT} is the satellite observed skin temperature and T_S^{MOD} is the WRF modeled skin temperature.

$$C_T^{NEW} = C_T^{OLD} \frac{\frac{\partial T_S^{SAT}}{\partial t}}{\frac{\partial T_S^{MOD}}{\partial t}} \qquad (3)$$

See Mackaro et al. (2011) and McNider et al. (2005) for further details. Because tendencies can sometimes have high frequency oscillations when the budget is perturbed, a regressed best fit was developed to provide a best estimate of 20 minute tendencies used in the adjustment. Model evaluation of the impact of the heat capacity adjustment is provided in Chapter 5.

4.4 Task 4: Vegetative Fraction

In the last biennium project it was found that the seasonally adjusted USGS vegetation used in the P-X scheme was producing erroneous values especially in the Western U.S. (See Figure 4-2 below). This was communicated directly with Jon Pleim and he agreed and said that a new paper by Ran et al. (2015) found similar results. Because of the importance of vegetative fraction and in view of Ran et al. (2015) it was decided to employ a MODIS derived vegetative fraction in the land surface model. Case et al. (2014) has developed a MODIS-derived 1-km CONUS Green Vegetation Fraction (GVF) dataset which extends back to June 2011. Figure 4-3 shows the MODIS Greenness product. Thus, it is believed the satellite vegetative approach is consistent and perhaps ahead of EPA. It is believed that not only are seasonal adjustments needed but that these can depend on specific years. For example, the Texas greenness is likely much different for the drought years 2010 and 2011 from 2013.

The MODIS greenness data has been processed and used only in the 2013 simulations. Model control cases using USGS data and the satellite greenness values were evaluated using standard performance statistics to assess the impact/validity of the new data set. These results are discussed in Chapter 5.

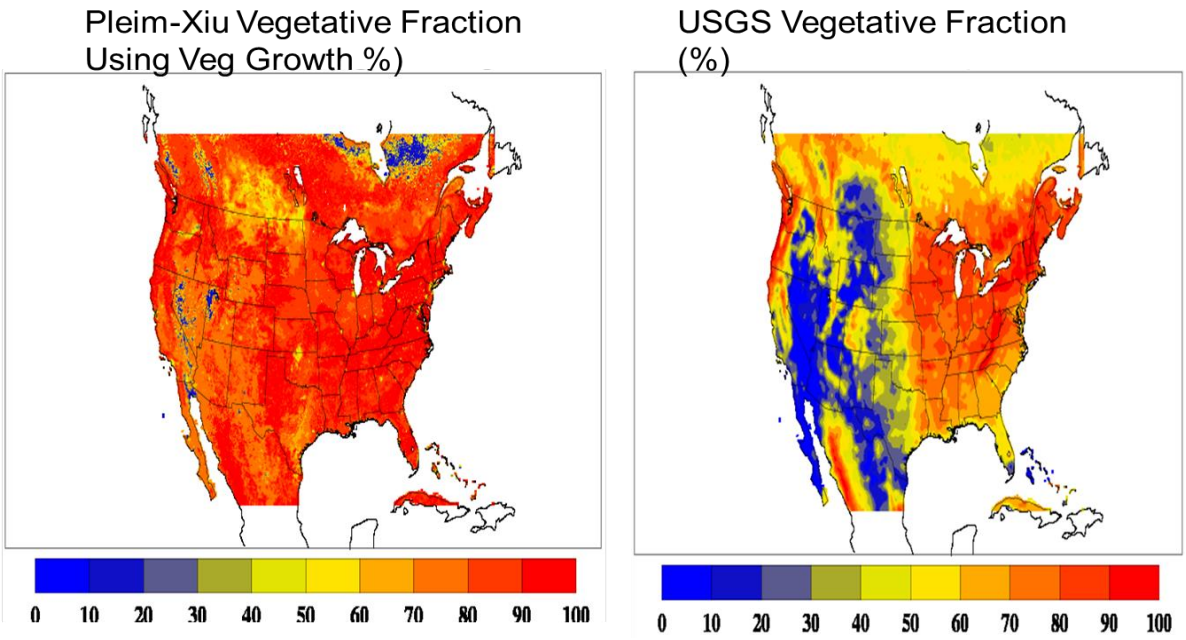

Figure 4-2 *The seasonal growth in the P-X scheme produced erroneous vegetation in the West in September (right). Last year's project used a USGS vegetative fraction data set. However, this is based on climatology and may not represent conditions in a given year or land use change.*

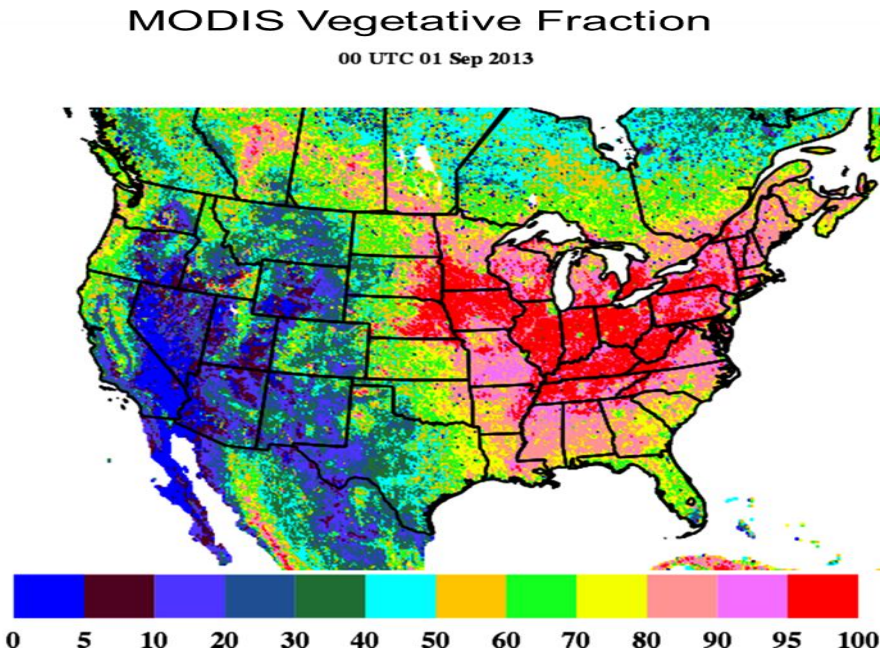

Figure 4-3 *Example of MODIS greenness vegetative fraction for 1 September, 2013. This data*

have been incorporated into WRF simulations.

4.5 Task 5: Tool for Investigating Sensitivity of Land Surface Model Components

The 2012-17 AQRP call suggested that model analysis tools be developed to help understand over or under-prediction of ozone. In the meteorological model there is the same need to understand why 2-m air temperatures (or skin temperatures) are over or under-predicted. A model analysis tool based on forward stepwise regression (Efroymson 1960) to develop a linear regression equation for a selected dependent variable was constructed to be used in the model framework. At each step the variable with the highest correlation with the dependent variable is the candidate for inclusion if certain statistical measures are met. This tool can help determine what variables may be correlated with various surface energy budget errors or other model residual errors.

In Chapter 9 this tool is applied to examine the correlation of several model variables and physical variables with the remaining error in the model simulations.

4.6 Task 6: Satellite Derived Insolation and Albedo

Net shortwave radiation is one of the largest terms in the energy in the daytime boundary layer and is dependent on insolation and surface albedo. Models can have clouds at the incorrect place or time. In last year's project GOES satellite derived insolation (McNider et al. 1995) was used but with the USGS land use albedo rather than a satellite-derived albedo. Since that time additional evaluation of the GOES product has been carried out. Figure 4-4 shows the comparison of the insolation product for Goodwin Creek Mississippi between the satellite and a surface-based pyranometer for 13 June 2013. The satellite derived insolation is nearly identical to the pyranometer for the clear sky case and also captures the cloud signal. Chapter 5 provides model runs with the new insolation products.

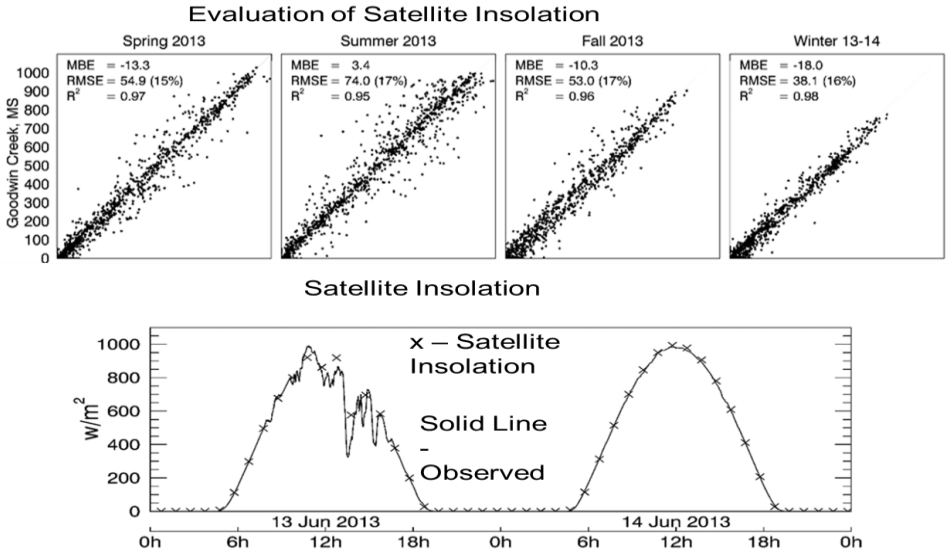

Figure 4-4 *Evaluation of satellite insolation for Goodwin Creek Mississippi. Note clear sky agreement at lower right is almost perfect and satellite product does detect clouds in lower left.*

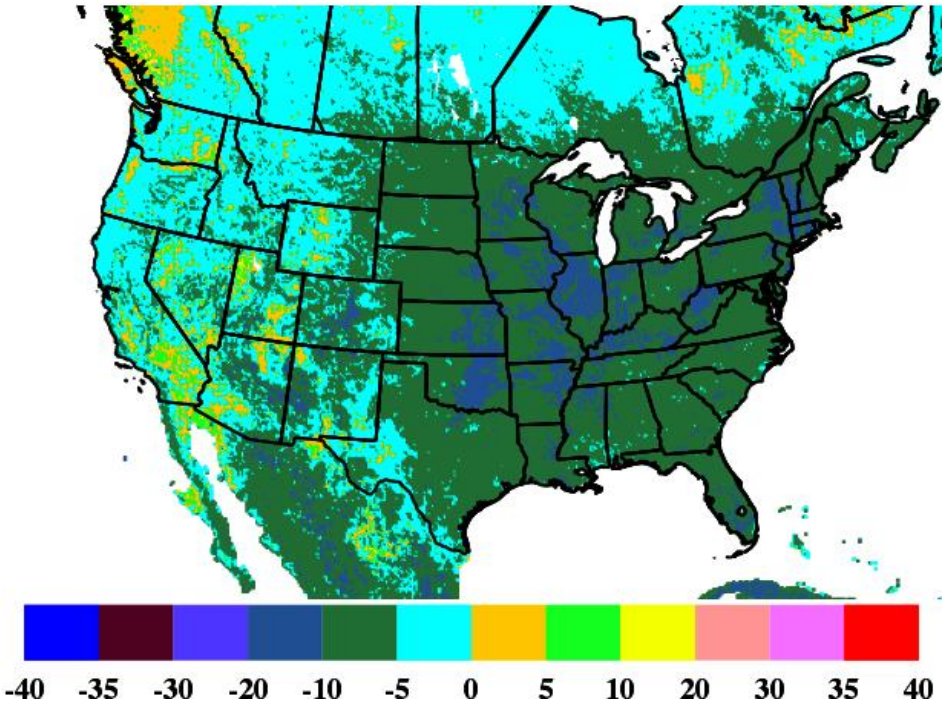

Figure 4-5 *Difference between GOES satellite derived albedo and WRF albedo (Satellite Albedo –WRF Albedo) (units of %) for 1800 UTC 17 August 2013. Note satellite albedo is generally lower than WRF albedo*.

There are also differences between a satellite derived albedo and the model albedo. Figure 4-5 shows the difference between the GOES satellite derived albedo and WRF albedo. The satellite albedo is less than the WRF model albedo. This would result in greater net energy in the surface energy budget. The implications of this lower albedo in model performance are discussed in Chapter 5.

4.7 Task 7: Additional Model Evaluation Period

Under the last biennium project, the model evaluation period was the DISCOVER-AQ Period flight period September 1-30, 2013. However, this period was selected in the AQRP RFP because of the aircraft data availability - not because it was representative of extreme ozone events in the past. The synoptic situation for the month was especially active with multiple fronts producing excess cloudiness and higher winds in Texas and the Southeast (see Alrick et al. 2015). They showed that the DISCOVER-AQ Period was not as conducive to high levels of ozone as TEXAQS II. While last biennium project showed that the satellite technique provided substantial improvement in land surface performance, the cloudiness reduced the number of times that the skin temperature data could be used. Examination of MODIS skin temperatures for the month of September 2013 showed virtually no thermal signal for Dallas (compared to Atlanta) indicating high winds may be reducing thermal gradients. Thus, the skin temperature technique may have even greater positive impact under other episodes where clear skies and light wind conditions most associated with high ozone events dominate.

In consultation with TCEQ another episode was selected. As part of the Good Neighbor SIP process May – September was of interest. Thus, for this project August 2012 was selected. It is a drier period than September 2013 and should have fewer clouds to interfere with skin temperatures.

Figure 4-6 shows an initial skin temperature result from the 2012 August control simulation. As discussed in Chapter 3 both the August 2012 and September 2013 control simulations for this year's project have much larger bias and RMSE than the control run in last biennium project.

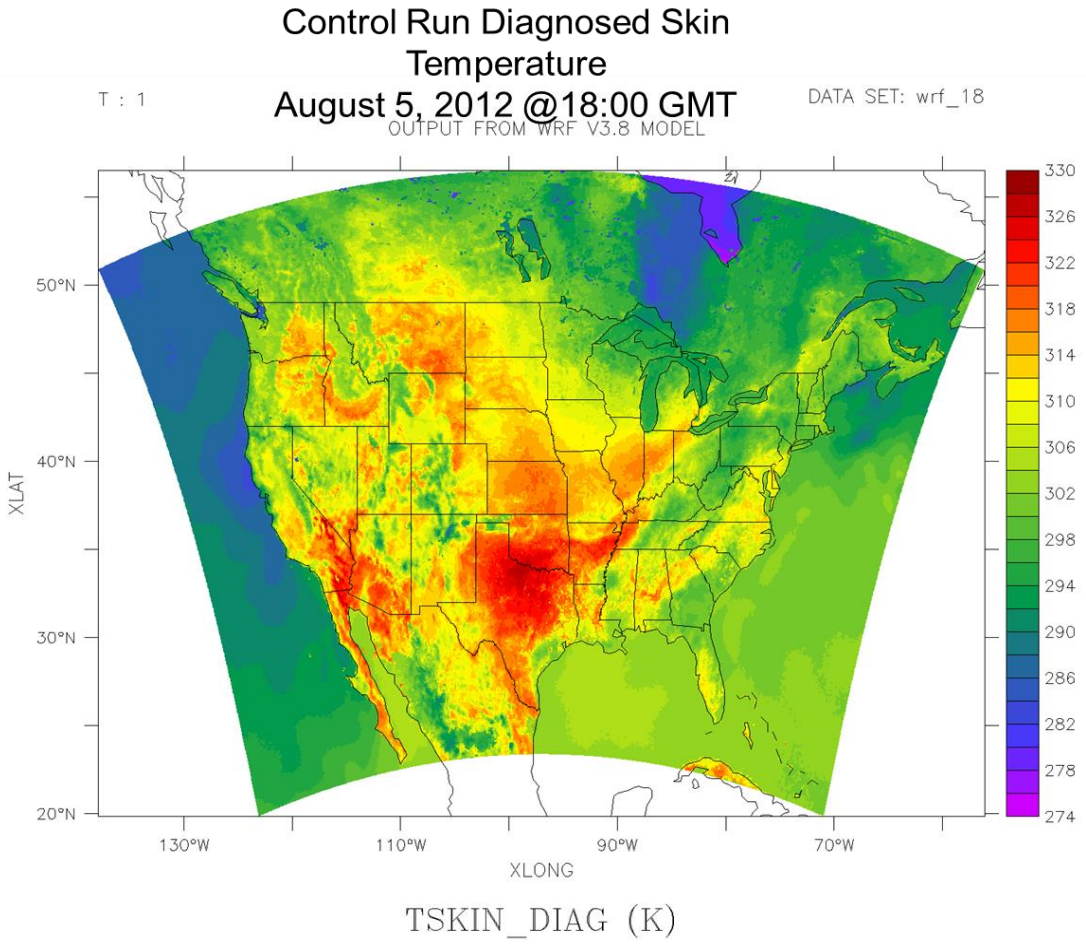

Figure 4-6 Diagnosed skin temperature from the 2012 control simulations. Note higher temperatures in Texas due to dry conditions.

4.8 References

Alrick, D. M., C. P. MacDonald, and G. A. Morris, 2015: Characterization of boundary-layer meteorology during DISCOVER-AQ, Texas Air Quality Research Program Workshop, Austin, TX, June 18, 2015

Case, J. L., F. J. LaFontaine, J. R. Bell, G. J. Jedlovec, S. V. Kumar, and C. D. Peters-Lidard, 2014: A Real-Time MODIS Vegetation Product for Land Surface and Numerical Weather

Prediction Models, *IEEE Transactions on Geoscience and Remote Sensing*, **52**(3), 1772-1786.

Efroymson, M.A., 1960: *Multiple Regression Analysis*, in Mathematical Methods for Digital Computers, Vol 1, Wiley, pp 191-203.

Mackaro, S., R.T. McNider and A. Pour-Biazar, 2011: Some physical and computational issues in land surface data assimilation of satellite skin temperatures. *Pure Appl. Geophys*. Springer Basel AG DOI 10.1007/s00024-011-0377-0

McNider, R. T., J. A. Song, and S. Q. Kidder: Assimilation of GOES-Derived Solar Insolation into a Mesoscale Model. *Int. Journal of Remote Sensing, Vol***. 16**, No. 12, 2207-2231, 1995.

McNider, R. T., W.M. Lapenta, A. Biazar, G. Jedlovec, R. Suggs, and J. Pleim, 2005: Retrieval of grid scale heat capacity using geostationary satellite products: Part I: Case-study application, *J. Appl. Meteor., **88***, 1342-1360

McNider, R.T., A.J. Song, D.M. Casey, P.J. Wetzel, W.L. Crosson, and R.M. Rabin, 1994: Toward a dynamic-thermodynamic assimilation of satellite surface temperature in numerical atmospheric models. *Mon. Wea. Rev.*, **122,** 2784-2803.

Pleim, Jonathan E., Robert Gilliam, 2009: An Indirect Data Assimilation Scheme for Deep Soil Temperature in the Pleim–Xiu Land Surface Model. J. Appl. Meteor. Climatol., 48, 1362–1376

Ran, L., R. Gilliam, F. S. Binkowski, A. Xiu, J. Pleim, and L. Band, 2015: Sensitivity of the Weather Research and Forecast/Community Multiscale Air Quality modeling system to MODIS LAI, FPAR, and albedo, *J. Geophys. Res. Atmos*., **120**, 8491–8511, doi:10.1002/2015JD023424.

5 Satellite Assimilation Runs for 2013

5.1 Model Cases and Descriptions

Beginning with the base control case described in Chapter 3 a series of model runs were made with different levels of satellite assimilation described in the task descriptions in Chapter 4. The following lists the series of model runs made and a short description.

(1) Control Using EPA setups (CNTRL)

This is the base case using the recommended set ups obtained by EPA described in Chapter 3

(2) Satellite Insolation with Satellite Albedo (INSL-1)

This run uses the satellite insolation and albedo described in Task 6 in Chapter 4.

(3) Satellite Insolation with WRF Model Albedo (INSL-2)
This run uses the satellite insolation and WRF model albedo described in Task 6 in Chapter 3.

(4) Veg Fraction – adding MODIS derived vegetation fraction (VEG)
This run uses the satellite derived vegetation fraction rather than the USGS vegetation fraction as described in Task 4 in Chapter 4 . It also includes the INSL-2 product.

(5) Soil Moisture Nudging (SM-1)
This run uses the soil moisture nudging using satellite observed skin temperatures described in Chapter 2 using a nudging time scale of 30 minutes. This includes the INSL-2 product as well as the VEG product.

(6) Soil Moisture Nudging (SM-2)
This run uses the soil moisture nudging using satellite observed skin temperatures described in Chapter 2 using nudging time scale of 60 minutes (weaker nudging). This includes the INSL-2 product as well as the VEG product.

(7) Heat Capacity Nudging (HC-1)
This run uses the adjustment to the heat capacity as described in Task 3 in Chapter 4. This includes the INSL-2 product, the VEG product and the SM-2 product.

(8) Heat Capacity Nudging (HC-2)
This run uses the tendency technique described in Task 2 in Chapter 4.

5.2 Model Evaluation Against Surface Observations

The above cases were evaluated against surface weather observations maintained by NCAR. These surface observations include National Weather Service and airport observations across the continental U.S. (CONUS) as well as private or other governmental observations provided to the National Weather Service. In the following time series plots of the bias (B) and root mean square error (RMSE) are provided. Additionally tables are provided for the actual numerical statistics. The evaluation is carried out separately for CONUS and Texas domains. Spatial plots of bias and RMSE are also provided.

5.2.1 Model Response to Satellite Albedo (INSOL-1), Satellite Insolation (INSOL-2) and Vegetative Fraction (VEG)

Figure 5-1 through Figure 5-6 provides diurnal plots of bias and RMSE as three levels of satellite assimilation are included. They first show the control case (see Chapter 3) bias compared to the observations then runs where successive levels of satellite products are added. As an example Figure 5-1 shows the control bias in blue for 2-m temperature. As the first insolation product with the satellite albedo is added the orange line shows an increase in bias during the day. This is because that the satellite albedo is larger contributing to greater net solar energy in the land surface. The satellite insolation with the model albedo (grey line) shows a reduction in bias

during the day. When the satellite vegetation is included (orange line) additional reduction in bias was found.

Figure 5-2 shows a slight improvement in humidity when the satellite vegetation is included. For wind speed at 10-m Figure 5-3 shows the satellite products slightly decrease an over-prediction in the night but a larger under prediction during the day. However, these changes are small and perhaps close to the errors of observations in wind speeds.

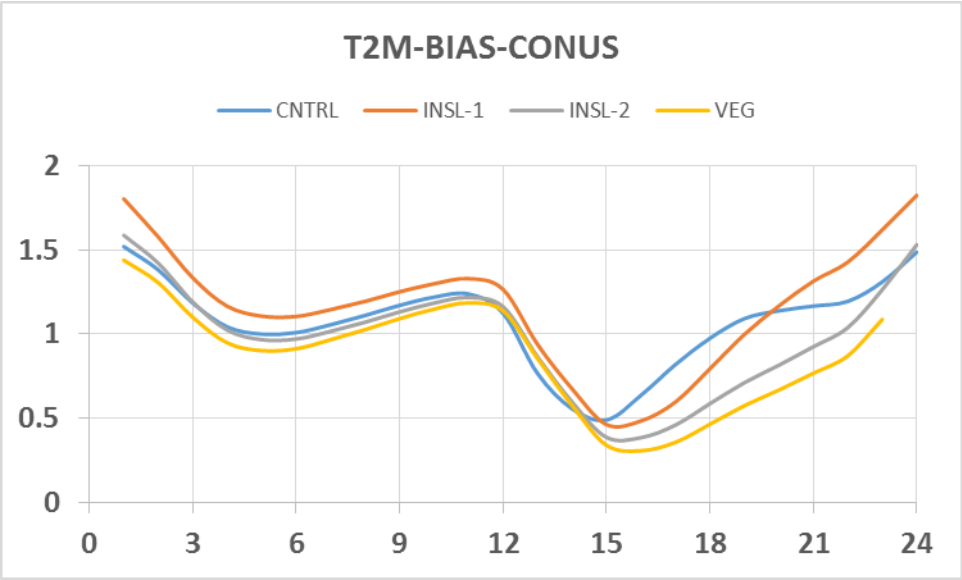

Figure 5-1 *Average hourly bias values (K) for temperature at 2-m for various WRF simulations for the entire 12-km grid for 1-30 September 2013. Values calculated at all surface observing stations. Times are in UTC with 00 being near sunset and 12 near sunrise.*

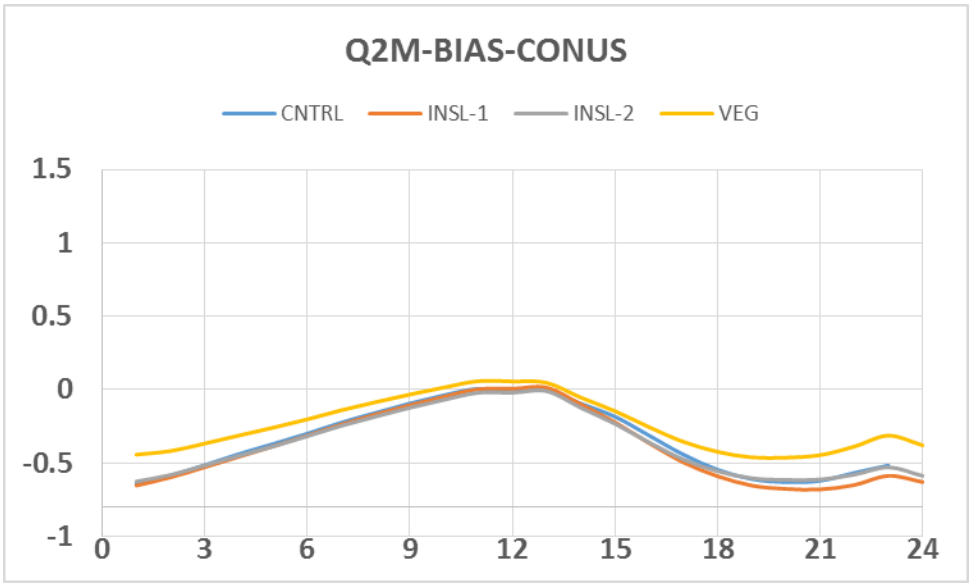

Figure 5-2 *Average hourly bias values (g kg^{-1}) for specific humidity at 2-m for various WRF simulations for the entire 12-km grid for 1-30 September 2013. Values calculated at all surface observing stations.*

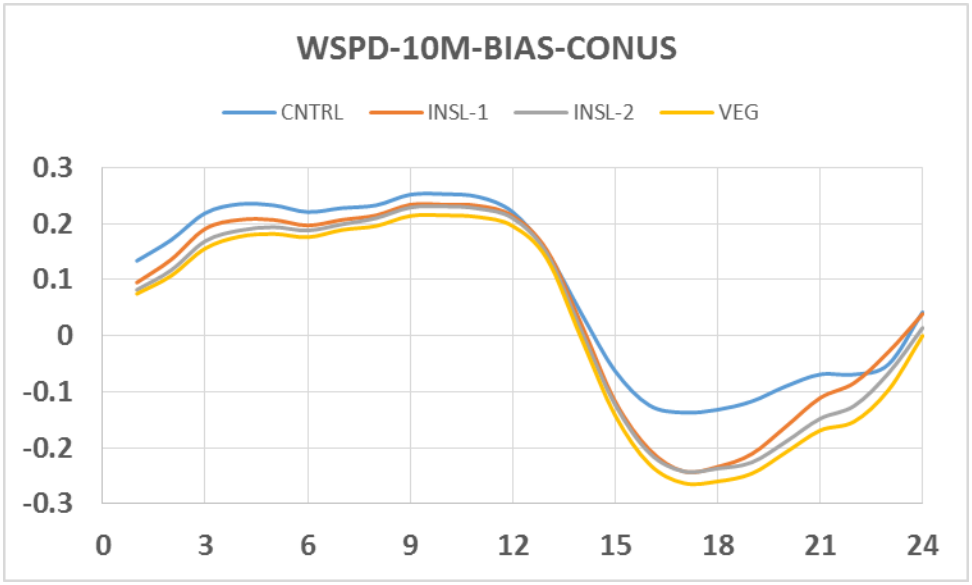

Figure 5-3 *Average hourly bias values (m s^{-1}) for wind speed at 10-m for various WRF simulations for the entire 12-km grid for 1-30 September 2013. Values calculated at all surface observing stations.*

Figure 5-4 through Figure 5-6 show similar plots for the root mean square error statistic (RMSE). The RMSE for 2-m temperature is reduced for the satellite insolation with model albedo and

satellite vegetation assimilation during the day. Small improvements are found in humidity and wind speed with the satellite assimilation.

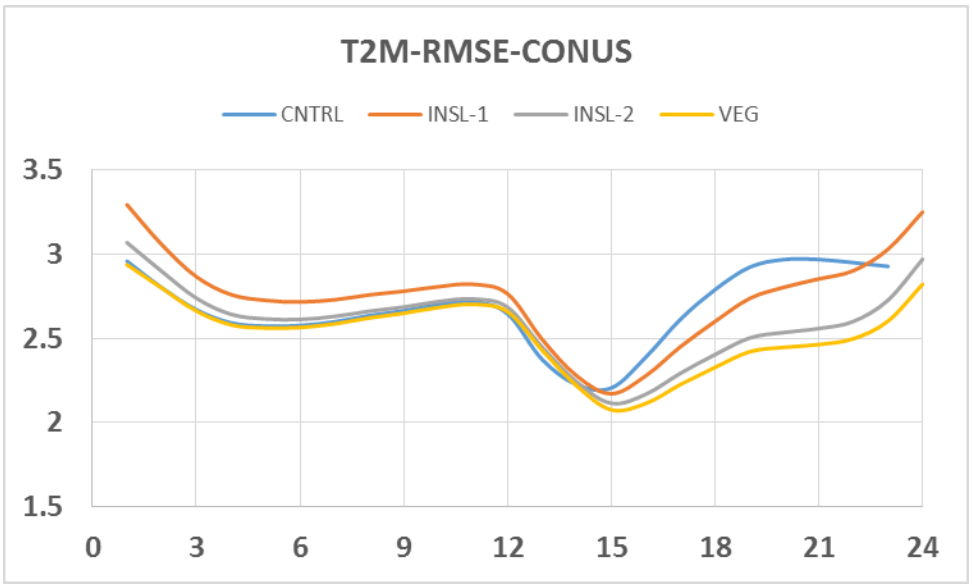

Figure 5-4 *Hourly root mean square error (RMSE) values (K) for temperature at 2-m for various WRF simulations for the entire 12-km grid for 1-30 September 2013. Values calculated at all surface observing stations.*

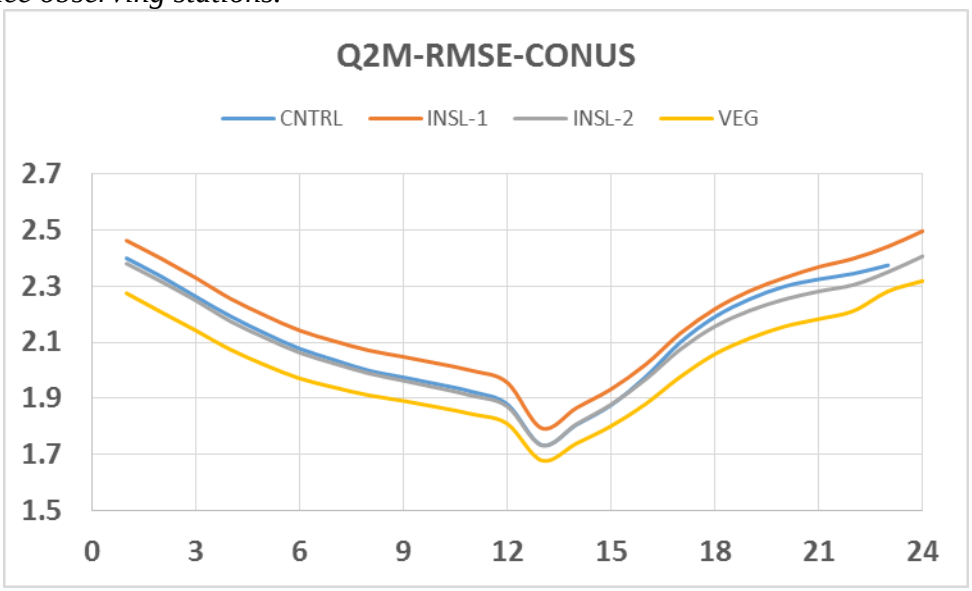

Figure 5-5 *Hourly root mean square error (RMSE) values (g kg^{-1}) for specific humidity at 2-m for various WRF simulations for the entire 12-km grid for 1-30 September 2013. Values calculated at all surface observing stations.*

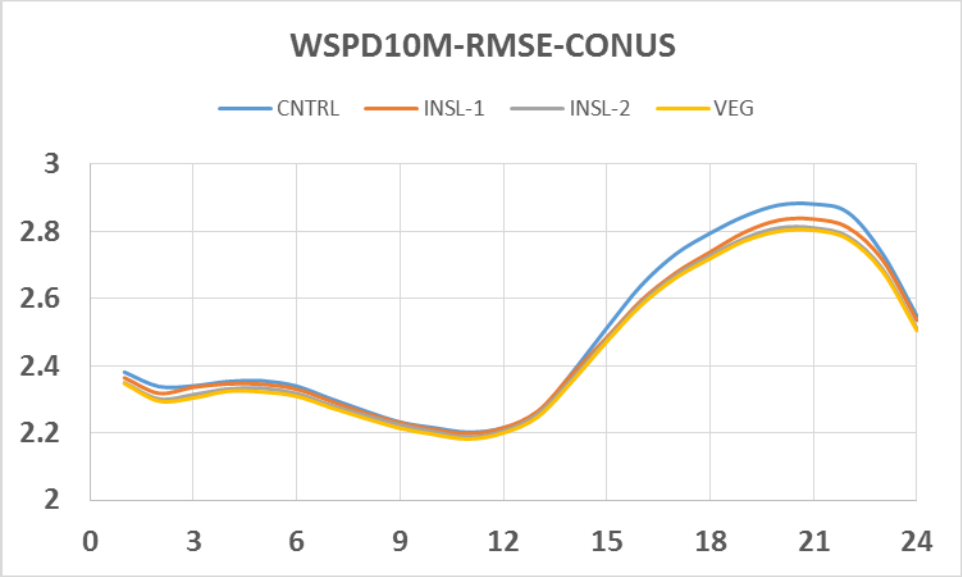

Figure 5-6 *Hourly root mean square error (RMSE) values (m s^{-1}) for wind speed at 10-m for various WRF simulations for the entire 12-km grid for 1-30 September 2013. Values calculated at all surface observing stations.*

Figure 5-7 shows the spatial pattern of changes in bias due to including satellite insolation with model albedo. Note over most areas the bias is improved with a few areas such as coastal Carolina showing a degradation. Figure 5-8 shows a similar plot when satellite vegetation is included (VEG) and satellite insolation (INSOL-2). As can be seen the bias is improved over most areas.

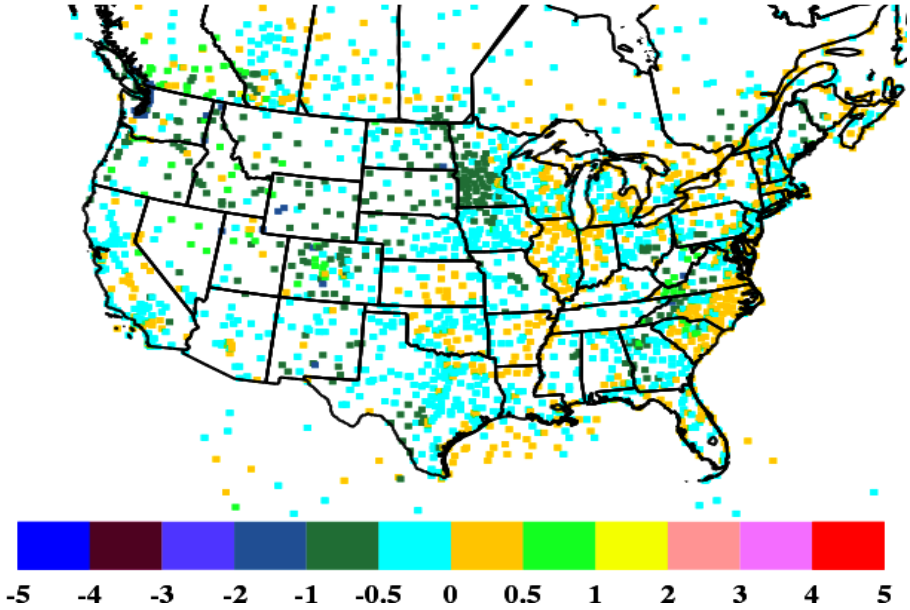

Figure 5-7 *Difference in the magnitudes of the respective bias values (units of degrees K) INSL-2 minus CNTRL of 2-m temperatures for the period 1-30 September 2013 for daytime conditions.*

Negative values indicate a decrease in the magnitude of the bias and vice versa.

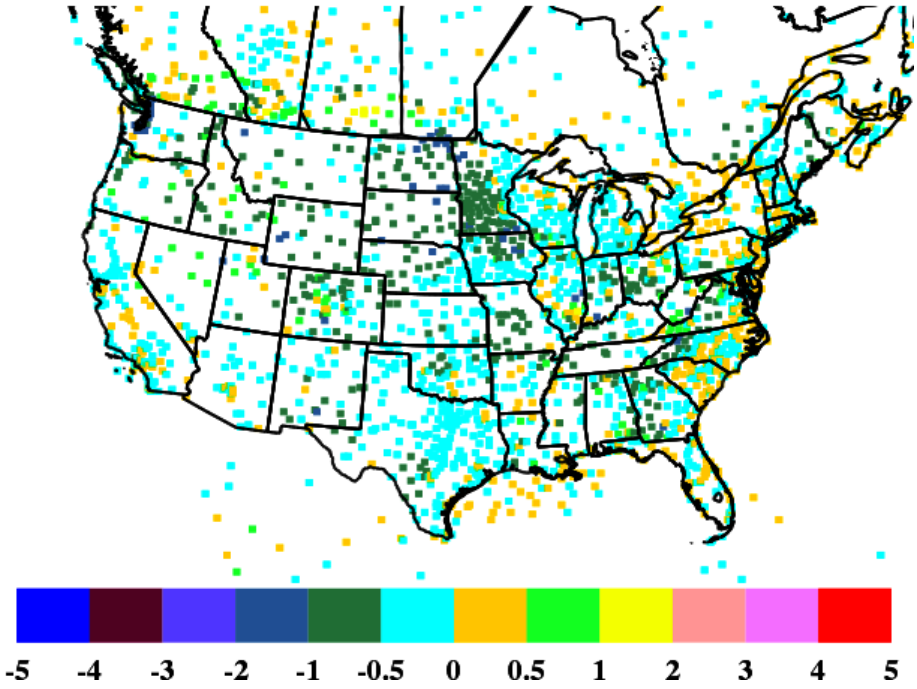

Figure 5-8 *Difference in the magnitudes of the respective bias values (units of degrees K) VEG minus CNTRL of 2-m temperatures for the period 1-30 September 2013 for daytime conditions. Negative values indicate a decrease in the magnitude of the bias and vice versa.*

5.2.2 CONUS Model Response to Satellite Skin Temperature Nudging (SM-1, SM-2) and Satellite Heat Capacity Adjustment (HC-1)

The satellite assimilation for soil moisture nudging and heat capacity adjustments as described in Chapter 4 were performed. The base case for the moisture nudging (SM-1 and SM-2) experiments is the case with satellite insolation, model albedo, and satellite vegetation that is the VEG run. The heat capacity adjustment case (HC-1) was carried out with the SM-2 moisture nudging on. In essence the HC-1 case includes all the satellite assimilation.

Figure 5-9 below shows the model 2-m bias for all the experiments. The moisture nudging (SM-1 - Red) shows a dramatic improvement in the daytime temperature bias. In fact it reverses the sign of the bias so that now daytime temperatures are too cool rather than too warm. In examining this it was felt that the satellite adjustment was too large. Therefore a second experiment was made (SM-2 - Green) in which the nudging factor was decreased (that is a longer time scale from 30 minutes to 60 minutes). This reduces the cool bias to almost zero in the daytime.

The moisture nudging increases the soil moisture leading to cooler daytime temperatures. Figure 5-10 shows that this has increased the bias in humidity. It has also increased the soil moisture

which in turn increases the surface heat capacity. This increases the high nighttime bias in 2-m temperature.

However, Figure 5-9 shows that when the heat capacity adjustment is implemented that this greatly reduces the nighttime positive bias in the model. Thus, the satellite adjustments as proposed in this project are working in that the soil moisture nudging improves the daytime temperatures and the heat capacity adjustment is improving the nighttime temperatures.

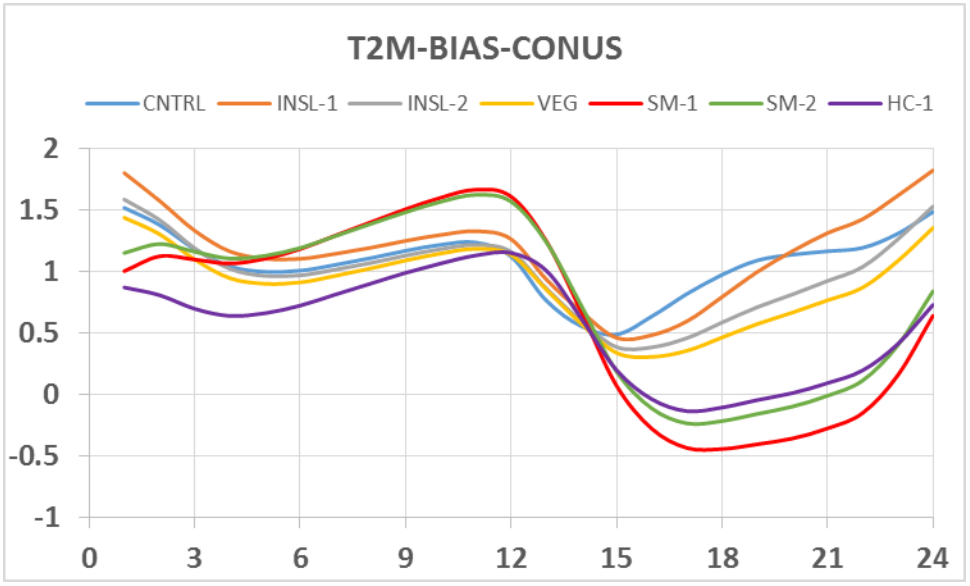

Figure 5-9 *Average hourly bias values (K) for temperature at 2-m for various WRF simulations for the entire 12-km grid for 1-30 September 2013. Values calculated at all surface observing stations.*

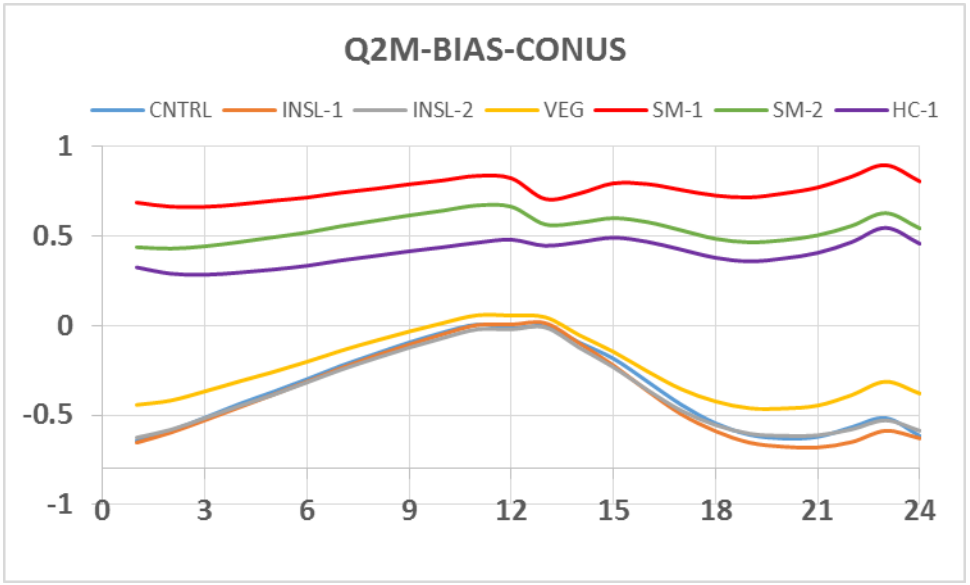

Figure 5-10 *Average hourly bias values (g kg^{-1}) for specific humidity at 2-m for various WRF simulations for the entire 12-km grid for 1-30 September 2013. Values calculated at all surface*

observing stations.

In terms of wind speed it appears that the satellite adjustments have increased the under-prediction of 10-m daytime winds. This may be due to a less unstable boundary layer which is reducing the downward transport of momentum. However, the few tenths of m s^{-1} difference is perhaps not far from the accuracy of the wind measurement. Additional evaluation against wind profiler data is given below.

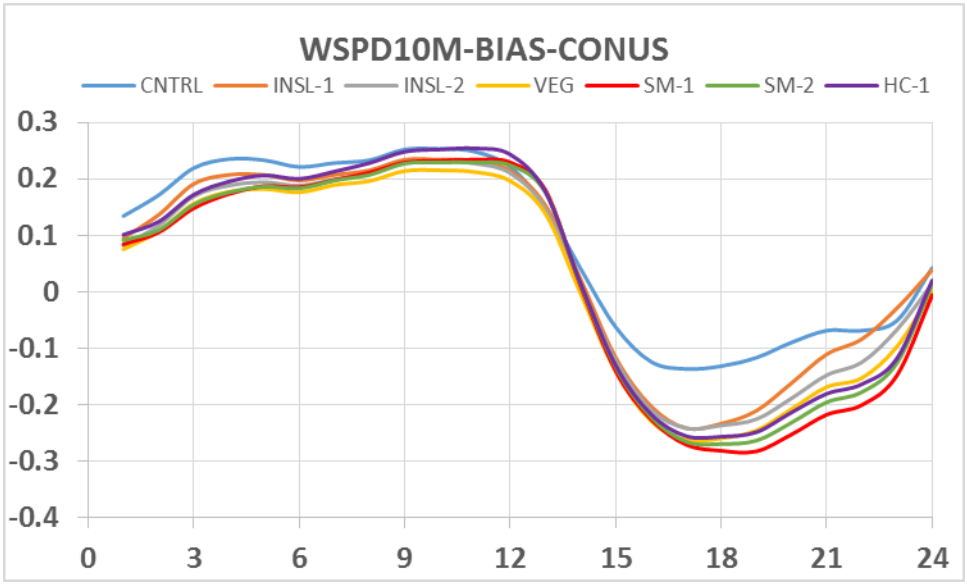

Figure 5-11 *Average hourly bias values (m s^{-1}) for wind speed at 10-m for various WRF simulations for the entire 12-km grid for 1-30 September 2013. Values calculated at all surface observing stations.*

In addition to the bias statistic the root-mean-square error statistics were evaluated. Figure 5-12 shows the RMSE for 2-m temperature. It shows that the RMSE has been reduced substantially in the daytime by nearly a full degree. However, a nighttime RMSE shows a slight deterioration.

Figure 5-13 shows the RMSE for 2-m specific humidity. It shows that the RMSE in humidity has been reduced over the domain. Thus, while the bias was slightly increased the spatial patterns of humidity have improved.

Figure 5-14 shows the RMSE in 10-m wind speed. It shows that the daytime RMSE has been improved although the improvement is small.

Table 5-2 provides numerical values of the statistics for NWS sites. It shows that for 2-m temperature that the bias is reduced by about 0.8 K and RMSE by about 0.5 K. For wind speed the bias is degraded by about 0.1 m s^{-1} and RMSE is only marginally improved.

In addition to the domain statistics described above, spatial plots of model improvement due to the satellite assimilation were also developed. Figure 5-15 shows that improvement is especially strong over the corn-belt in Iowa and Minnesota which is due both to the vegetative assimilation and skin temperature nudging. Texas also shows substantial improvement which will be

discussed further below. Figure 5-16 shows the sign of the improvement. As can be seen most areas show improvement especially in the middle of the country. Deterioration is scattered but mostly in the East and Central Valley of California.

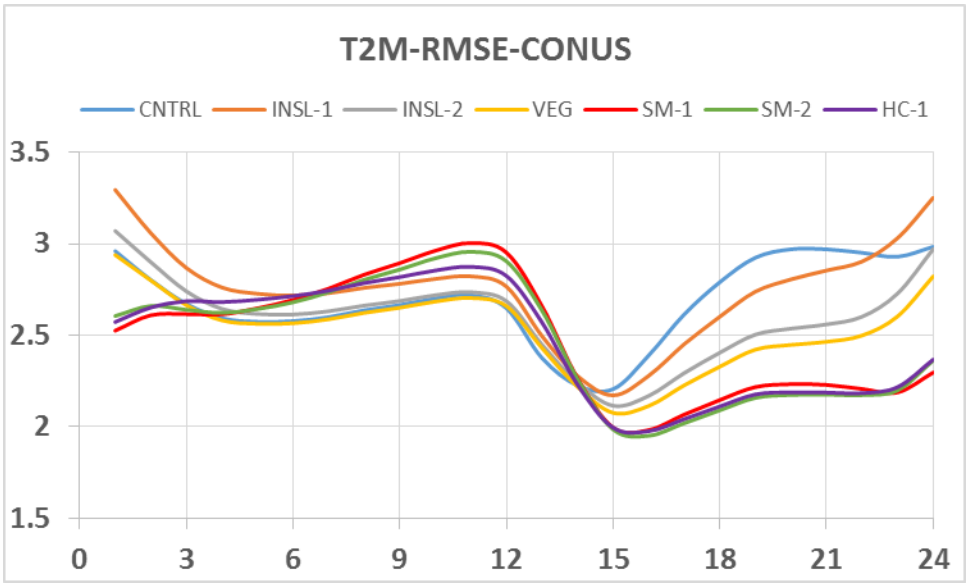

Figure 5-12 *Hourly root mean square error (RMSE) values (K) for temperature at 2-m for various WRF simulations for the entire 12-km grid for 1-30 September 2013. Values calculated at all surface observing stations.*

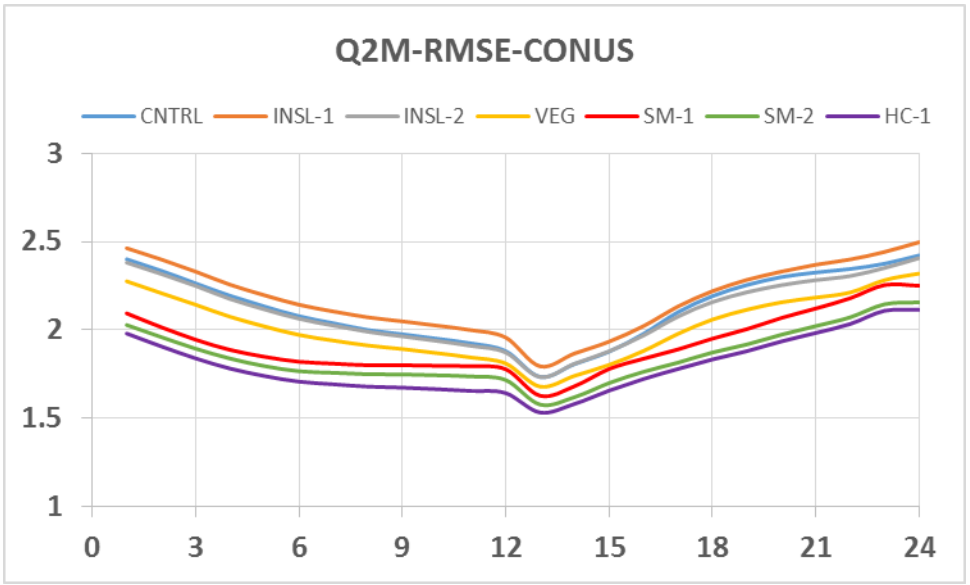

Figure 5-13 *Hourly root mean square error (RMSE) values (g kg^{-1}) for specific humidity at 2-m for various WRF simulations for the entire 12-km grid for 1-30 September 2013. Values calculated at all surface observing stations.*

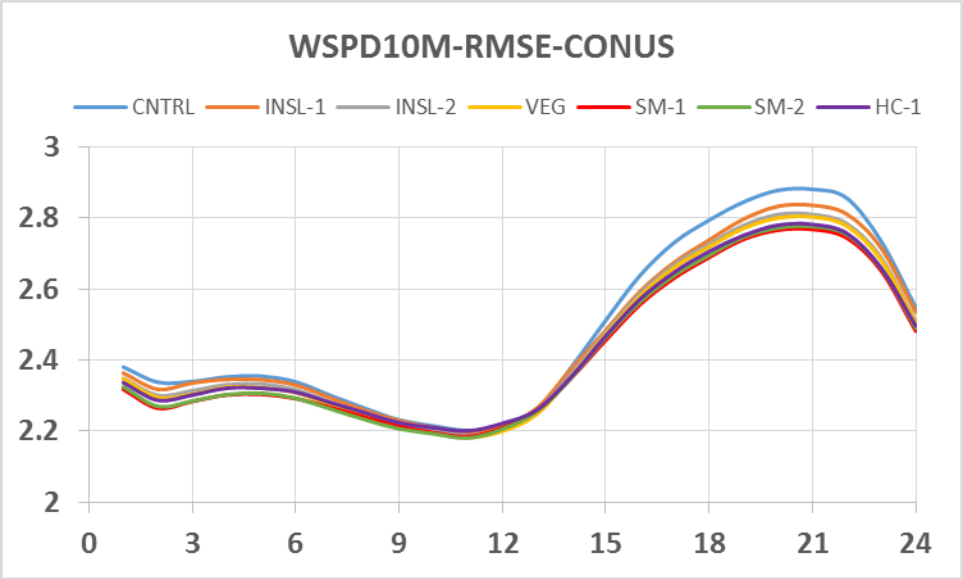

Figure 5-14 Hourly root mean square error (RMSE) values (m s^{-1}) for wind speed at 10-m for various WRF simulations for the entire 12-km grid *for 1-30 September 2013*. Values calculated at all surface observing stations.

RUN	T2M-B	Q2M-B	WSPD10M-B	T2M-R	Q2M-R	WSPD10M-R
CNTRL	0.938	-0.426	-0.055	2.697	2.152	2.680
INSL-1	0.964	-0.461	-0.107	2.641	2.198	2.645
INSL-2	0.750	-0.435	-0.122	2.452	2.126	2.629
VEG	0.644	-0.306	-0.140	2.378	2.039	2.622
SM-1	0.038	0.752	-0.152	2.220	1.975	2.600
SM-2	0.216	0.526	-0.140	2.191	1.891	2.606
HC-1	0.253	0.421	-0.132	2.194	1.853	2.611

Table 5-1 *Bias (-B) and Root Mean Square Error (-R) for standard observations sites for temperature at 2-m (T2M), specific humidity at 2-m (Q2M), and wind speed at 10-m (WSPD10M) for various WRF simulations for the entire 12-km grid for daytime conditions for 1-30 September 2013.*

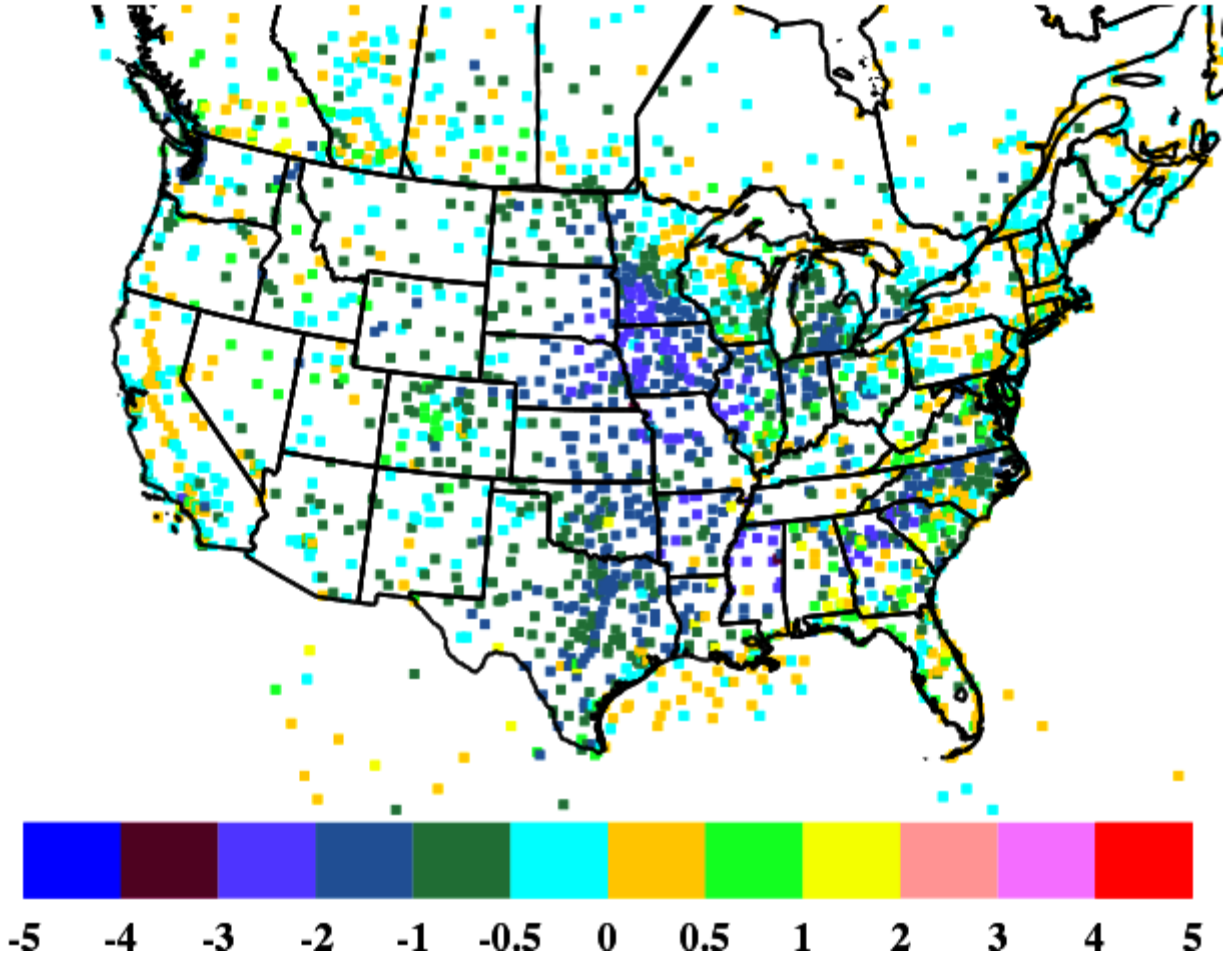

Figure 5-15 *Difference in the magnitudes of the respective bias values (units of degrees K) HC minus CNTRL of 2-m temperatures for the period 1-30 September 2013 for daytime conditions. Negative values indicate a decrease in the magnitude of the bias and vice versa.*

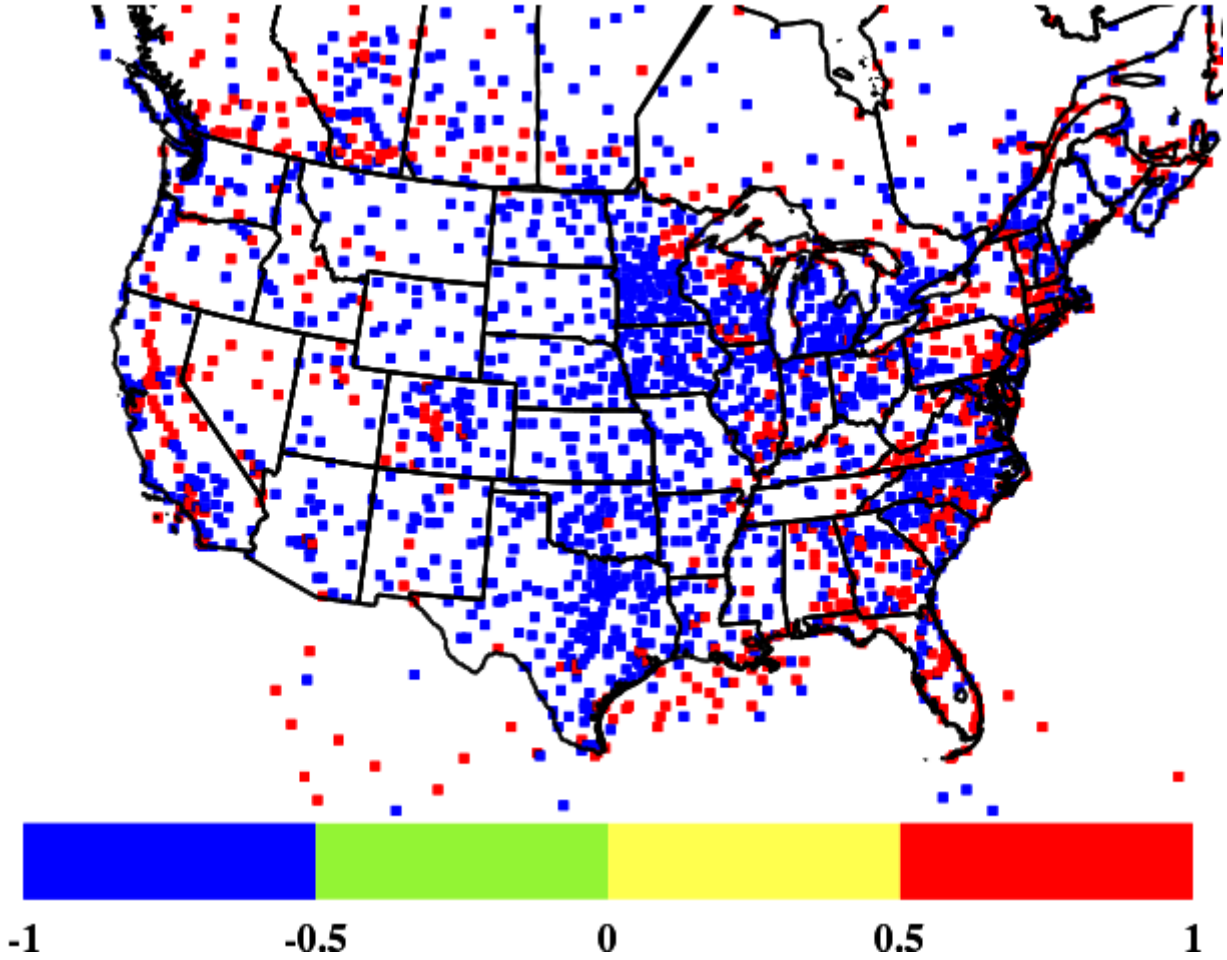

Figure 5-16 *The sign of the difference in the magnitude of bias values (HC – CONTRL) as shown in* Figure 5-15. *Blue (red) grid locations indicate a decrease (increase) in the magnitude of the bias.*

5.2.3 Texas Model Response to Satellite Skin Temperature Nudging (SM-1, SM-2) and Satellite Heat Capacity Adjustment (HC-1)

This section parallels section 5.2.2 providing the impacts of the assimilation but focuses on the Texas domain. The satellite assimilation for soil moisture nudging was performed and heat capacity adjustments as described in Chapter 4. The base case for the moisture nudging (SM-1 and SM-2) experiments is the case with satellite insolation model albedo and satellite vegetation that is the VEG run. The heat capacity adjustment case (HC-1) included the SM-2 moisture nudging. In essence the HC-1 case includes all the satellite assimilation.

Figure 5-17 below shows the model 2-m bias for all the experiments for the Texas. The moisture nudging (SM-1 - Red) shows a dramatic improvement in the daytime temperature bias. In fact it reverses the sign of the bias so that now daytime temperatures are slightly cool rather too warm. In examining this it was felt that the satellite adjustment was too large. Thus, a second experiment was made (SM-2 - Green) in which the nudging factor was decreased (that is a longer

time scale from 30 minutes to 60 minutes). This reduces bias substantially compared to the control run but maintains a warm bias especially in the nighttime.

The moisture nudging increases the soil moisture leading to cooler daytime temperatures. Figure 5-18 shows that this has moistened the surface over the control and has reduced the bias in humidity. It has also increased the soil moisture which in turn increases the surface heat capacity. This increases the high nighttime bias in 2-m temperature (see Figure 5-17).

However, Figure 5-17 shows that when the heat capacity adjustment is used that this greatly reduces the nighttime positive bias in the model. Thus, the satellite adjustments as proposed in this project are working in that the soil moisture nudging improves the daytime temperatures and the heat capacity adjustment is improving the nighttime temperatures.

In terms of wind speed it appears that the satellite adjustments SM-2 and HC-1 have little changed 10-m daytime winds. But nighttime winds have improved. Additional evaluation against wind profiler data is given below.

In addition to the bias statistic the root-mean-square error statistics were evaluated. Figure 5-20 shows the RMSE for 2-m temperature. It shows that the RMSE has been reduced substantially in the daytime by nearly a full degree. However, a nighttime RMSE shows little change.

Figure 5-21 shows the RMSE in 2-m specific humidity. It shows that the RMSE in humidity has been reduced over the domain for both day and night. Thus, while the bias was slightly increased the spatial patterns of humidity have improved.

Figure 5-22 shows the RMSE in 10-m wind speed. It shows that the daytime RMSE unchanged and a slight nighttime increase in RMSE.

Table 5-3 provides numerical values of the statistics for the satellite statistics compared to NWS sites. It shows that for 2-m temperature that the bias is reduced by about a 1 K and RMSE by about 0.7 K. For wind speed the bias is slightly improved by about .05 m s^{-1} and RMSE is only marginally improved.

In addition to the domain statistics described above, spatial plots of model improvement due to the satellite assimilation were also developed. Figure 5-23 shows that improvement is especially strong over central Texas. There are a few scattered areas of deterioration with one cluster in the Houston area. Figure 5-24 shows the sign of the improvement. Figure 5-25 shows the difference in RMSE in 2-m temperature. Over most all the domain the RMSE is improved.

Wind speed performance was also evaluated spatially. Because the magnitudes of the changes are small only the sign of the differences are shown in Figure 5-26.

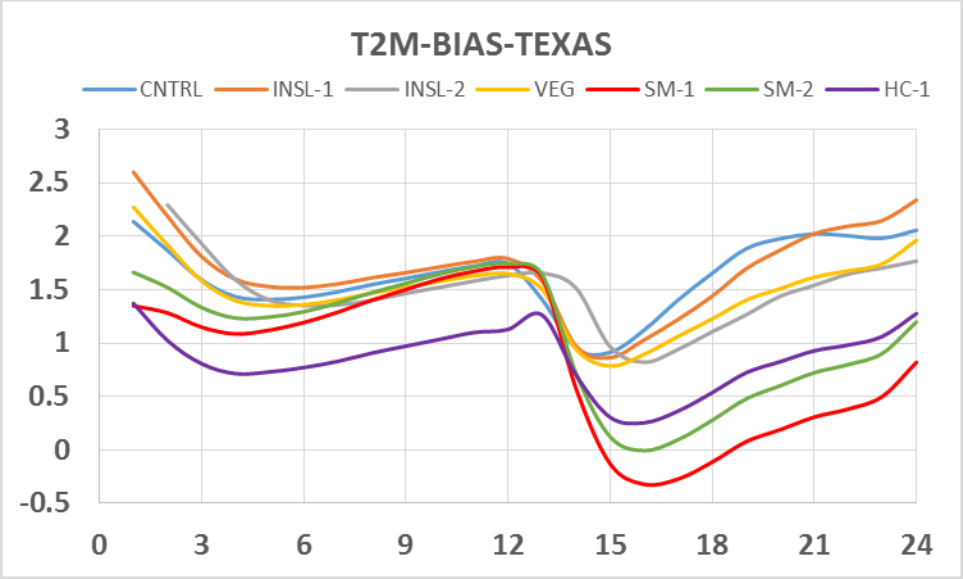

Figure 5-17 *Average hourly bias values (K) for temperature at 2-m for various WRF simulations for the state of Texas for 1-30 September 2013. Values calculated at all surface observing stations.*

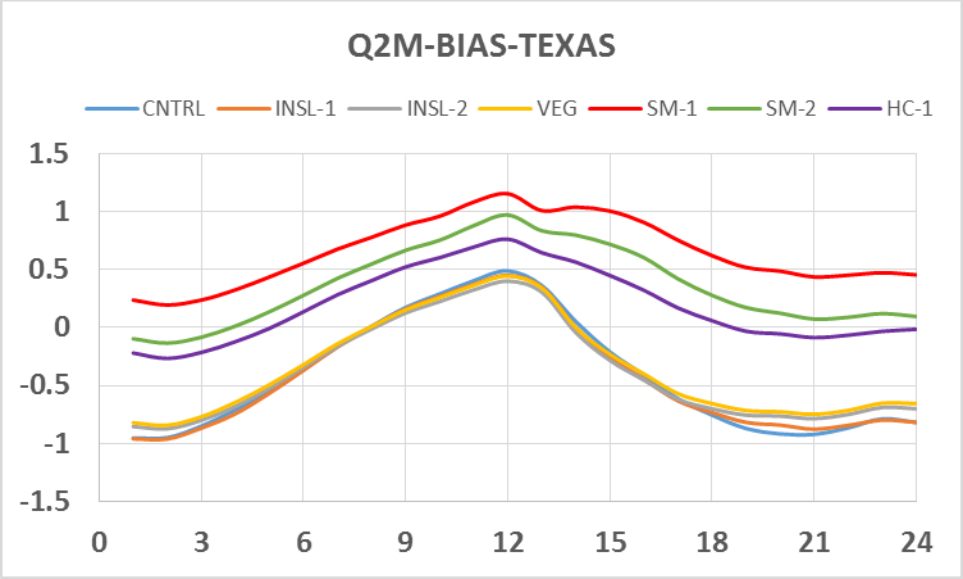

Figure 5-18 *Average hourly bias values (g kg^{-1}) for specific humidity at 2-m for various WRF simulations for the state of Texas for 1-30 September 2013. Values calculated at all surface observing stations.*

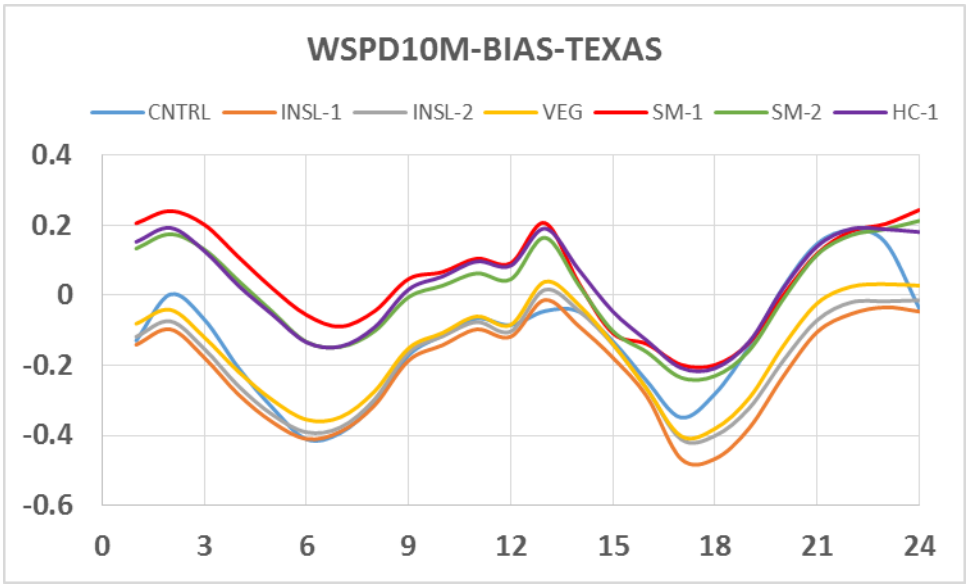

Figure 5-19 *Average hourly bias values (m s^{-1}) for wind speed at 10-m for various WRF simulations for the state of Texas for 1-30 September 2013. Values calculated at all surface observing stations.*

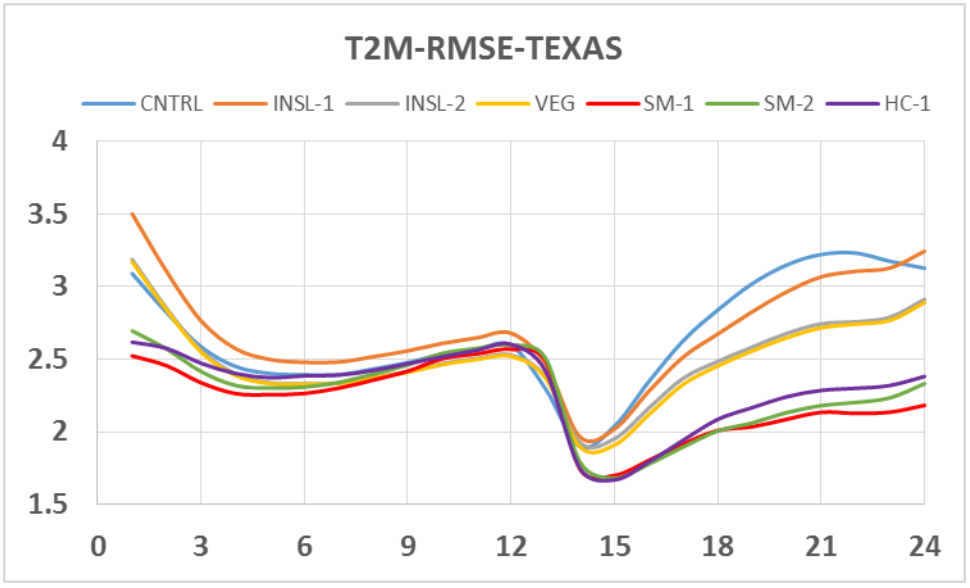

Figure 5-20 *Hourly root mean square error (RMSE) values (K) for temperature at 2-m for various WRF simulations for the state of Texas for 1-30 September 2013. Values calculated at all surface observing stations.*

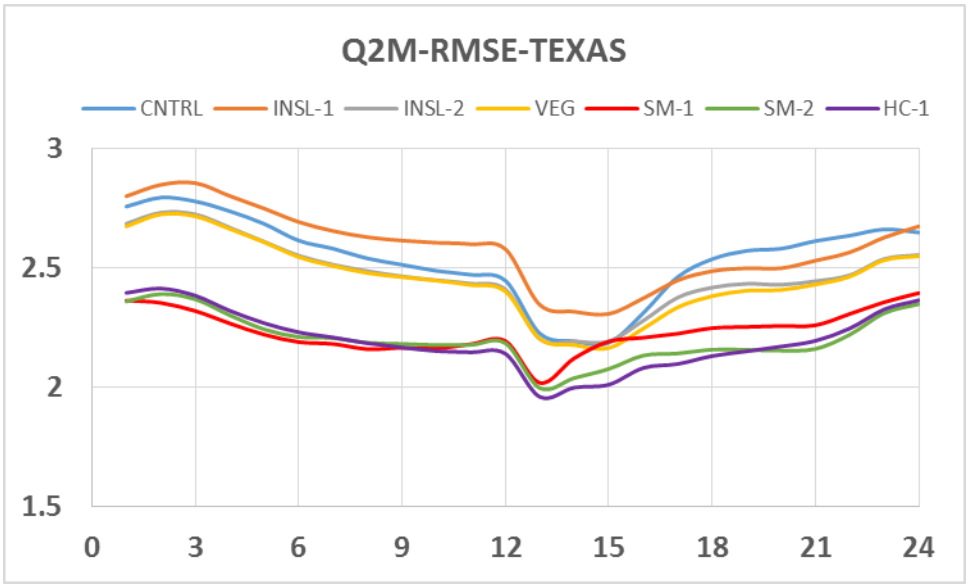

Figure 5-21 *Hourly root mean square error (RMSE) values (g kg^{-1}) for specific humidity at 2-m for various WRF simulations for the state of Texas for 1-30 September 2013. Values calculated at all surface observing stations.*

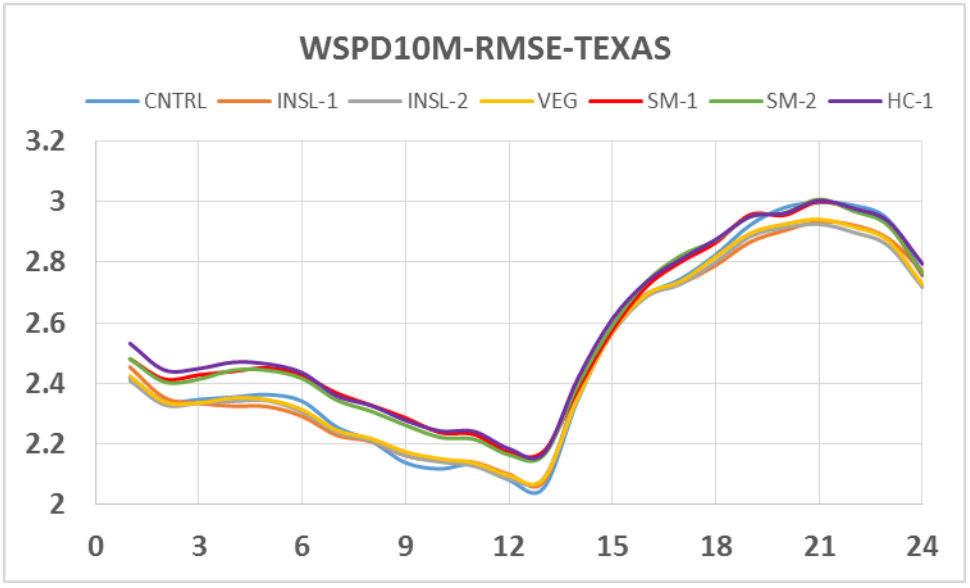

Figure 5-22 *Hourly root mean square error (RMSE) values (m s^{-1}) for wind speed at 10-m for various WRF simulations for the state of Texas for 1-30 September 2013. Values calculated at all surface observing stations.*

RUN	T2M-B	Q2M-B	WSPD10M-B	T2M-R	Q2M-R	WSPD10M-R
CNTRL	1.830	-0.707	-0.131	2.876	2.557	2.673
INSL-1	1.823	-0.710	-0.251	2.808	2.556	2.651
INSL-2	1.589	-0.659	-0.228	2.568	2.456	2.630
VEG	1.554	-0.613	-0.204	2.540	2.436	2.638
SM-1	0.397	0.673	-0.089	2.073	2.307	2.636
SM-2	0.755	0.319	-0.104	2.116	2.221	2.653
HC-1	0.909	0.098	-0.078	2.167	2.207	2.665

Table 5-2 *Bias (-B) and Root Mean Square Error (-R) for standard observations sites for temperature at 2-m (T2M), specific humidity at 2-m (Q2M), and wind speed at 10-m (WSPD10M) for various WRF simulations for Texas for daytime conditions for 1-30 September 2013.*

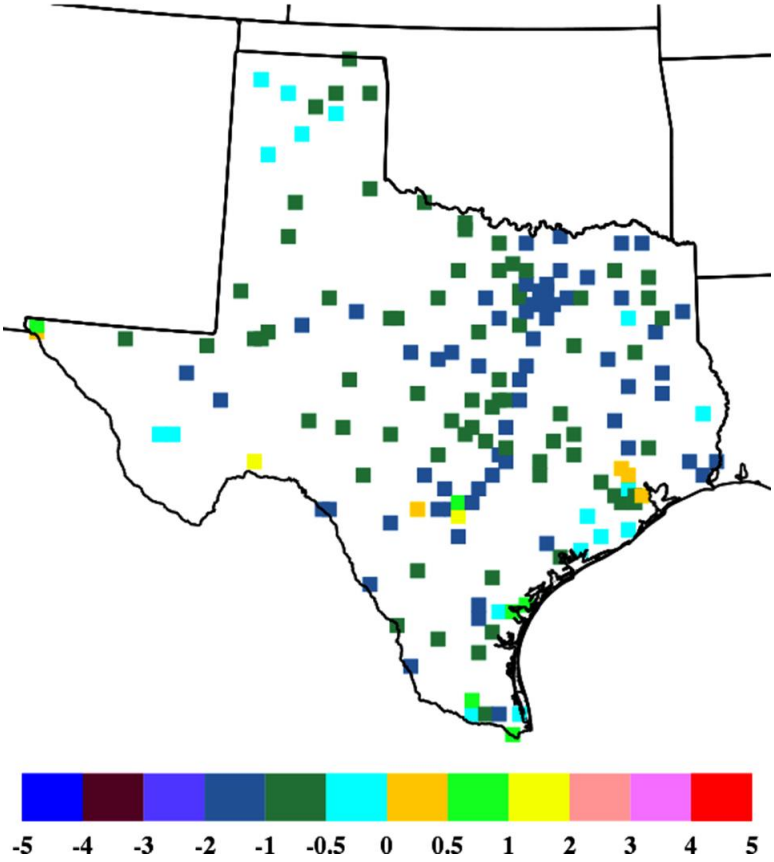

Figure 5-23 *Difference in the magnitudes of the respective bias values (units of degrees K) HC minus CNTRL of 2-m temperatures for the period 1-30 September 2013 for daytime conditions for the state of Texas. Negative values indicate a decrease in the magnitude of the bias and vice versa.*

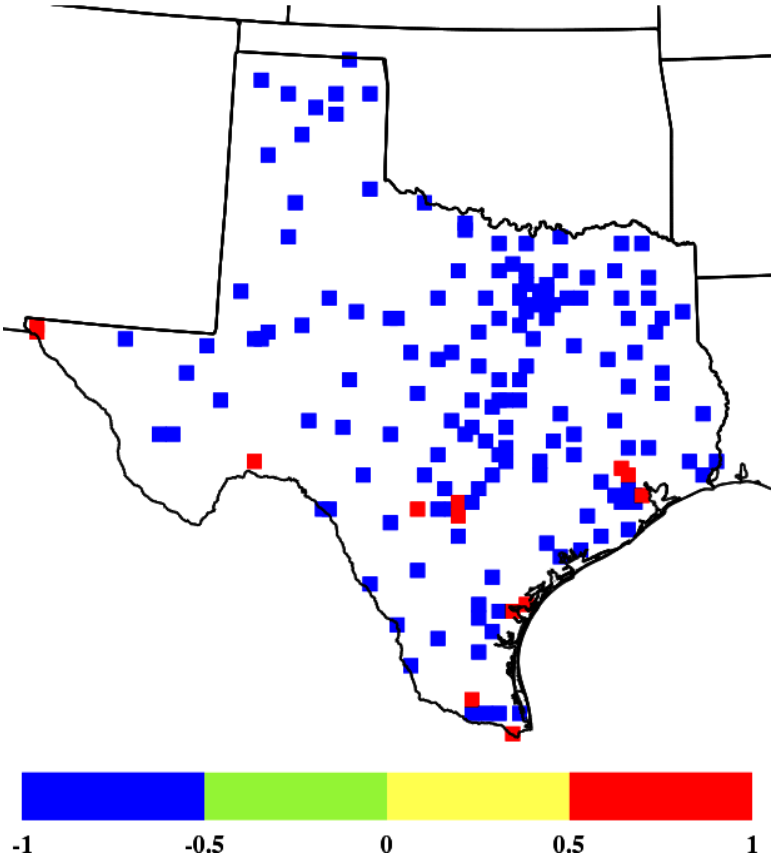

Figure 5-24 *The sign of the difference in the magnitude of bias values (HC – CONTRL) as shown in Figure* 5-23 *for the state of Texas. Blue (red) grid locations indicate a decrease (increase) in the magnitude of the bias.*

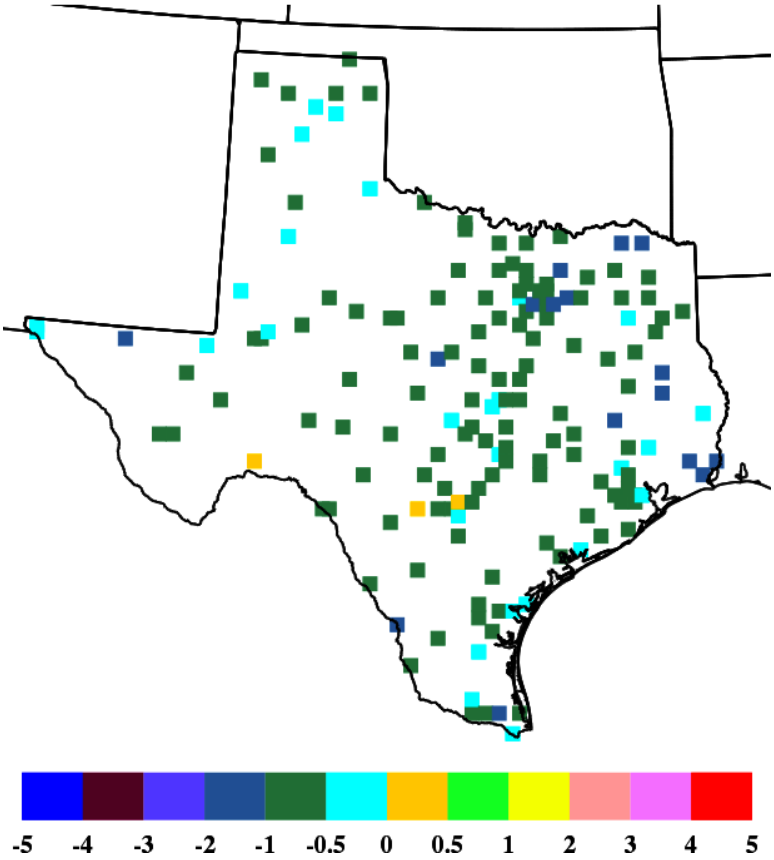

Figure 5-25 *Difference in the respective RMSE values (units of degrees K) HC minus CNTRL of 2-m temperatures for the period 1-30 September 2013 for daytime conditions for the state of Texas. Negative values indicate a decrease in the RMSE and vice versa*.

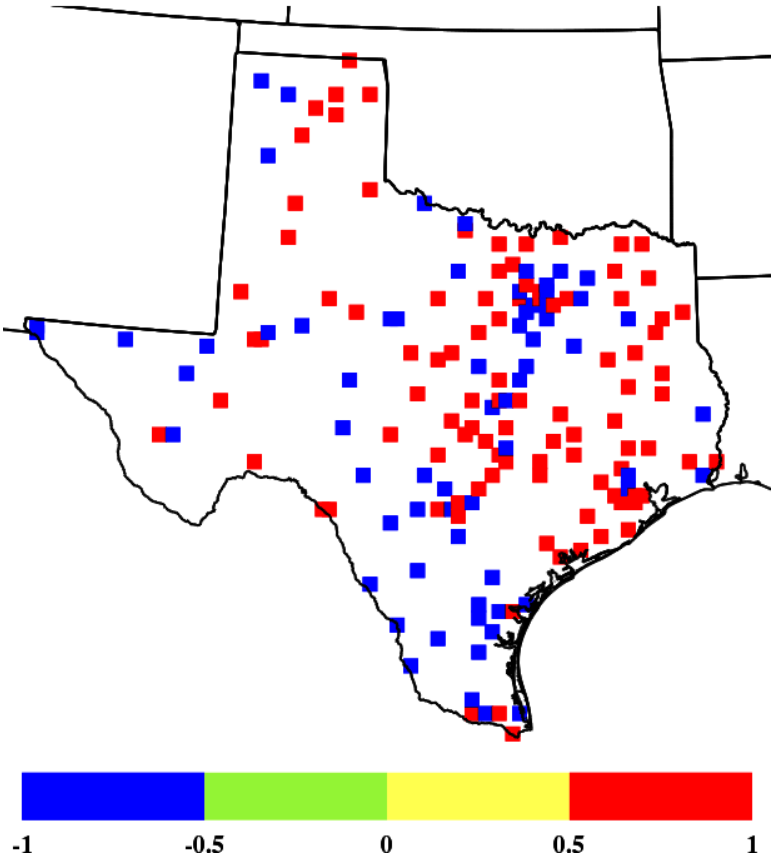

Figure 5-26 *The sign of the difference in the magnitude of the 10-m wind speed bias values (HC – CONTRL) for the state of Texas for daytime conditions. Blue (red) grid locations indicate a decrease (increase) in the magnitude of the bias*.

5.3 Model Evaluation Relative to Profiler Data

As part of the evaluation comparisons were made against profilers deployed for the Discover AQ period. Figure 5-27 shows the profiler locations and the acronym used for each of the sites.

Figure 5-28 shows a visual comparison between the profiler winds at Beaumont (BM) and the model runs with various levels of satellite assimilation employed for the first week of September 2013. While additional analysis will be required the results appear to show for this site that the initial control simulation generally over-predicted the low level nighttime winds. However, successive levels of assimilation appear to reduce model speeds more in keeping with the profiler data. Figure 5-29 shows a similar plot for College Station. Here there is not as much difference in wind speed between the model and observed winds and also less change with the satellite assimilation. Figure 5-30 is for the LaPorte location but with agreement similar to College Station. Other profiler locations have been analyzed but for brevity here the descriptions concentrate on these three sites.

In an attempt to understand the impact of the assimilation against profiler observations an analysis was made of the mean behavior of wind speed in the model and observations over the

entire 2013 data period (September 1-30, 2017). Figure 5-31 shows the impact of various levels of assimilation for the Beaumont location. The INSL-1 run seems to deteriorate over CNTRL (positive bias for daytime), while the VEG run recovers from INSL-1 run. The SM-1 and HC-1 runs fare better than the other runs, especially for the daytime boundary layer.

Figure 5-32 shows similar sensitivity studies for College Station. While all simulations seem to have negative bias (under-prediction), the SM-1 and HC-1 runs are even more pronounced and worse for the daytime part at this location, but with better performance for the aloft layer at night.

Figure 5-33 shows similar sensitivity studies for Laporte.

While there are cases that seem to improve the agreement with profiler wind speeds there is variation across the different experiments. Figure 5-34 shows a summary of the magnitude of the bias difference for the final assimilation experiment (HC1) described at the beginning of this chapter. It shows the increase or decrease in bias due to the full satellite assimilation. It shows that for BM (top) that bias (under-prediction of nighttime temperatures has decreased as are late afternoon over prediction. There is a slight increase in wind speed bias during early morning. For College Station (middle) wind speeds overnight are greatly improved but the bias in daytime winds is increased

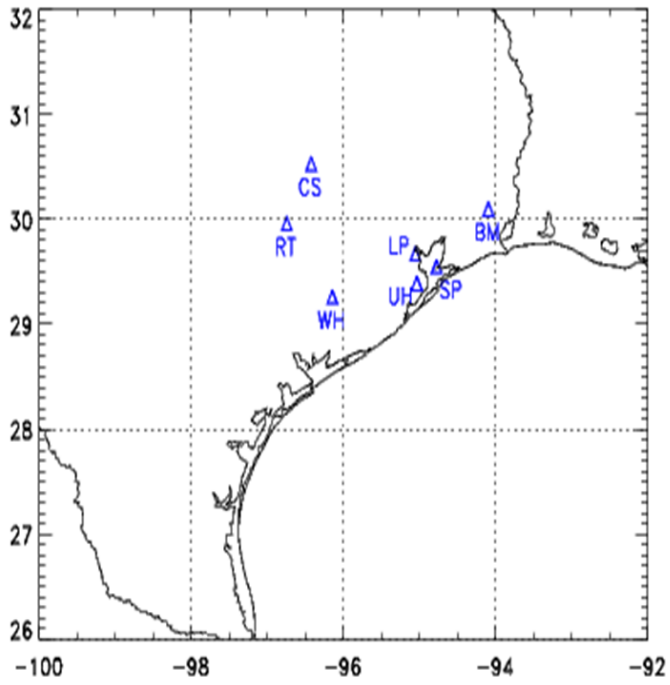

Figure 5-27 *Location of profilers and acronyms.*

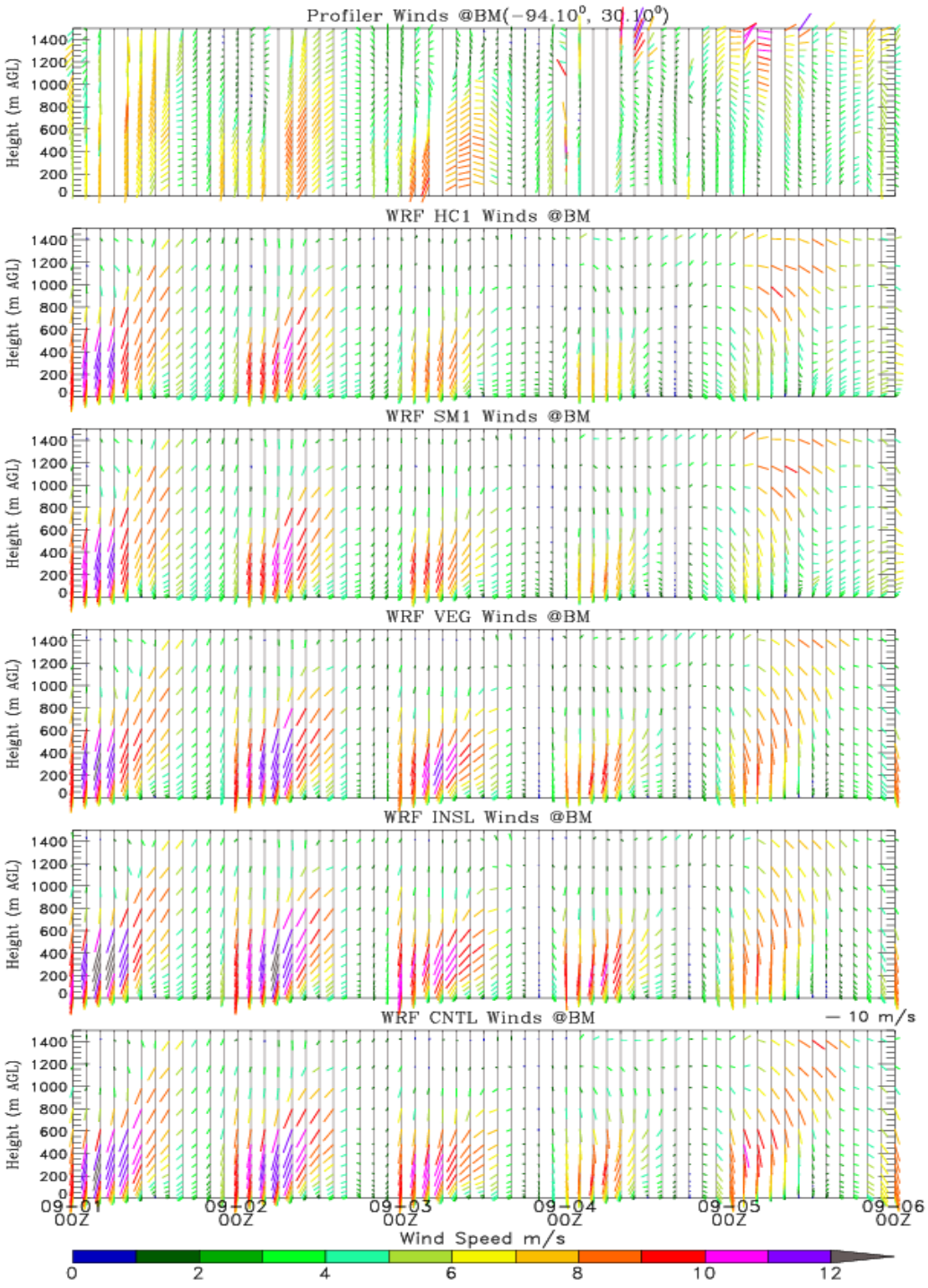

Figure 5-28 *Profiler (top panel) and WRF simulated winds at the Beaumont (BM) location for the 5-day period of Sep. 01-06 starting at 00 UTC. From bottom up, 5 WRF simulations are: control (CNTL) run, GOES Insolation (INSL-1), INSL with MODIS vegetation fraction (VEG); VEG with nudging of soil moisture using skin temperatures (SM-1) and with heat capacity adjustment (HC-1). BM is located east of Houston-Galveston Bay area.*

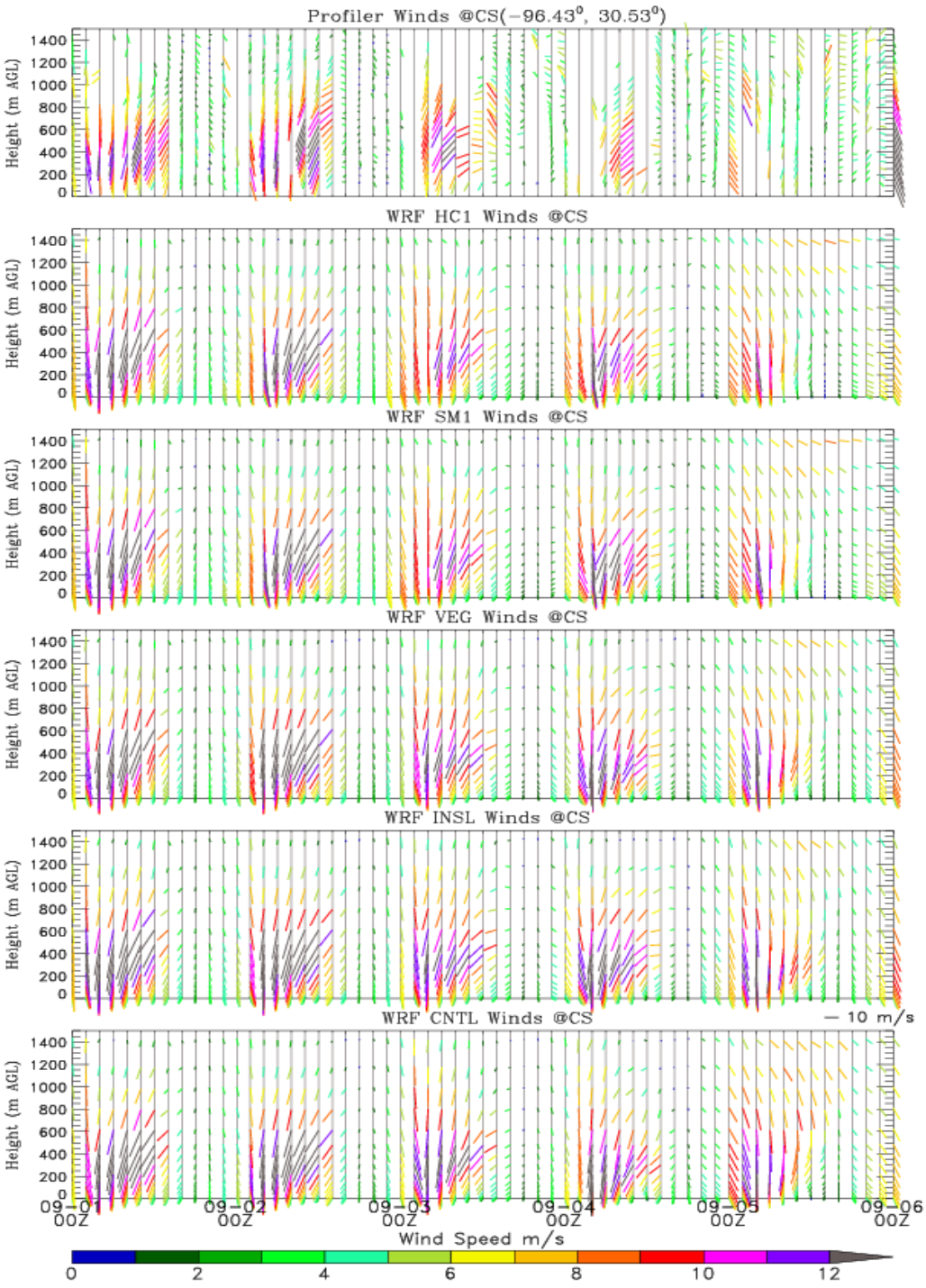

Figure 5-29 *Similar to Figure* 5-28 *but at the College Station (CS) location NW of the Houston*.

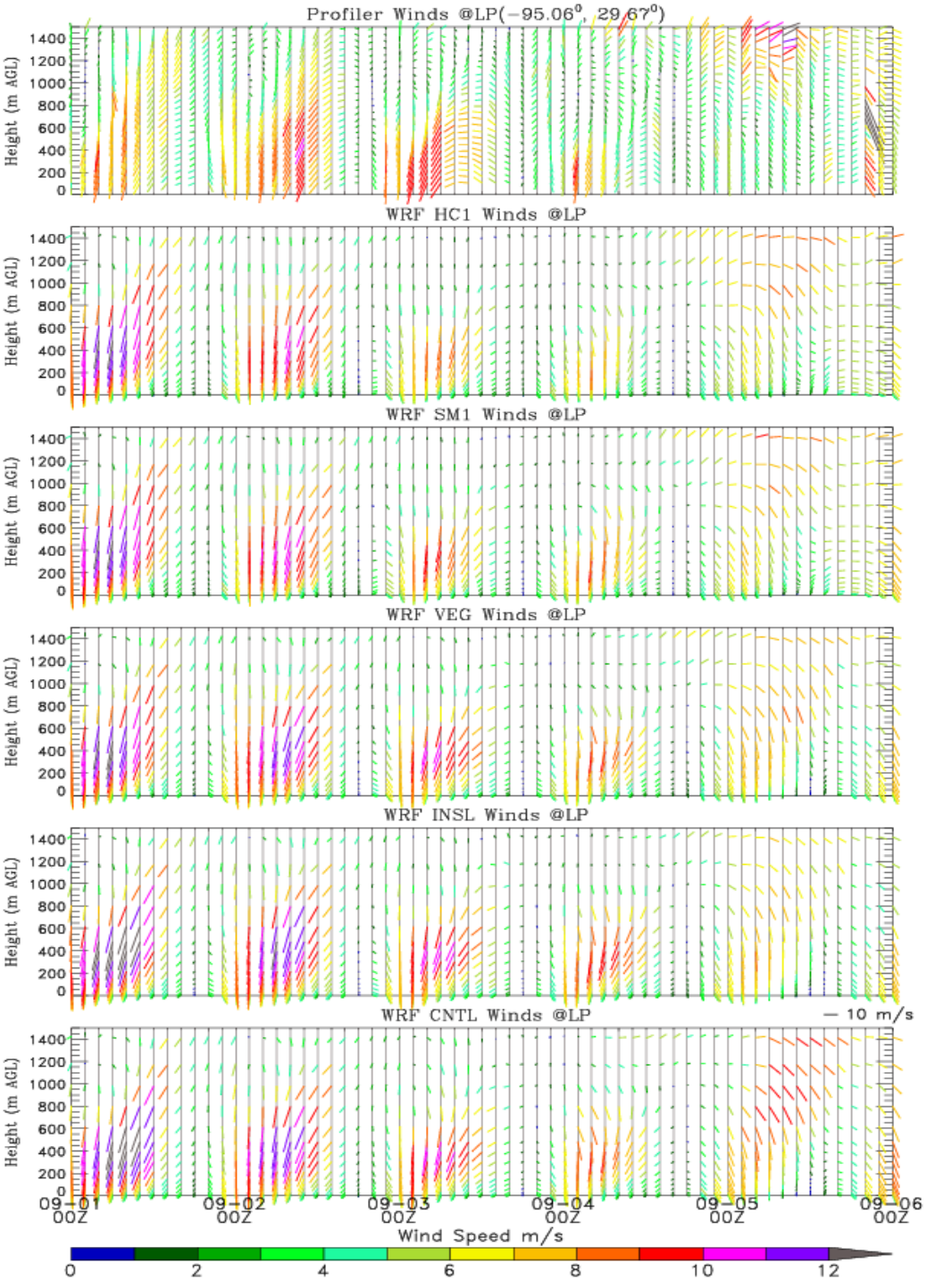

Figure 5-30 *Similar to Figure* 5-28, *but at the La Porte (LP) location in the Houston-Galveston Bay area.*

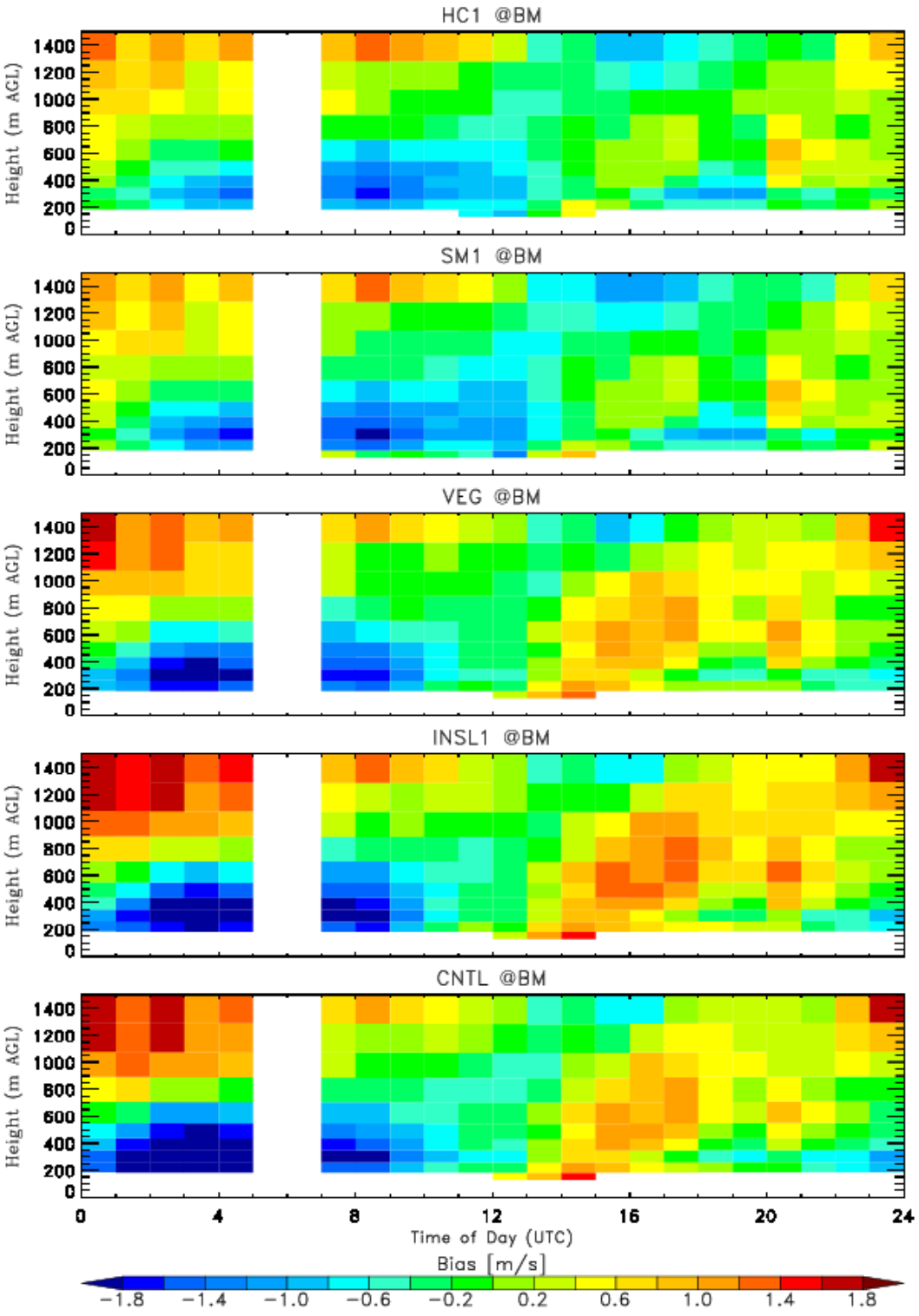

Figure 5-31 *Model wind bias (MBE) against profiler observation at the BM location. From bottom up, 5 WRF simulations are: control (CNTL) run, CNTL with GOES Insolation (INSL-1), INSL with MODIS vegetation fraction (VEG); VEG with nudging of soil moisture (SM-1); and SM1 with heat capacity adjustment (HC-1).*

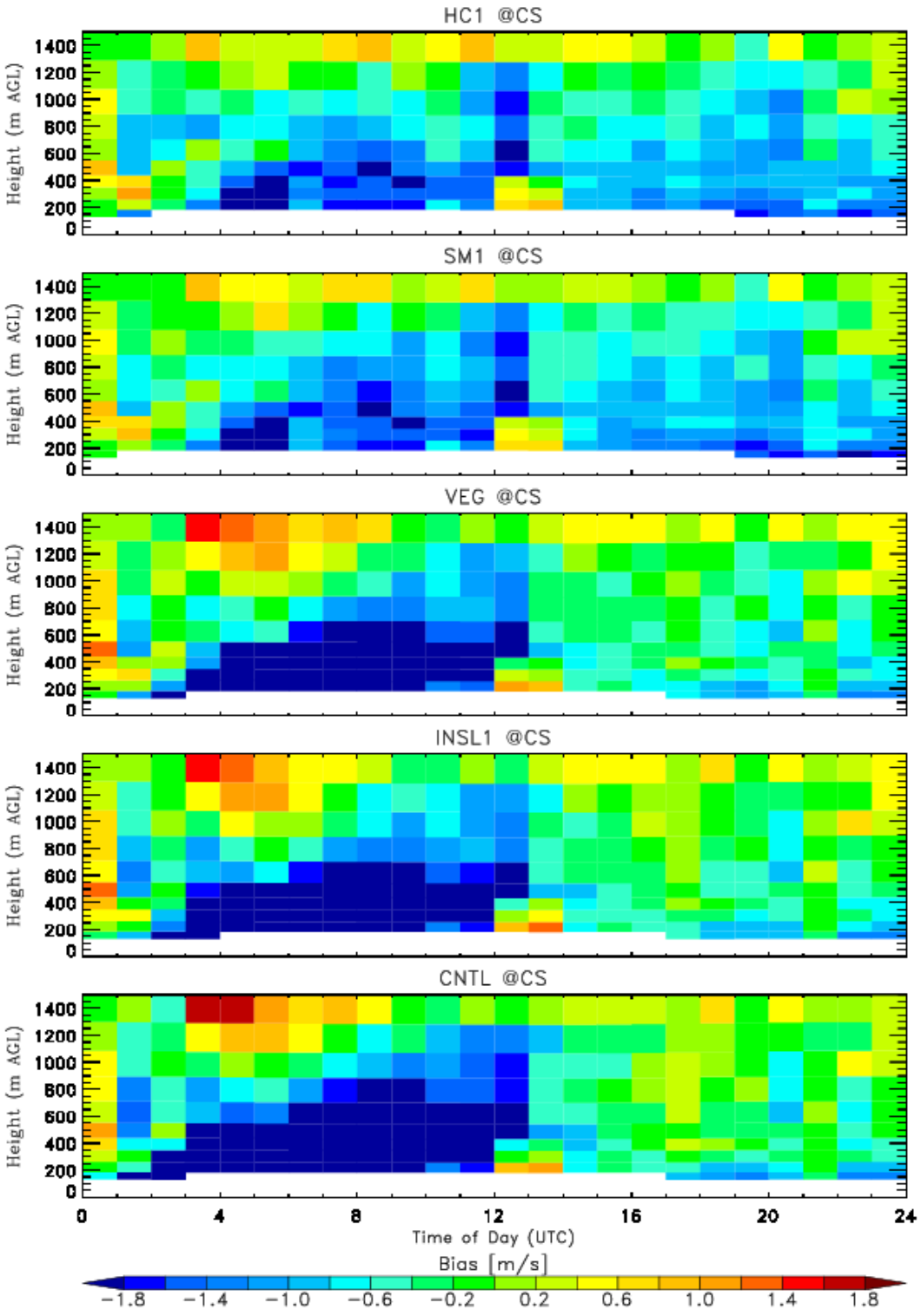

Figure 5-32 *Similar to Figure 5-31 but for MBE against profiler observation at CS.*

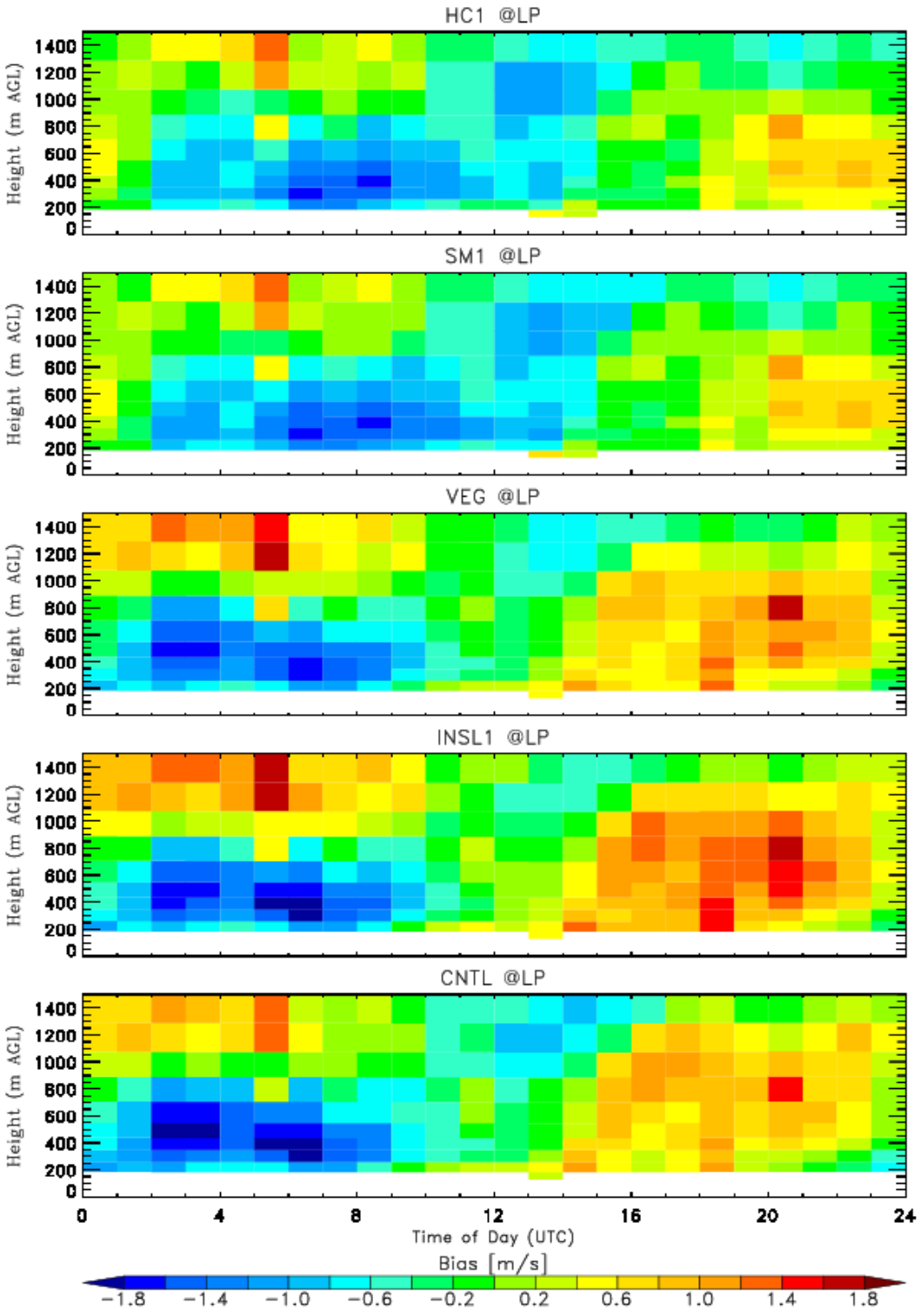

Figure 5-33 *Similar to Figure 5-31 but for MBE against profiler observation at LP.*

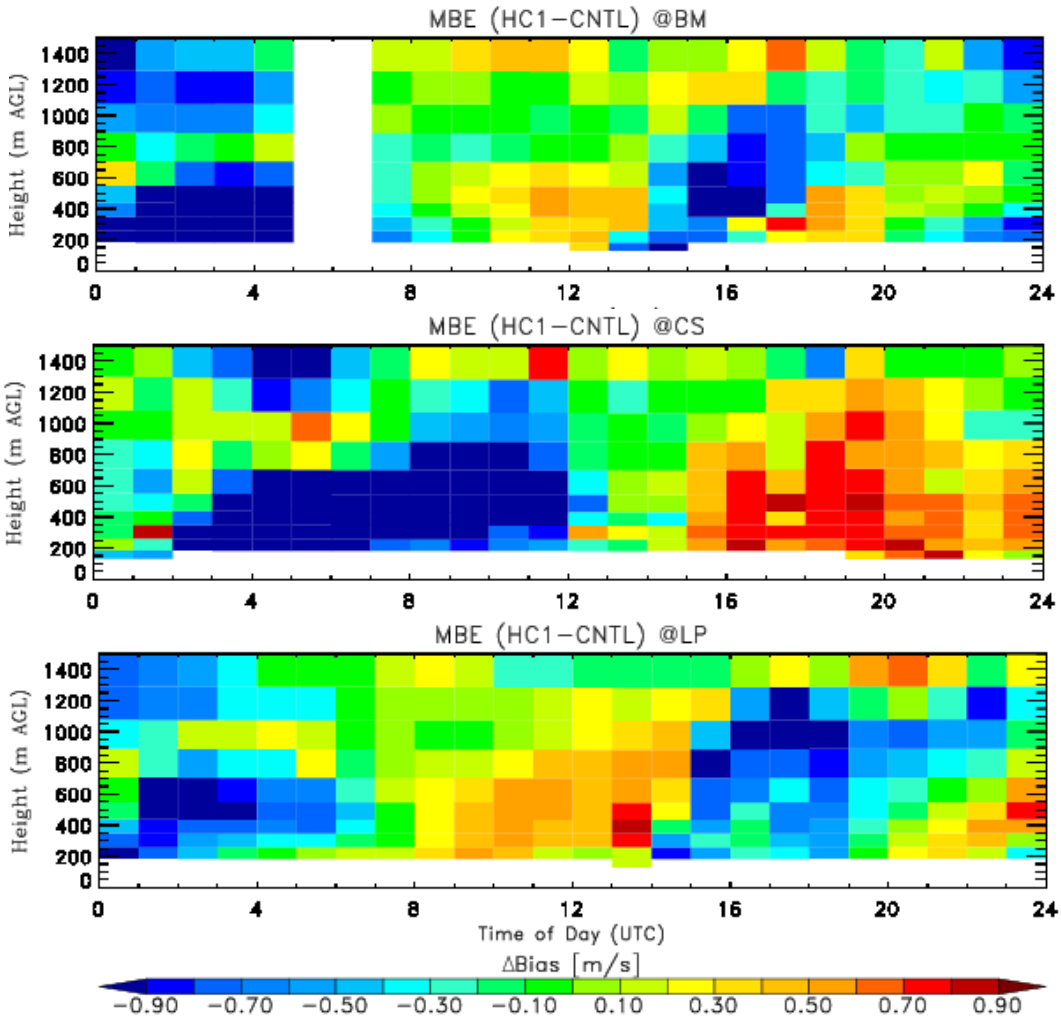

Figure 5-34 *Difference in Bias magnitude between the HC1 and CNTL runs at selected locations (top: BM; middle: CS; bottom: LP).*

5.4 Model Evaluation With Respect to Satellite Skin Temperature

As stated in the introduction satellite skin temperatures provide a much higher resolution than surface data sets. Thus, it can provide coverage across different land use conditions. The following provides model skin temperature evaluation against these observed skin temperatures.

5.4.1 Bias and RMSE Summary Statistics

Figure 5-35 shows the model 2-m temperature bias when insolation and vegetative fraction are added. The bias increases slightly in the daytime. This is similar to the NWS results except the INSOL-2 and VEG runs still have higher bias values than the CONTRL run. Figure 5-36 shows the RMSE. This statistic is mostly unchanged.

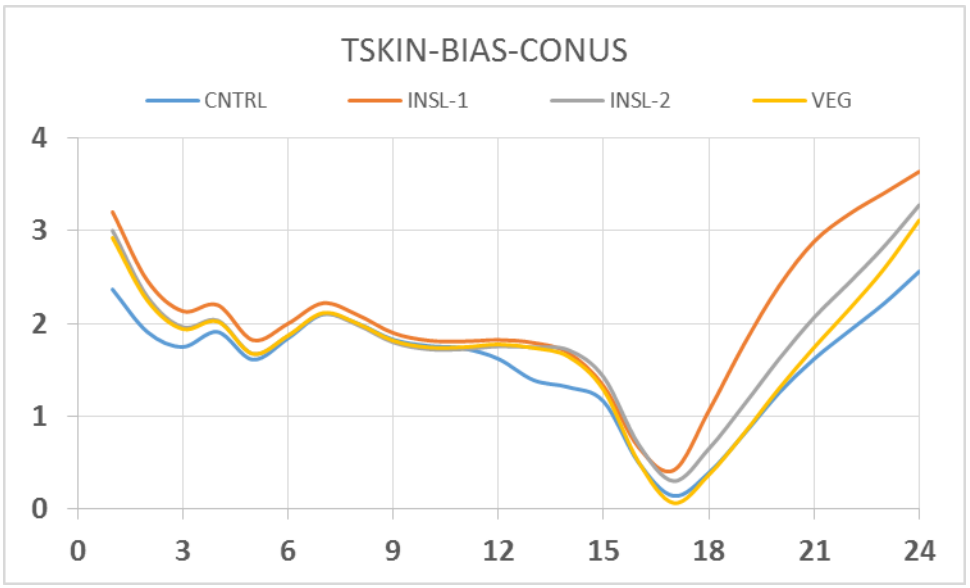

Figure 5-35 *Average hourly bias values (K) for skin temperature for various WRF simulations for the entire 12-km grid for 1-30 September 2013.*

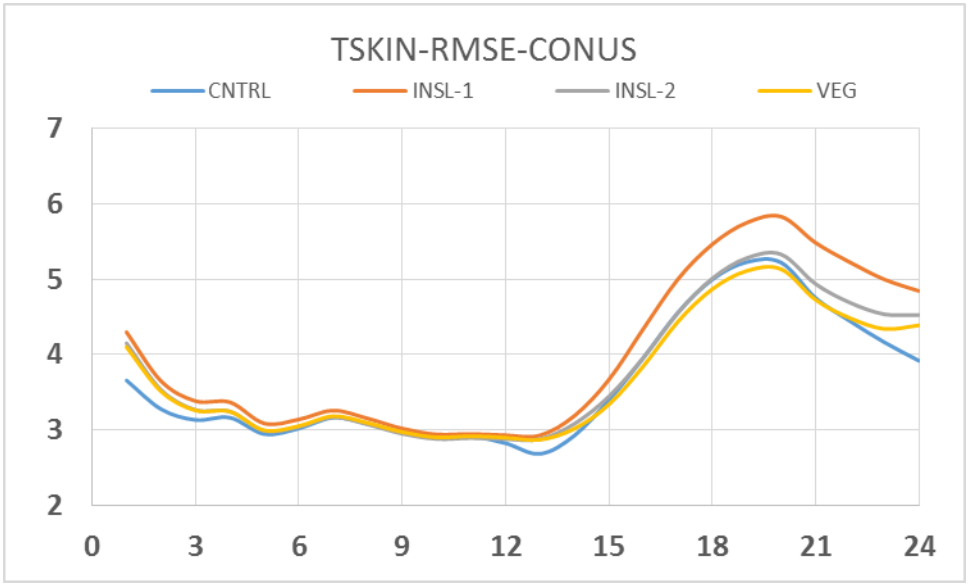

Figure 5-36 *Hourly root mean square error (RMSE) values (K) for skin temperature for various WRF simulations for the entire 12-km grid for 1-30 September 2013.*

Figure 5-37 shows the skin temperature bias results after all the satellite products are assimilated. This is similar to the NWS statistics except the assimilation impacts are larger. The moisture nudging (SM-1 Red) and (SM-2 Green– smaller nudging) show much improvement in the daytime. However, as with NWS the nighttime performance is deteriorated. The assimilation mostly decreases the daytime warm bias especially in the East (see below spatial discussions)

and moistens the soil. This causes an increase in heat capacity causing nighttime temperatures to become too warm.

When the heat capacity adjustment is added (HC-1) it changes the daytime temperatures little but does decrease the nighttime temperature. Thus, the HC-1 improves both daytime and nighttime performance.

The RMSE statistics for skin temperature for the whole domain are provided in Figure 5-38. It shows a reduction in RMSE in the daytime and early evening but increases RMSE in most of the nighttime period. This is discussed further in the spatial analysis.

Table 5-3 shows the numerical values over all times of bias and RMSE for the CONUS grid.

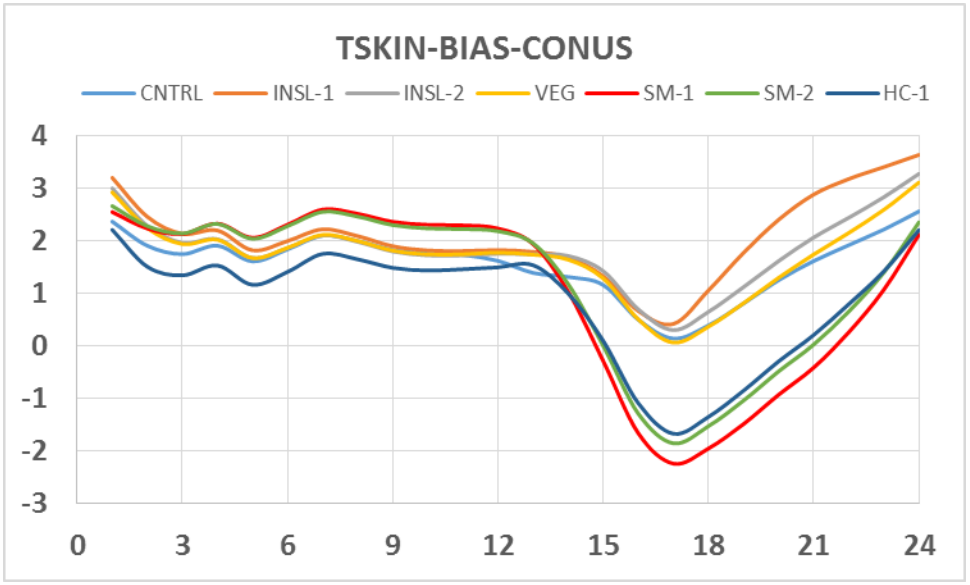

Figure 5-37 *Average hourly bias values (K) for skin temperature for various WRF simulations for the entire 12-km grid for 1-30 September 2013. Values calculated at all 12-km grid points. Values calculated at all 12-km grid points.*

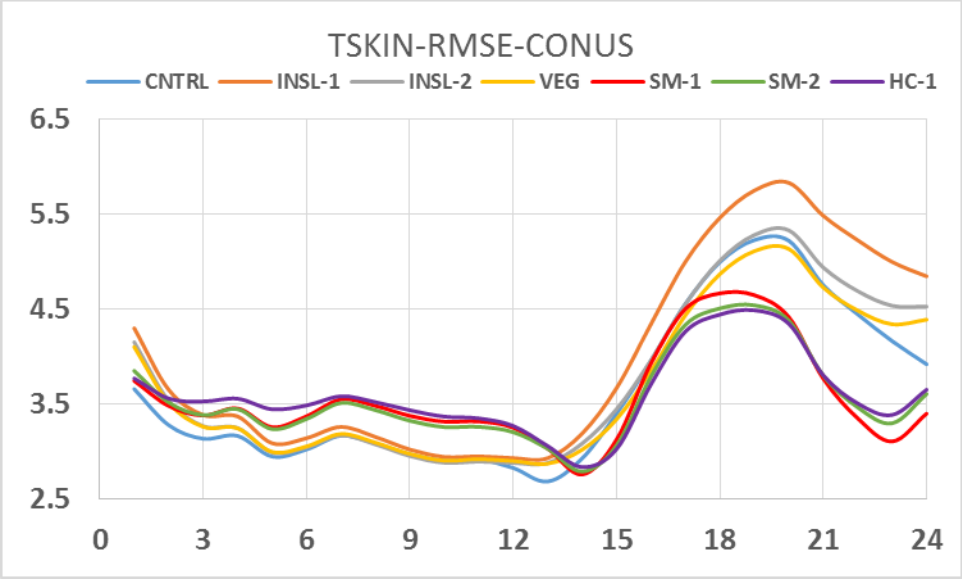

Figure 5-38 *Hourly root mean square error (RMSE) values (K) for skin temperature for various WRF simulations for the entire 12-km grid. Values calculated at all 12-km grid points.*

RUN	TSKIN-B	TSKIN-R
CNTRL	1.239	4.231
INSL-1	1.931	4.755
INSL-2	1.621	4.384
VEG	1.418	4.247
SM-1	-0.202	3.807
SM-2	0.117	3.779
HC-1	0.204	3.758

Table 5-3 *Bias (-B) and Root Mean Square Error (-R) for skin temperature for various WRF simulations for the entire 12-km grid for daytime conditions for 1-30 September 2013.*

5.4.2 Spatial Analysis of Bias and RMSE for CONUS

Figure 5-39 shows the skin temperature bias of the control run (CNTRL) for the entire domain. As can be seen the control generally has a warm bias in the East and a cool bias in the West. The warm bias is especially strong over the corn belt.

Figure 5-40 shows the comparable bias plot for the control run compared to NWS sites. The same warm bias is shown in the East again especially over the corn belt. However, the consistent cool bias in the West seen in the skin temperature is not evident in in the NWS spatial plot. This will be discussed more later after the assimilation plots.

Figure 5-41 shows the change in magnitude of the bias between the final satellite assimilation run (HC-1) and the control case (CNTRL). As can be seen it greatly reduced the bias in the Eastern U.S. but generally increased the bias in the West. In order to understand the source of the

degradation in the West, spatial plots of the incremental satellite assimilation are examined. Figure 5-42 shows the skin temperature bias change from the control case after the satellite insolation is added (INSOL-2). It shows a decrease in bias in the West so this is not the source of degradation.

Figure 5-43 shows a similar plot for the inclusion of the satellite vegetation (VEG). It also does not show a pattern of degradation in the West. So VEG is not the source of the degradation.

Figure 5-44 shows the plot for the inclusion of the satellite soil moisture nudging run (SM-1). It does now show a pattern of degradation in the West. Thus, it appears that the soil moisture nudging is the source of the degradation. This seems counter-intuitive since the direction of the nudging (though indirect through changes in soil moisture) should push the model skin temperature to the satellite value. This will need to be investigated further and may be due to some bias in the skin temperature product which changes over time.

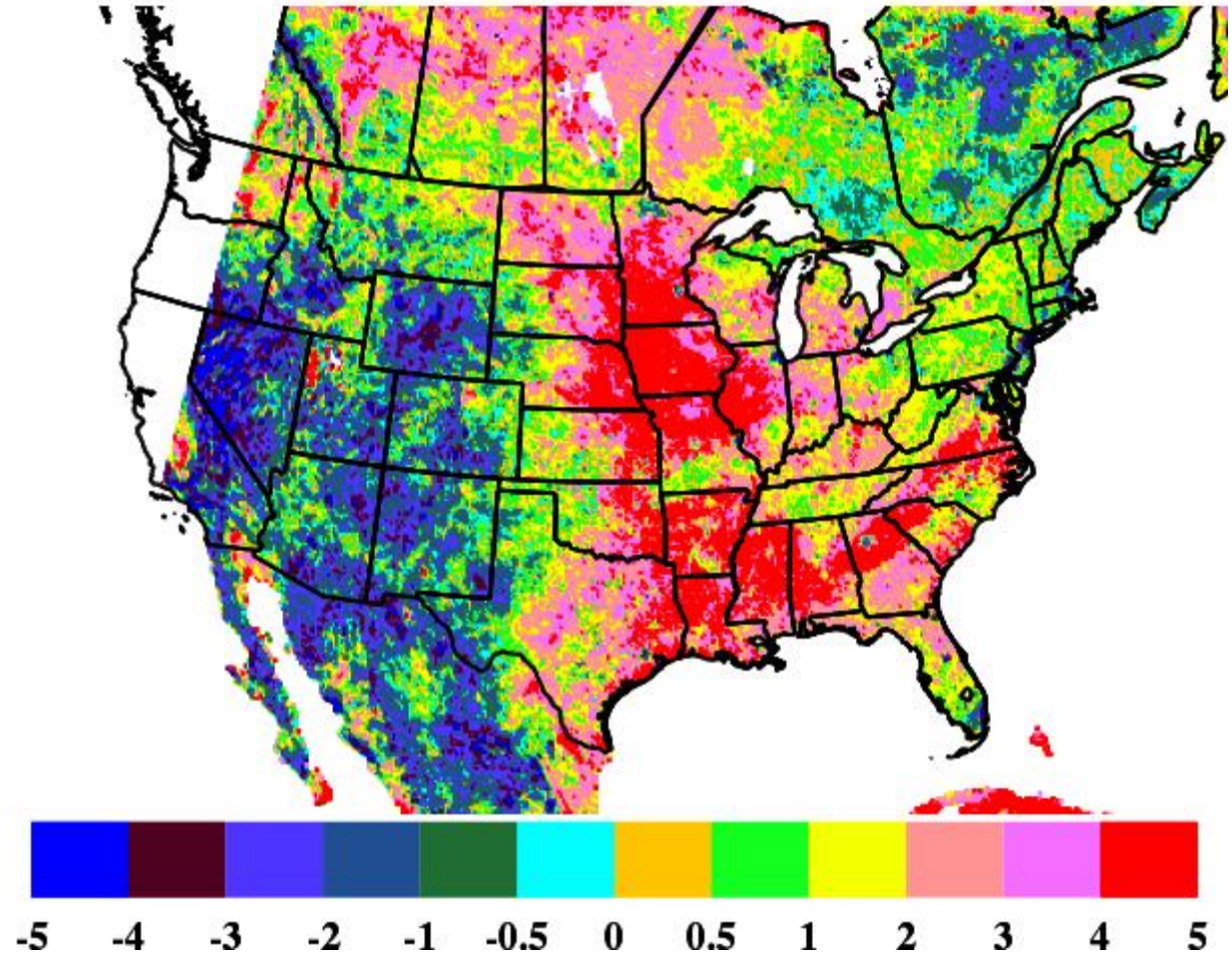

Figure 5-39 *Bias (model minus satellite) of skin temperature (units of degrees K) for the CNTRL simulation for the period 1-30 September 2013 for daytime conditions.*

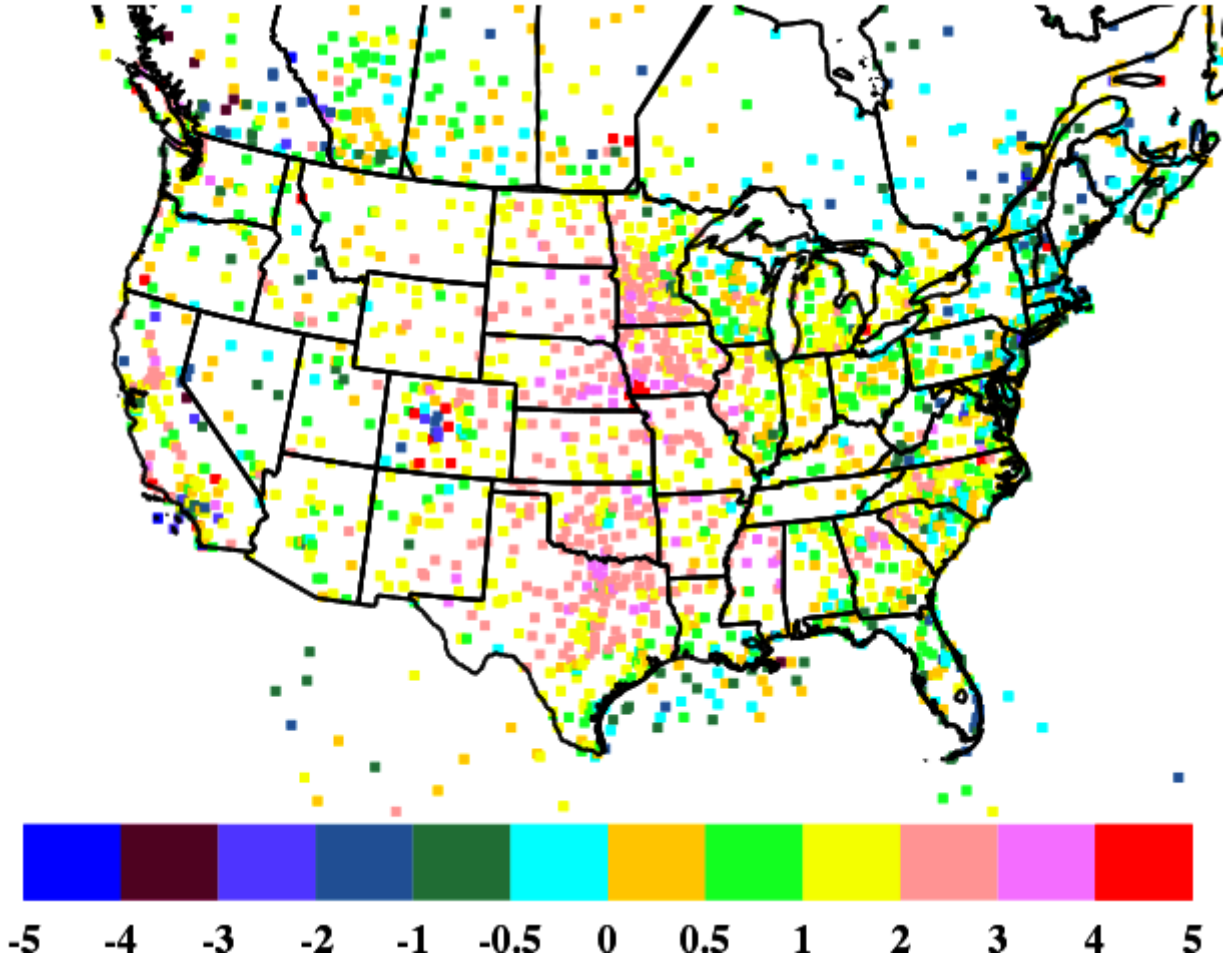

Figure 5-40 *Bias (model minus satellite) of 2-m temperature (units of degrees K) for the CNTRL simulation for the period 1-30 September 2013 for daytime conditions*.

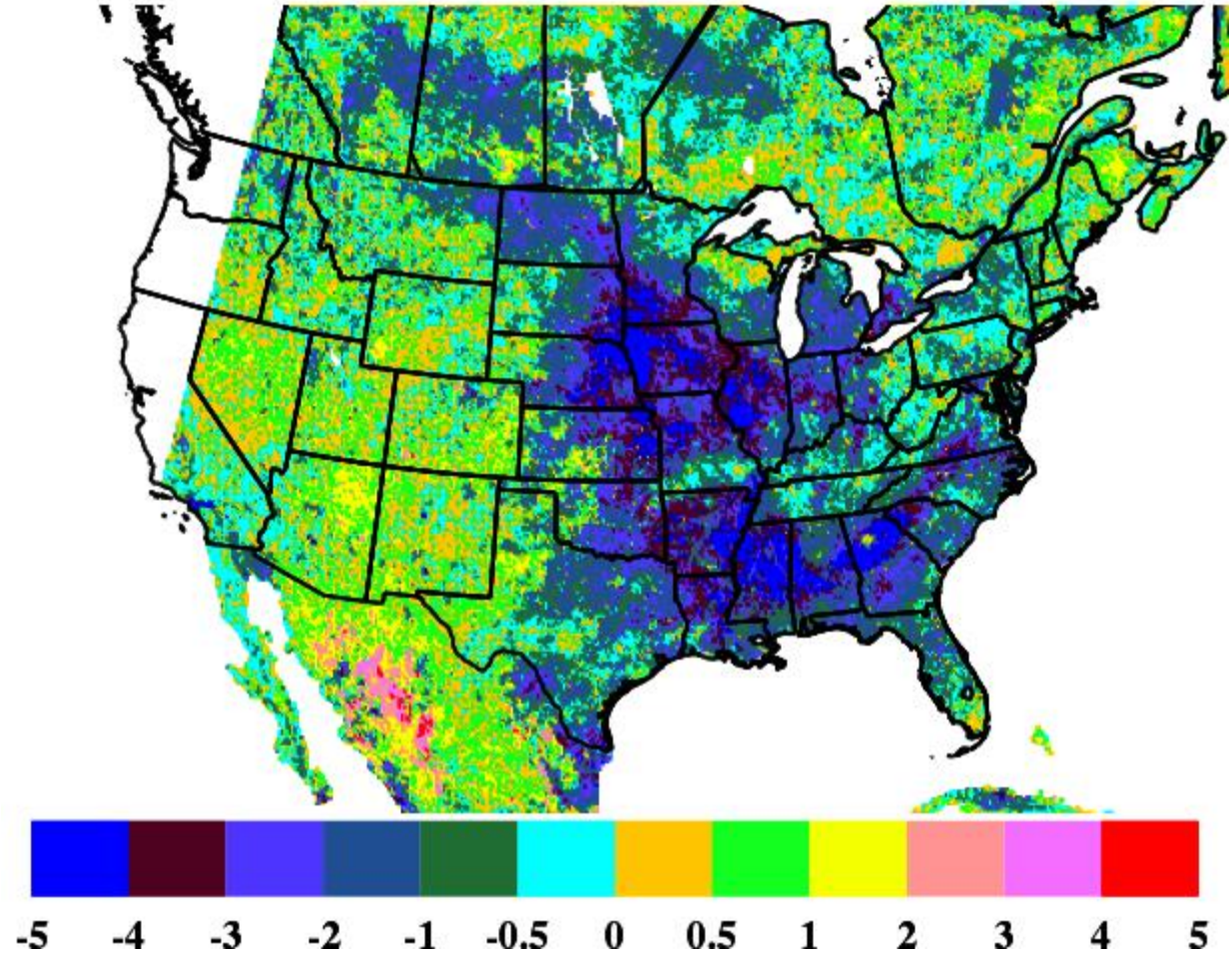

Figure 5-41 *Difference in the magnitudes of the respective bias values (units of degrees K) HC minus CNTRL of skin temperatures for the period 1-30 September 2013 for daytime conditions. Negative values indicate a decrease in the magnitude of the bias and vice versa*.

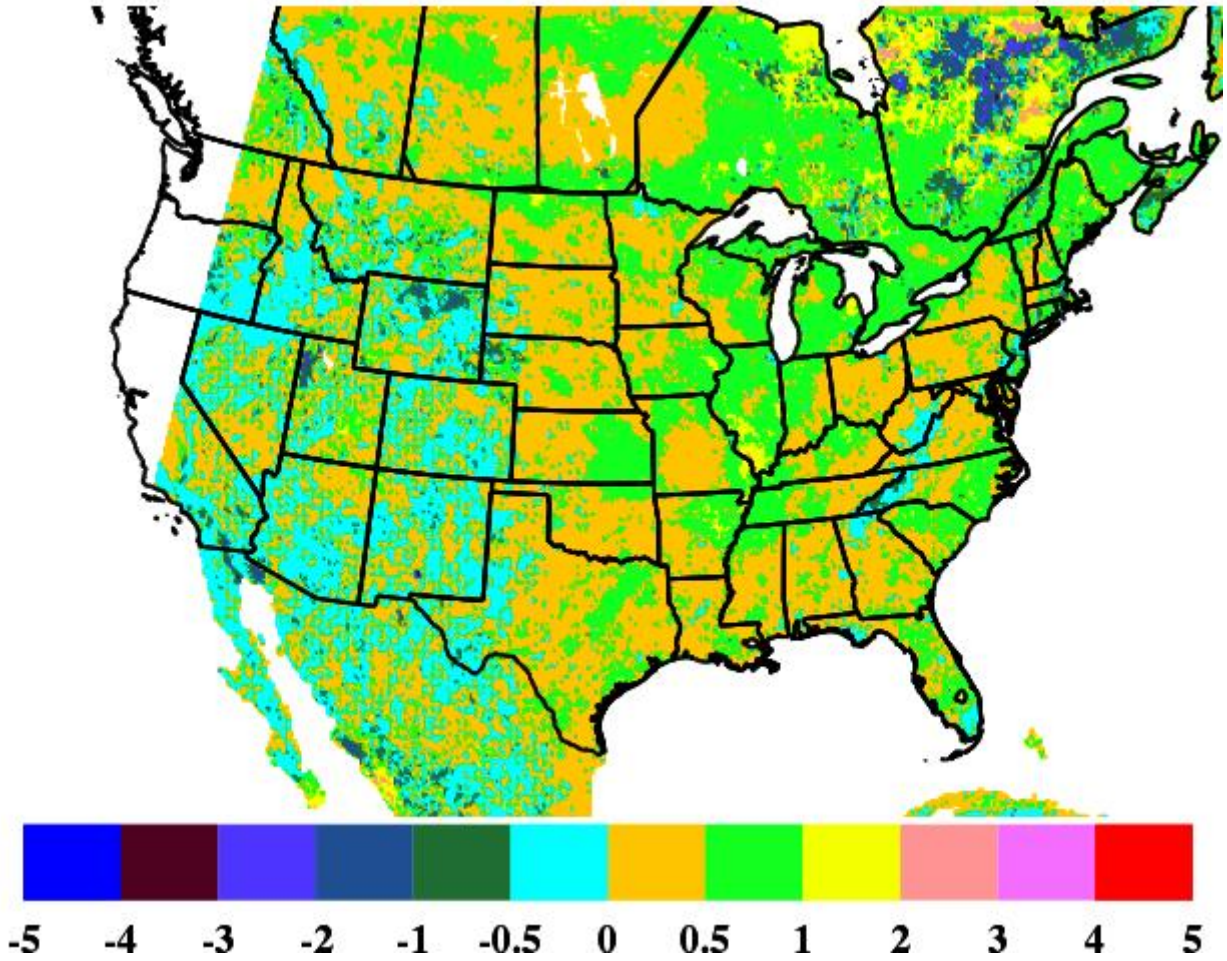

Figure 5-42 *Difference in the magnitudes of the respective bias values (units of degrees K) INSL-2 minus CNTRL of skin temperatures for the period 1-30 September 2013 for daytime conditions. Negative values indicate a decrease in the magnitude of the bias and vice versa*.

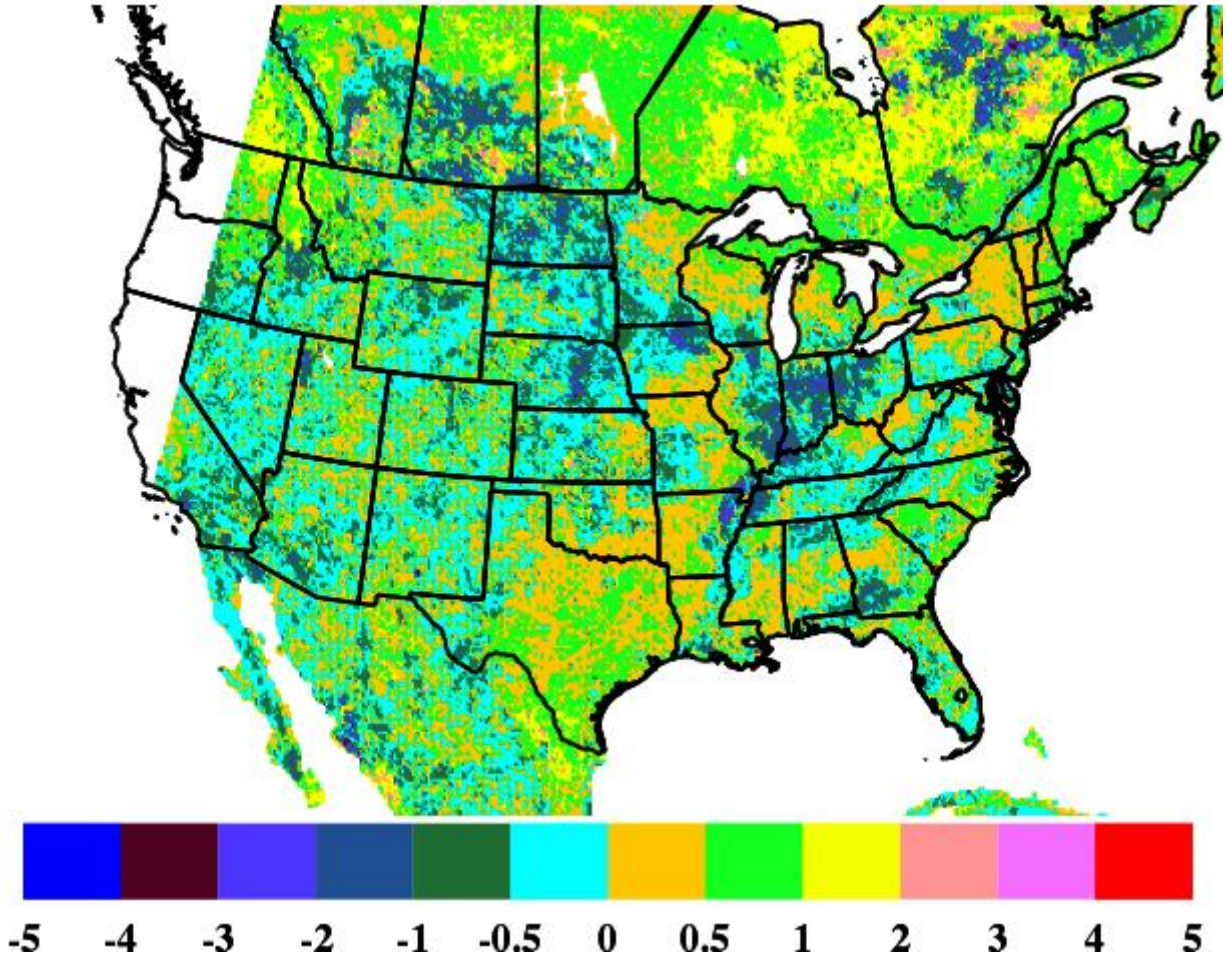

Figure 5-43 *Difference in the magnitudes of the respective bias values (units of degrees K) VEG minus CNTRL of skin temperatures for the period 1-30 September 2013 for daytime conditions. Negative values indicate a decrease in the magnitude of the bias and vice versa.*

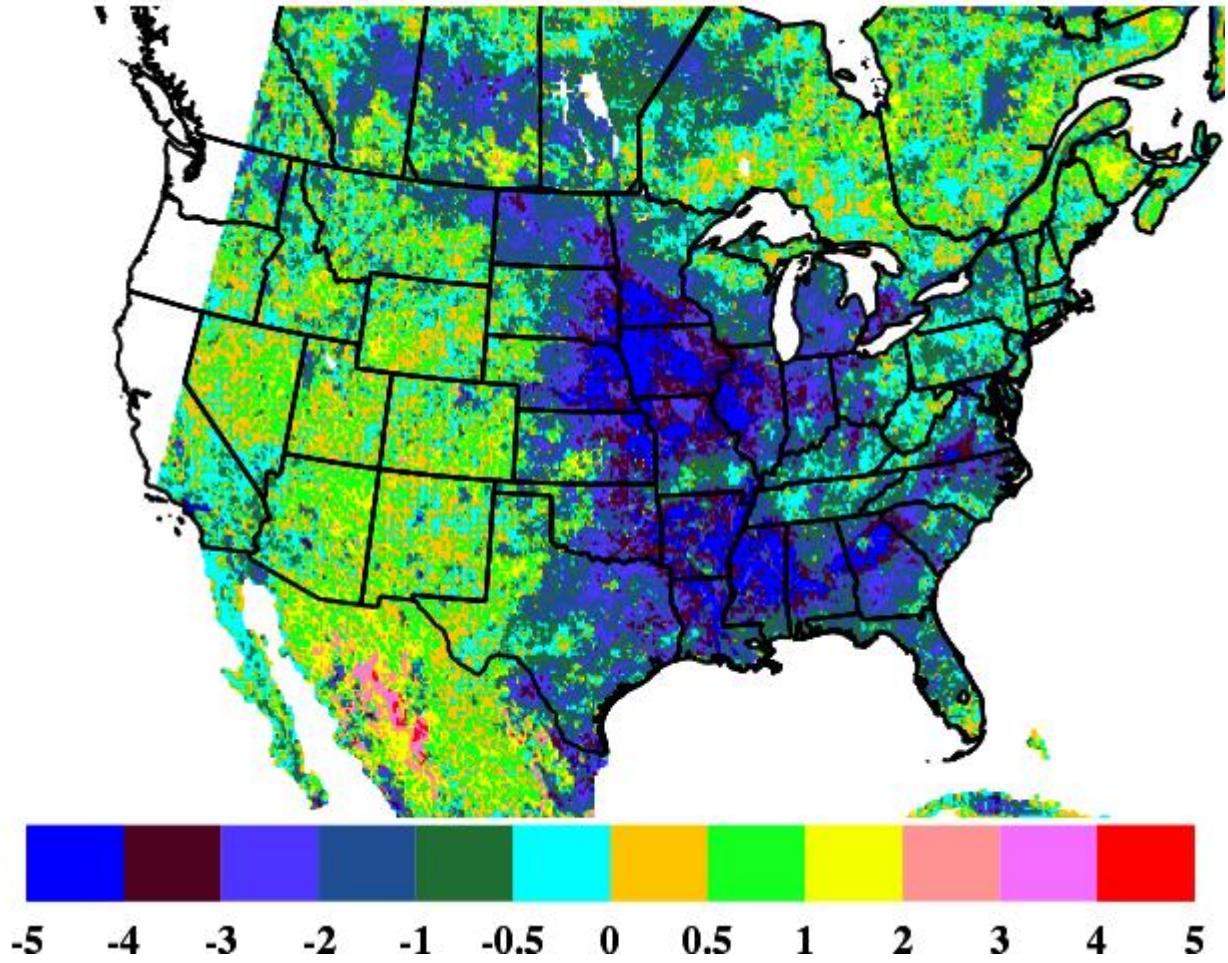

Figure 5-44 *Difference in the magnitudes of the respective bias values (units of degrees K) SM-2 minus CNTRL of skin temperatures for the period 1-30 September 2013 for daytime conditions. Negative values indicate a decrease in the magnitude of the bias and vice versa*.

5.4.3 Model Evaluation Against Skin Temperature for Texas Domain

As part of the evaluation statistics for skin temperature performance were made for only a Texas domain. Figure 5-45 shows the skin temperature for the Texas only domain. It shows similar results as for the CONUS except the bias is more improved for the Texas domain. The RMSE in Figure 5-46 shows improvement in daytime RMSE but degradation at night.

Table 5-4 shows corresponding numerical values over all times.

In Figure 5-47 the spatial distribution of the bias error in the control run indicates a warm bias over most of East Texas. A cold bias is indicated in far West Texas perhaps in areas of sparse vegetation or complex topography.

Figure 5-48 shows the spatial difference in the magnitude of the bias after the final satellite assimilation which includes all the satellite assimilation. As can be seen the bias is reduced over

most areas of Texas (light blue, blues and green). However, the warm colors show that over West Texas and a few scattered grid-boxes in the East the magnitude of the bias has increased. This is summarized in Figure 5-49 which indicates where the bias has been improved (blue) and where it has been degraded (red) by the satellite assimilation.

As noted above in the discussion of the CONUS results the fact that the model shows a cold bias in west Texas may be related to a satellite skin temperature being too warm. However, it is not clear why the satellite nudging of moisture using skin temperatures makes the bias worse.

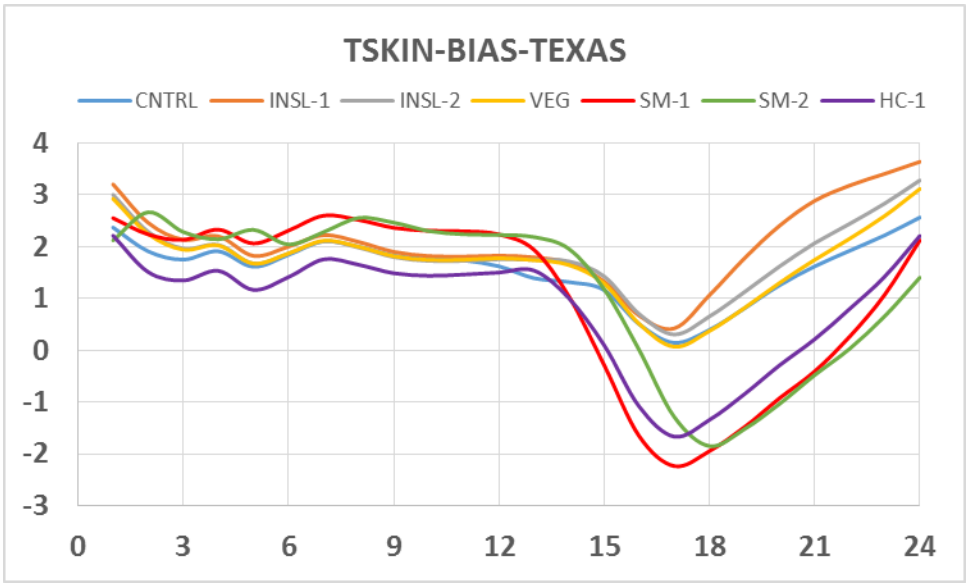

Figure 5-45 *Average hourly bias values (K) for skin temperature for various WRF simulations for the state of Texas for 1-30 September 2013. Values calculated at all 12-km grid points.*

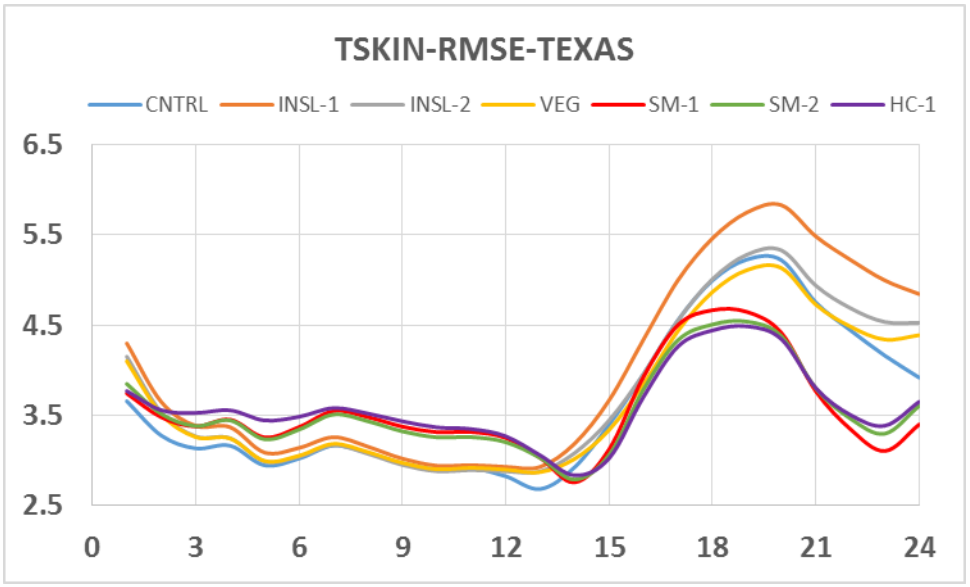

Figure 5-46 *Hourly root mean square error (RMSE) values (K) for skin temperature for various*

WRF simulations for the state of Texas for 1-30 September 2013. Values calculated at all 12-km grid points.

RUN	TSKIN-B	TSKIN-R
CNTRL	1.618	4.359
INSL-1	2.331	4.827
INSL-2	1.927	4.481
VEG	1.958	4.502
SM-1	-0.130	4.233
SM-2	0.449	4.137
HC-1	0.662	4.073

Table 5-4 *Bias (-B) and Root Mean Square Error (-R) for skin temperature for various WRF simulations for the state of Texas for daytime conditions for 1-30 September 2013.*

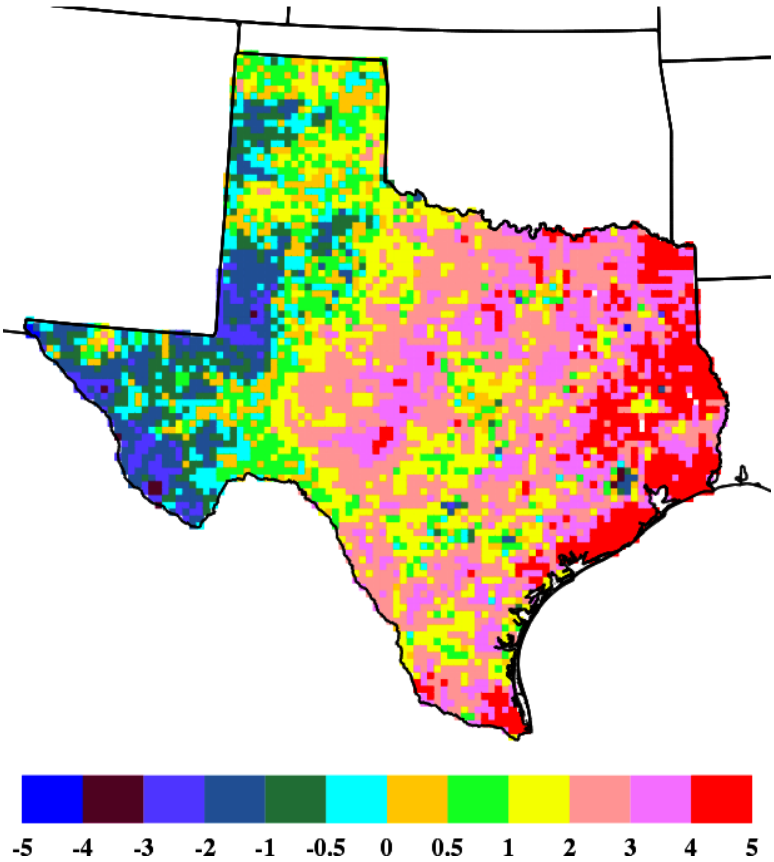

Figure 5-47 *Bias (model minus satellite) of skin temperature (units of degrees K) for the CNTRL simulation for the period 1-30 September 2013 for daytime conditions for the state of Texas.*

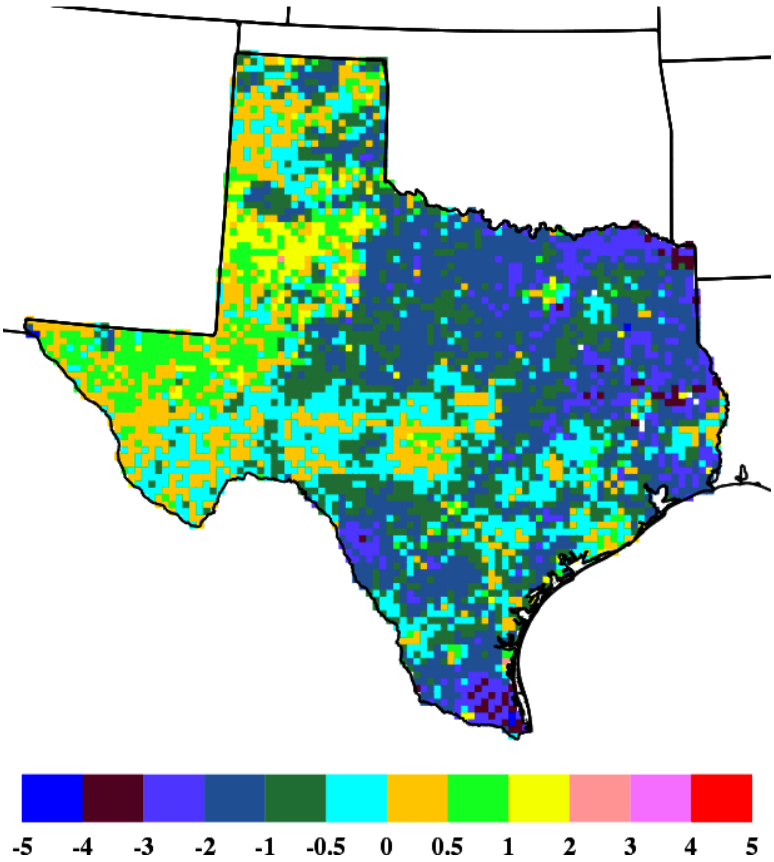

Figure 5-48 *Difference in the magnitudes of the respective bias values (units of degrees K) HC-1 minus CNTRL of skin temperatures for the period 1-30 September 2013 for daytime conditions for the state of Texas. Negative values indicate a decrease in the magnitude of the bias and vice versa.*

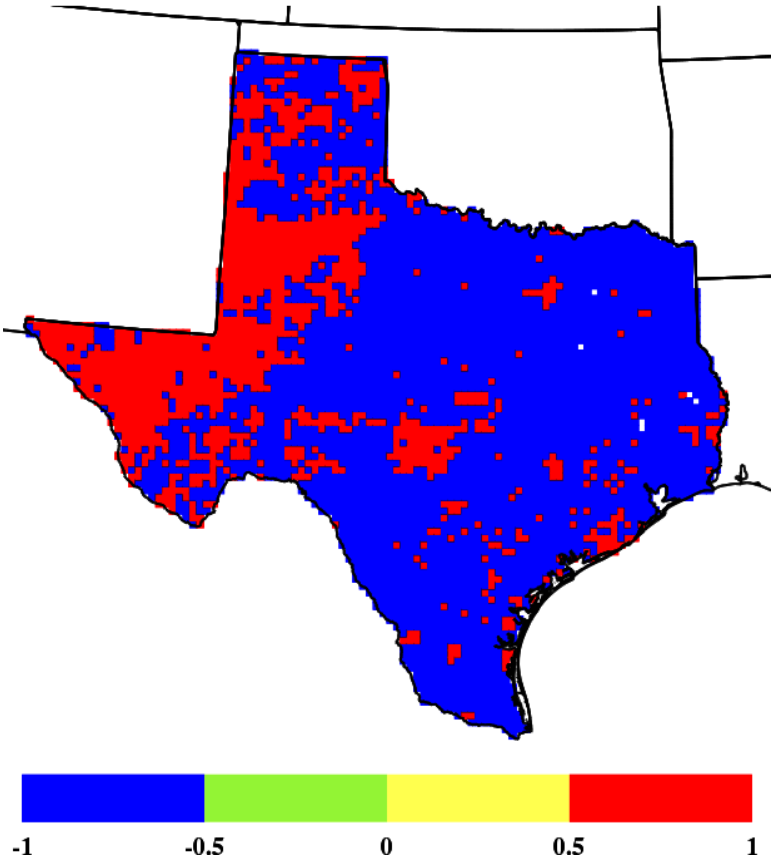

Figure 5-49 *The sign of the difference in the magnitude of the skin temperature bias values (HC-1 – CONTRL) for the state of Texas for daytime conditions. Blue (red) grid locations indicate a decrease (increase) in the magnitude of the bias.*

5.4.4 Skin Temperature Performance Around Houston

Most of the ozone SIP activity in Texas has centered on the Houston and Dallas areas. Additionally, Houston has been at the center of national field program activities including TEXAQ 2000, TEXAQ 2006 and Discover AQ. Model performance around Houston is then of special interest. Figure 5-50 shows the difference in the magnitudes of the respect bias values (units of degrees K) between the final satellite assimilation run and the control run (HC-1 minus CNTRL) of skin temperatures for the period 1-30 September 2013 for daytime conditions for the Houston area. Figure 5-51 shows the sign of the difference with blue indicating improvement and red degradation. As can be seen over most areas the bias has been improved. A few areas to the northwest and southwest of the city show degradation. This may be due to the sign of the bias changing during the day or errors in skin temperature or other model issues such as albedo or roughness.

Figure 5-52 shows the remaining bias after the satellite assimilation. It shows that the model remains too warm around most of the area except over the immediate down town area where the model remains too cool. This can be further evaluated in the future.

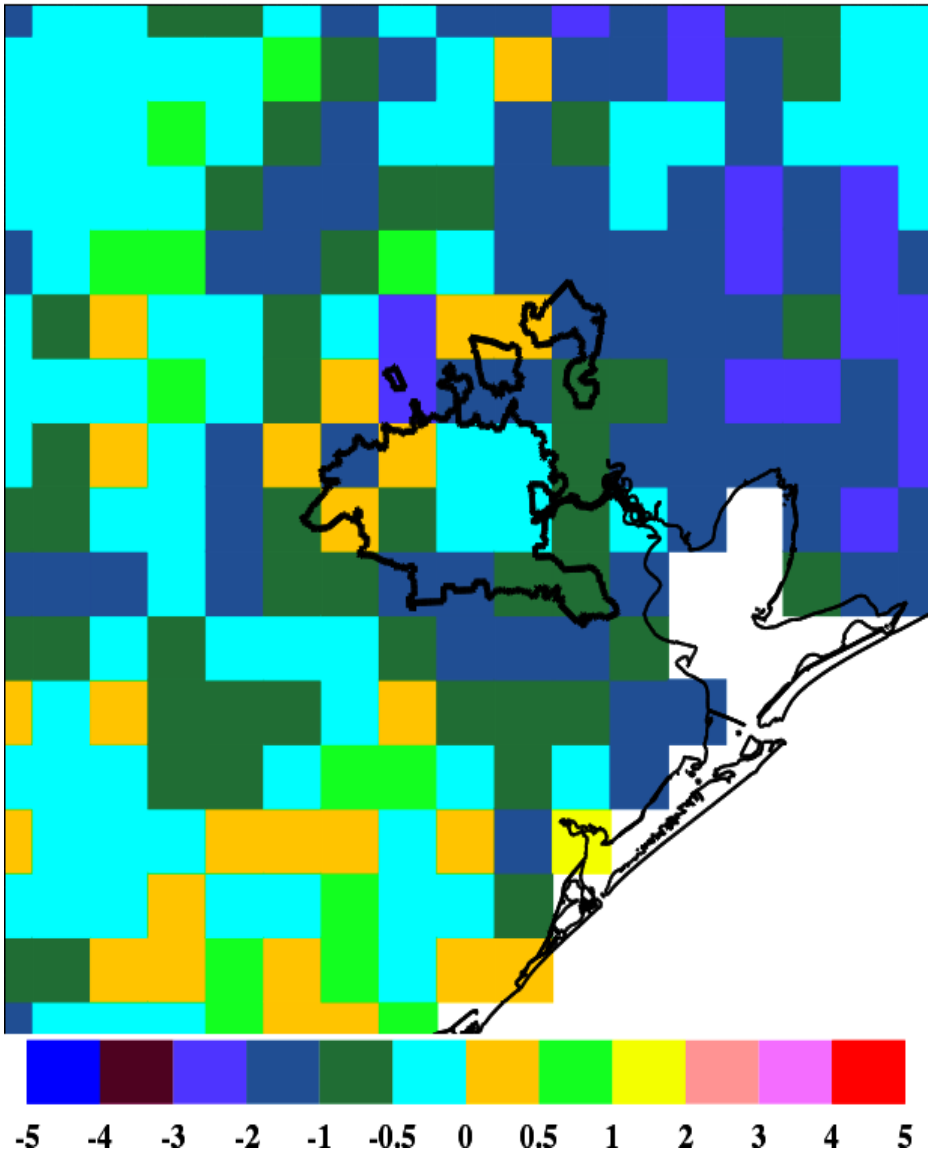

Figure 5-50 *Difference in the magnitudes of the respective bias values (units of degrees K) HC-1 minus CNTRL of skin temperatures for the period 1-30 September 2013 for daytime conditions for the Houston area. Negative values indicate a decrease in the magnitude of the bias and vice versa.*

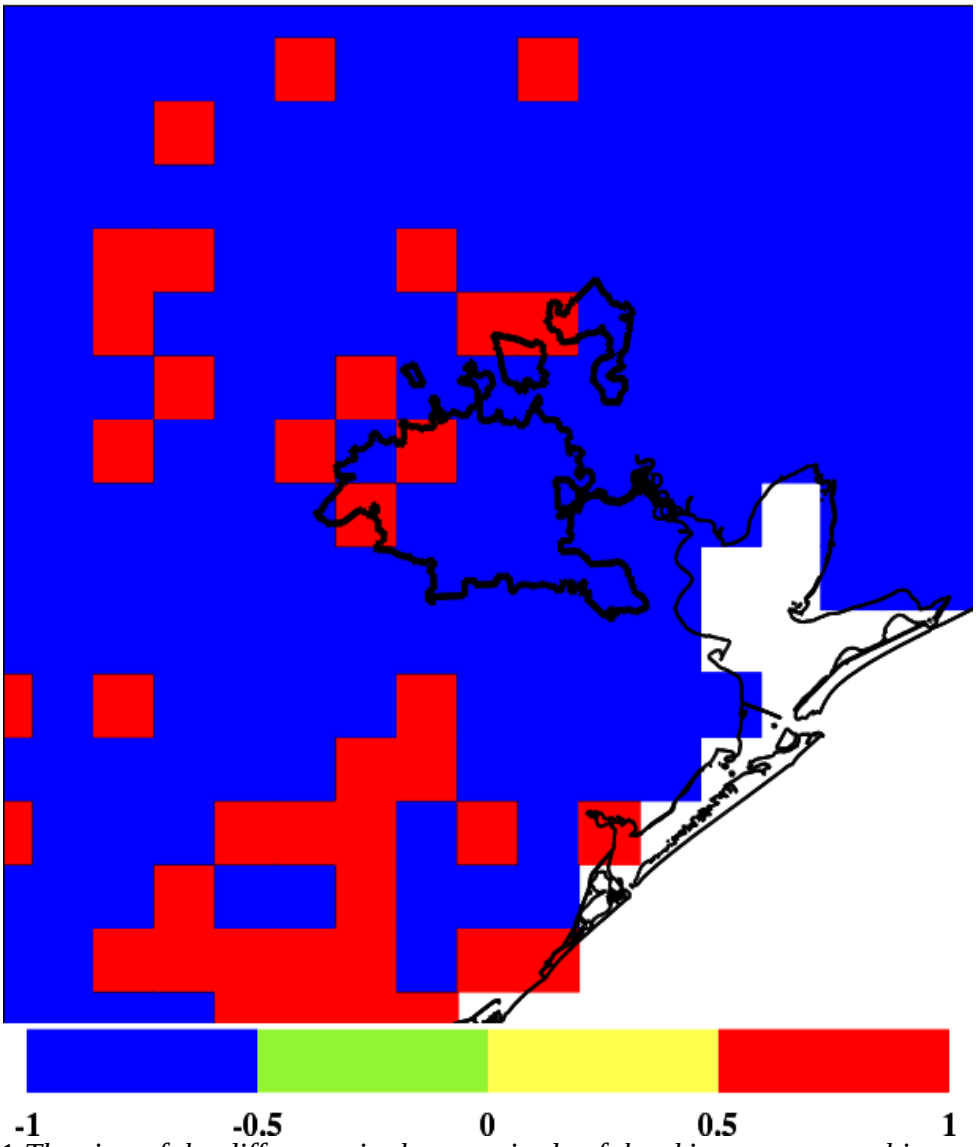

Figure 5-51 *The sign of the difference in the magnitude of the skin temperature bias values (HC-1 – CONTRL) for the state of Texas for daytime conditions. Blue (red) grid locations indicate a decrease (increase) in the magnitude of the bias.*

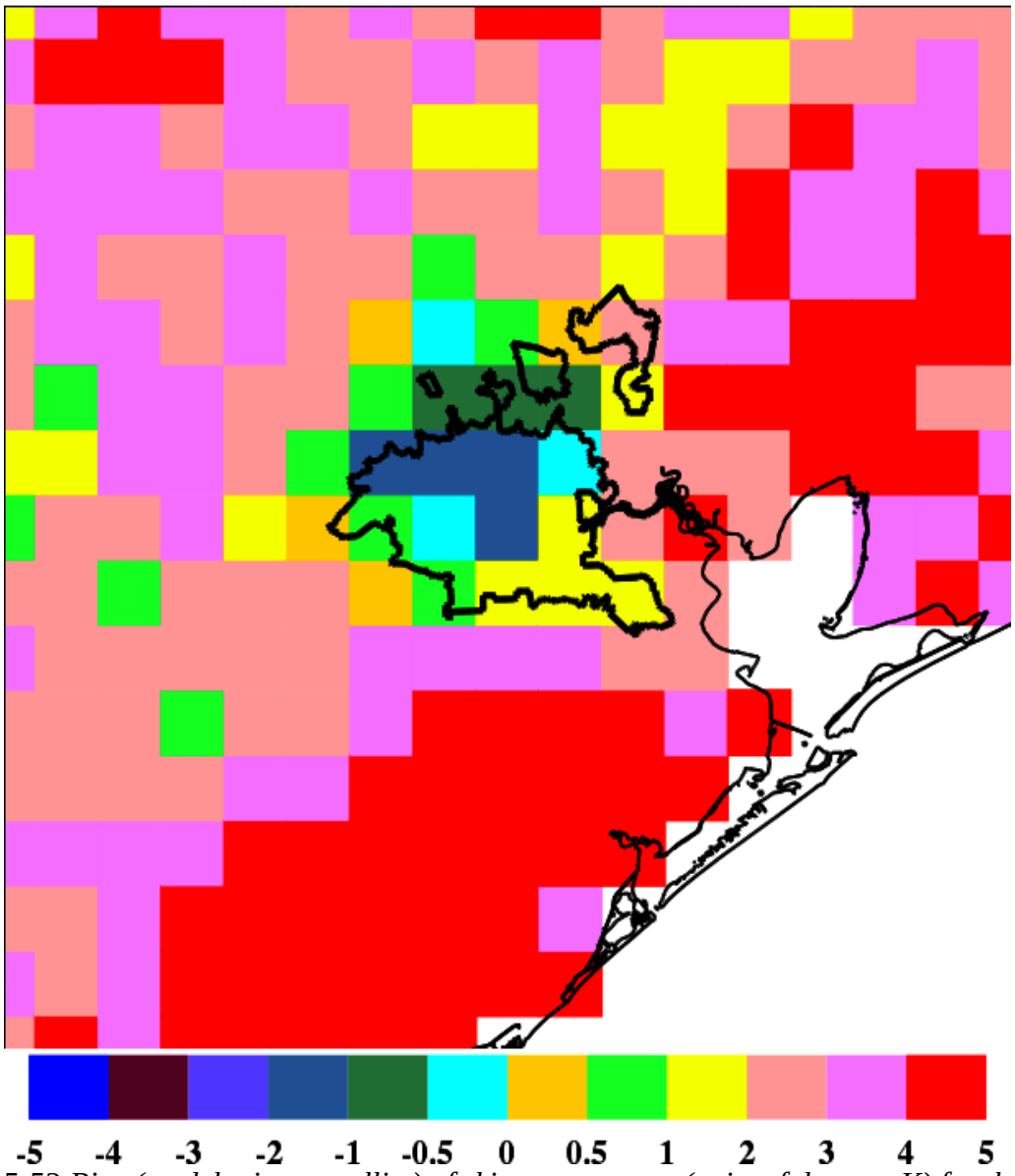

Figure 5-52 *Bias (model minus satellite) of skin temperature (units of degrees K) for the HC-1 satellite assimilation simulation for the period 1-30 September 2013 for daytime conditions for the Houston area.*

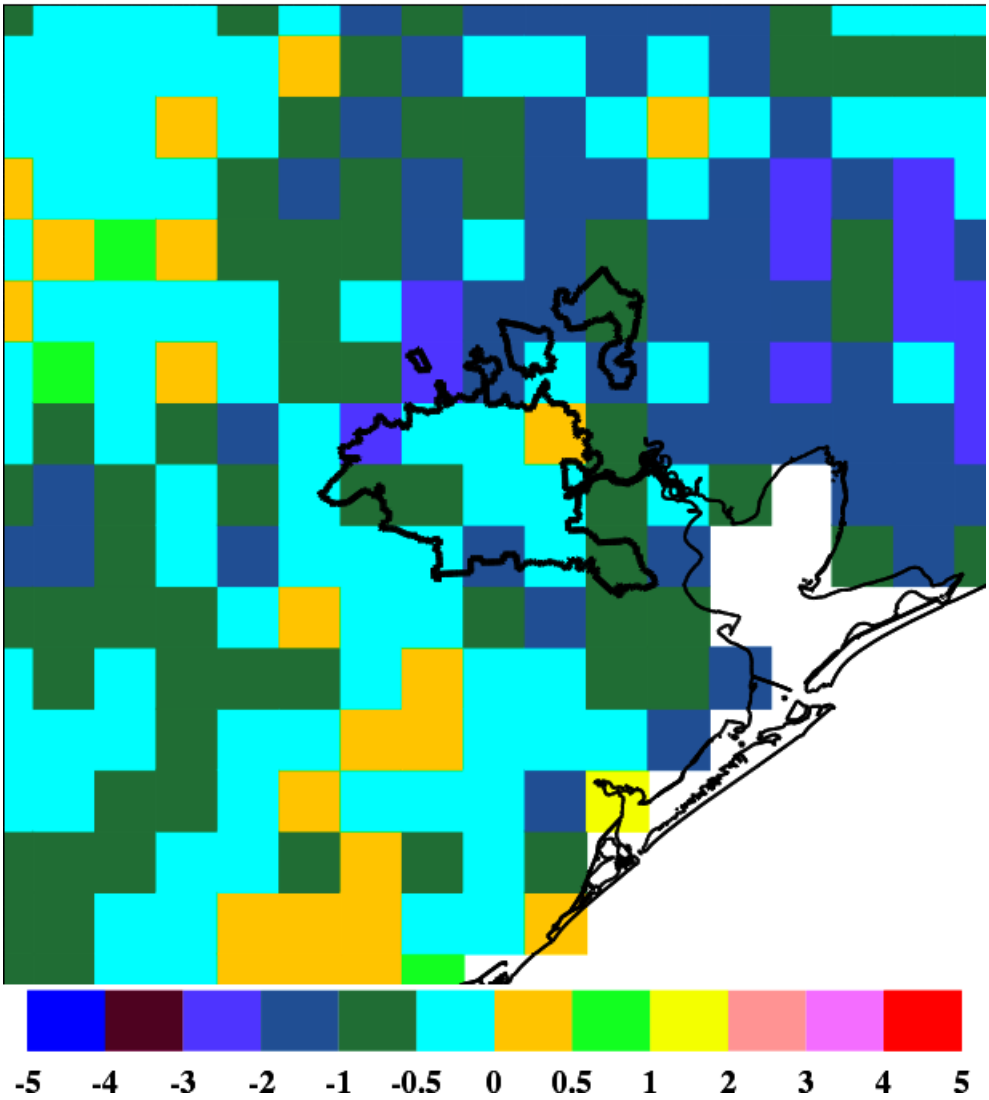

Figure 5-53 *Difference in the magnitudes of the respective RMSE values (units of degrees K) HC-1 minus CNTRL of skin temperatures for the period 1-30 September 2013 for daytime conditions for the Houston area. Negative values indicate a decrease in the magnitude of the RMSE and vice versa.*

5.4.5 Time Variation of Statistics and East West Domain Statistics

As seen above there are substantial differences in the model assimilation results for the Eastern U.S. and Western U.S. with skin temperature as the metric. Here the Eastern statistics are tabulated separately (see Figure 5-54). Table 5-5 shows the results for the red sub-domain. It shows that the satellite assimilation can provide substantial improvement in model performance in Eastern U.S. The bias statistic is improved by over a degree and a half and RMSE by about a degree.

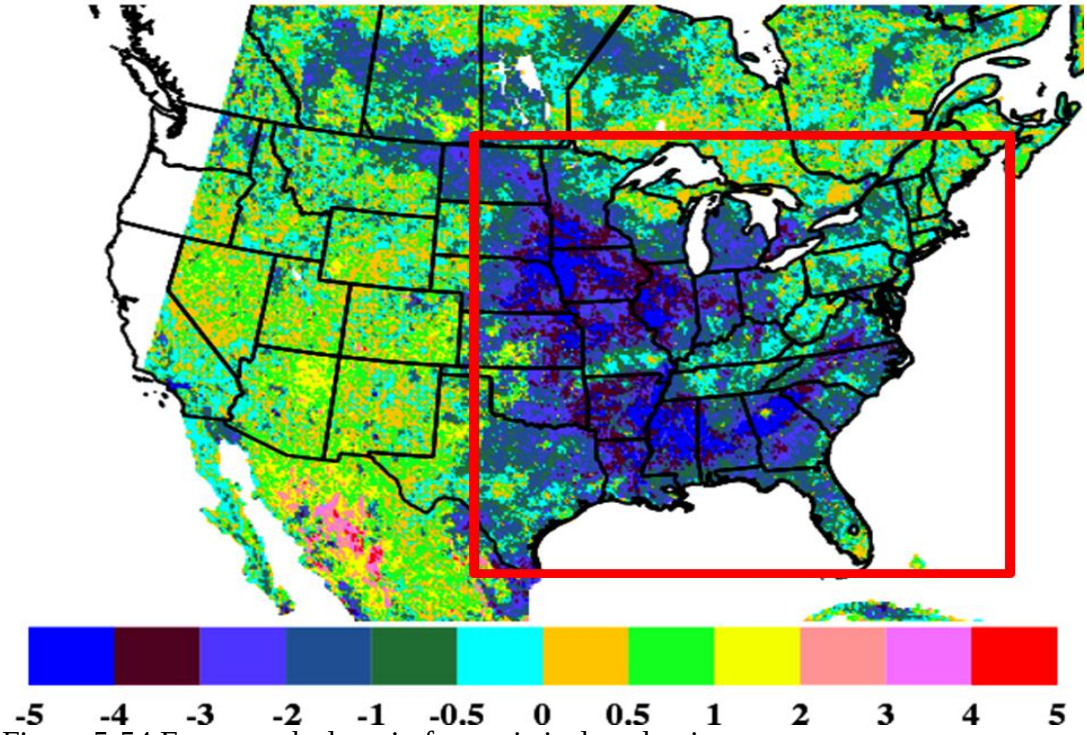

Figure 5-54 Eastern sub-domain for statistical evaluation.

RUN	TSKIN-B	TSKIN-R
CNTRL	2.590	4.559
INSL-1	3.728	5.391
INSL-2	3.039	4.773
VEG	2.633	4.495
SM-1	0.384	3.297
SM- 2	0.809	3.371
HC-1	0.957	3.387

Table 5-5 Statistics for the Eastern subdomain.

In carrying out the assimilation because of clouds and missing skin temperature data it must be remembered that it takes some time for the assimilation technique to reach all the grid points.

Figure 5-55 shows the time evolution of the 2-m bias statistics against NWS observations for the entire domain. It can be seen that the model performance for the satellite assimilation improves substantially over time. Performance in the second half of the simulation period is much better than in the first half.

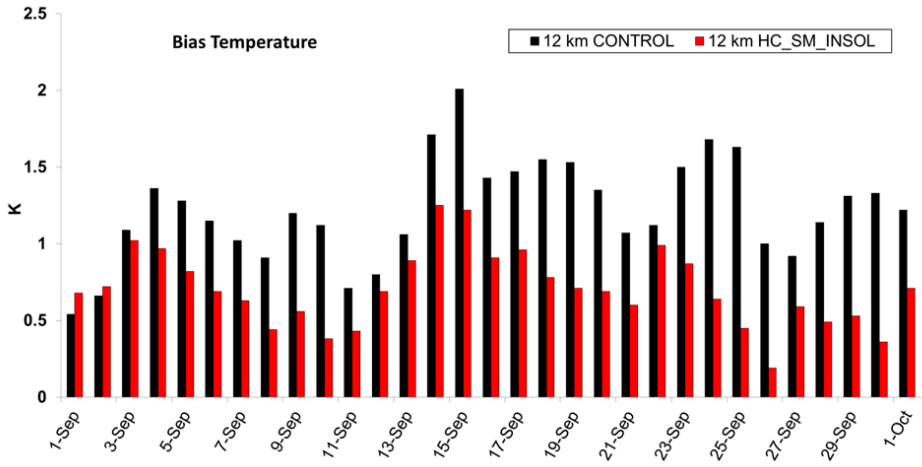

Figure 5-55 *Time series of bias for the control and final satellite assimilation (HC-1) for entire domain. It shows that as more assimilation data becomes available model performance generally improves.*

6 Model Satellite Results for the 2012 Model Evaluation Period

As described in Chapter 4 one of the tasks under this year's project was to carry out model evaluation for an additional period outside the Discover AQ 2013 period 1-30 September. In consultation with TCEQ another episode was selected. As part of the Good Neighbor SIP process May – September was of interest. Thus, for this project August 2012 was selected. It is a drier period than September 2013 and should have fewer clouds to interfere with skin temperatures.

The following describes the results for this August 2012 period. Over much of the East and Midwest this was a dry period and a dry period for most of Texas. Because most of the model set-ups were described in Chapter 4 and the model assimilation cases described in Chapter 5, the discussions here focuses on 2012 performance. The acronyms for the different runs are the same as in Chapter 5 except there is an additional control run, labeled as CNTRL-2. In the latter run the initial soil moisture and temperature of the top soil layer were derived from the previous 5.5 day simulation.

Figure 6-1 through Figure 6-9 shows the changes in the 2-m temperature for the control and subsequent assimilation runs. The results show improvement with the satellite assimilation in the daytime for 2012 as for 2013. However, a significant part of the improvement in the assimilation is due to the satellite insolation assimilation. The subsequent improvement by soil moisture nudging is small. There is improvement even at night due to the insolation assimilation which may be due to improved daytime temperatures that persist through the night.

The 2-m specific humidity performance in bias seen in Figure 6-2. It also shows an improvement especially in daytime. The 10-m wind speed improvement in Figure 6-3 is more mixed with nighttime performance improving slightly but daytime performance slightly deteriorating.

Figure 6-7 shows the spatial depiction of bias in the control run (CNTRL-1). It shows the model is too warm across most of the country especially in the drought areas of 2012. This may be due to inadequate handling of moisture in the model or in clouds.

Figure 6-8 shows the spatial change in magnitude of the bias for the final satellite assimilation run which includes satellite insolation, satellite vegetation, soil moisture nudging from satellite skin temperatures and heat capacity nudging using satellite skin temperatures. It shows over most of the domain that the bias has been reduced especially in the corn-belt region of the Midwest. Figure 6-9 shows where the bias is decreased (blue) and where it is degraded (red). It shows improvement in most areas of the country.

6.1 Evaluation Compared with NWS Observations

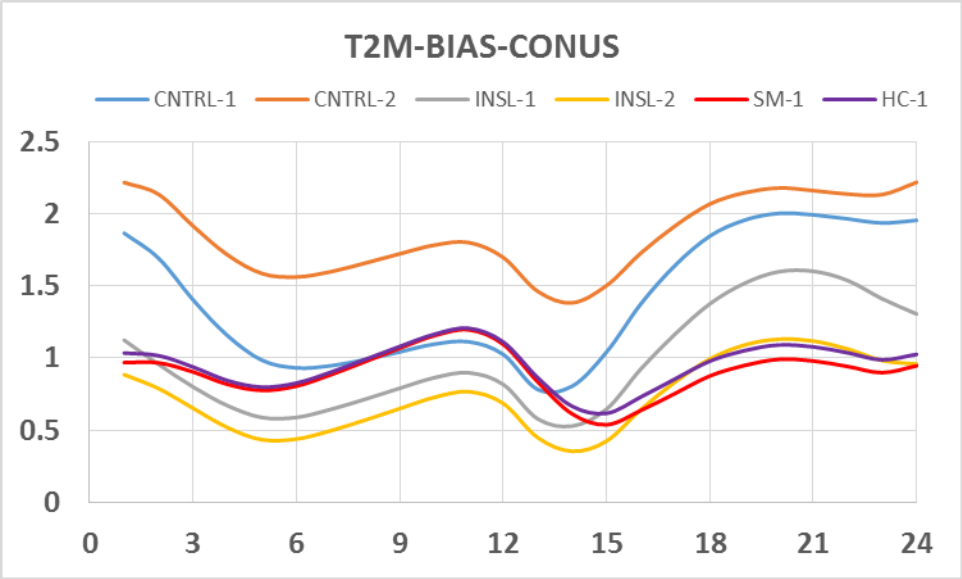

Figure 6-1 *Average hourly bias values (K) for temperature at 2-m for various WRF simulations for the entire 12-km grid for 1-31 August 2012. Values calculated at all surface observing stations.*

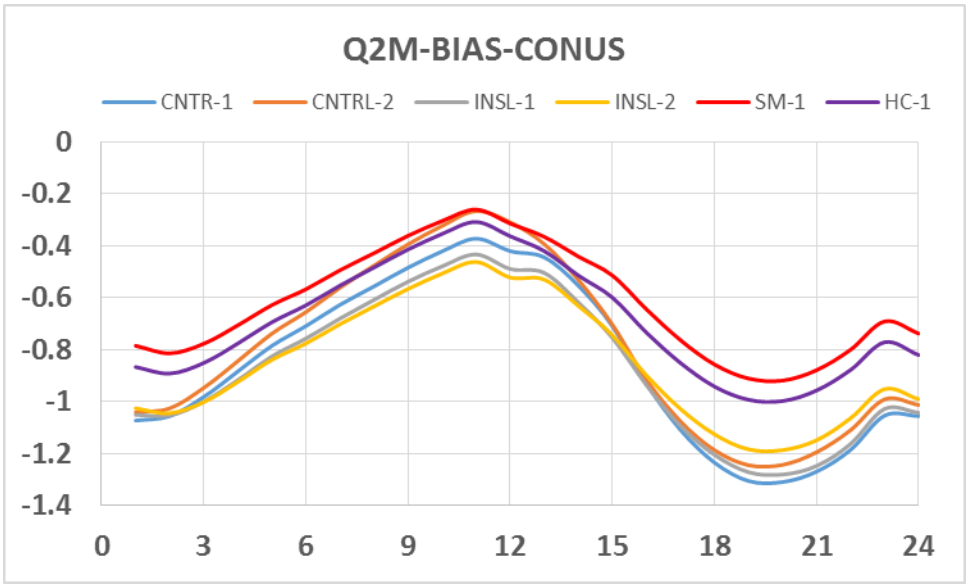

Figure 6-2 *Average hourly bias values (g kg^{-1}) for specific humidity at 2-m for various WRF simulations for the entire 12-km grid for 1-31 August 2012. Values calculated at all surface observing stations.*

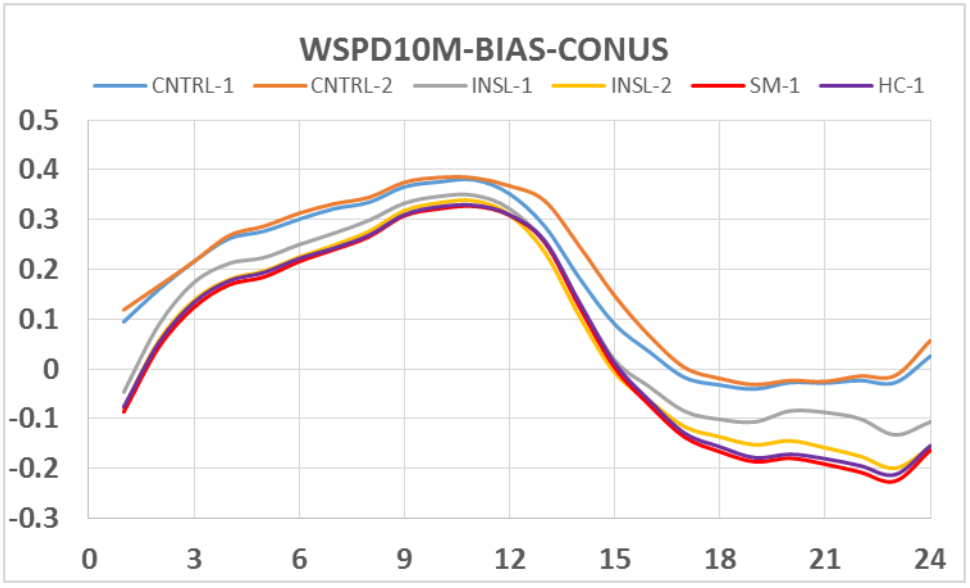

Figure 6-3 *Average hourly bias values (m s^{-1}) for wind speed at 10-m for various WRF simulations for the entire 12-km grid for 1-31 August 2012. Values calculated at all surface observing stations.*

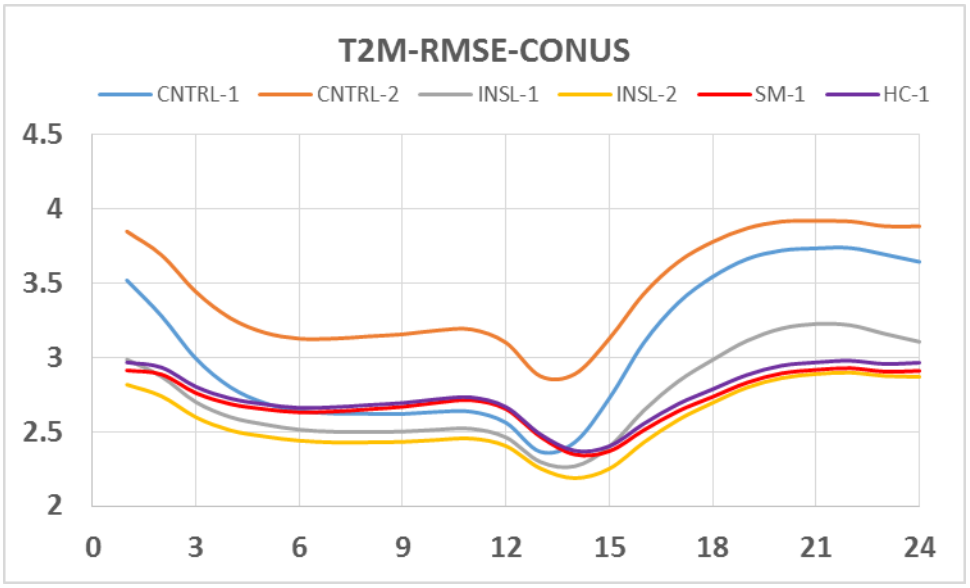

Figure 6-4 *Hourly root mean square error (RMSE) values (K) for temperature at 2-m for various WRF simulations for the entire 12-km grid for 1-31 August 2012. Values calculated at all surface observing stations.*

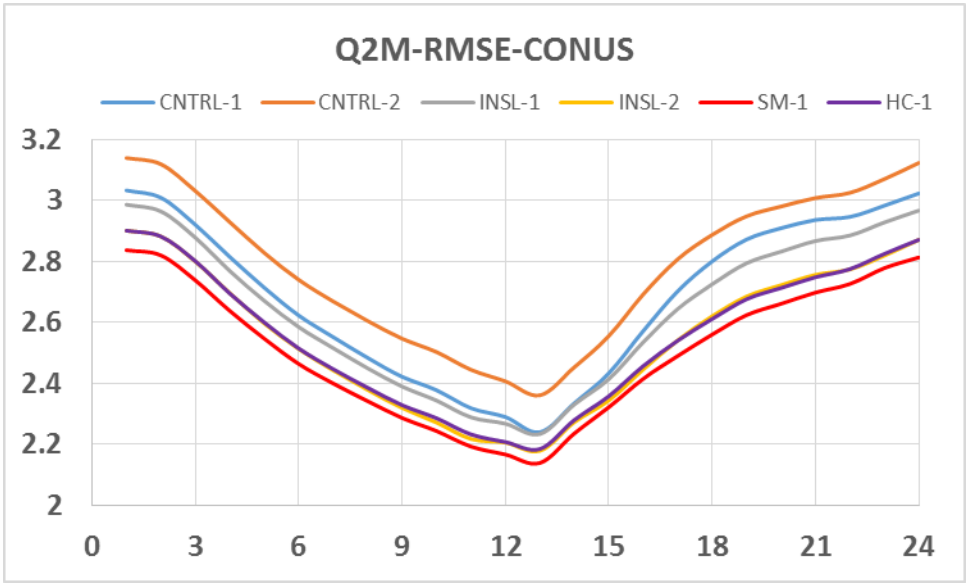

Figure 6-5 *Hourly root mean square error (RMSE) values (g kg^{-1}) for specific humidity at 2-m for various WRF simulations for the entire 12-km grid for 1-31 August 2012. Values calculated at all surface observing stations.*

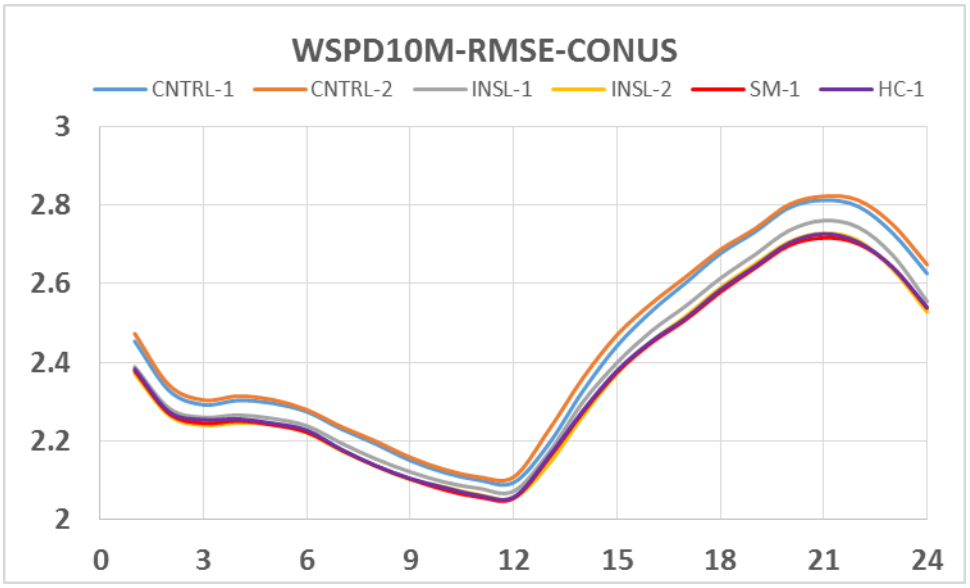

Figure 6-6 *Hourly root mean square error (RMSE) values (m s^{-1}) for wind speed at 10-m for various WRF simulations for the entire 12-km grid for 1-31 August 2012. Values calculated at all surface observing stations.*

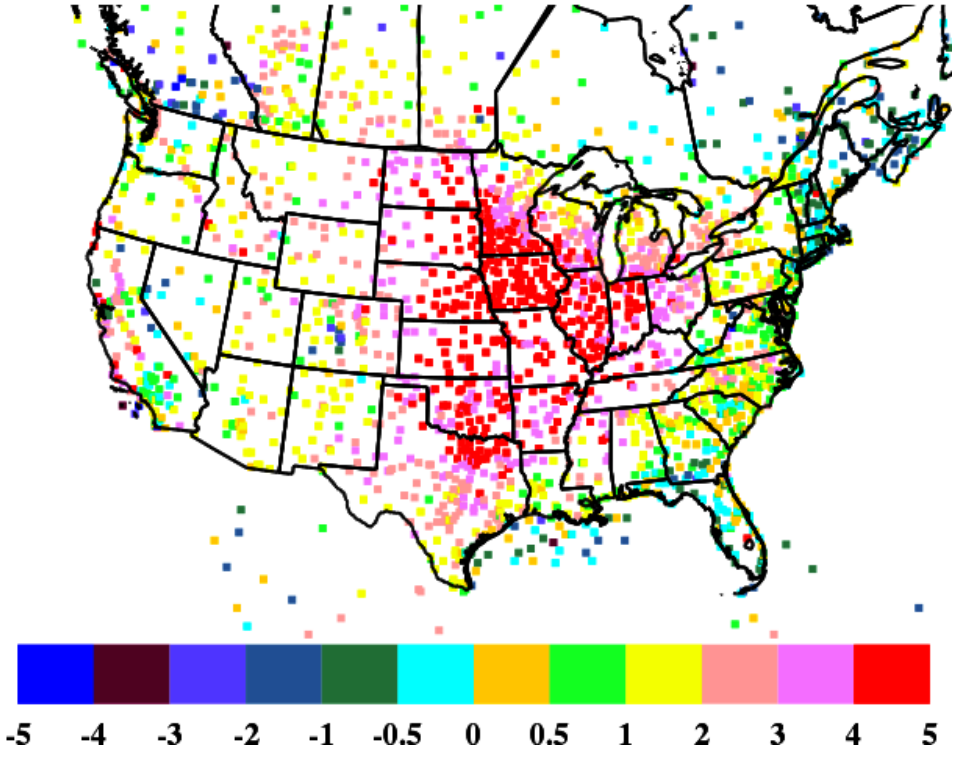

Figure 6-7 *Bias (model minus observed) of 2-m temperature (units of degrees K) for the CNTRL simulation for the period 1-31 August 2012 for daytime conditions.*

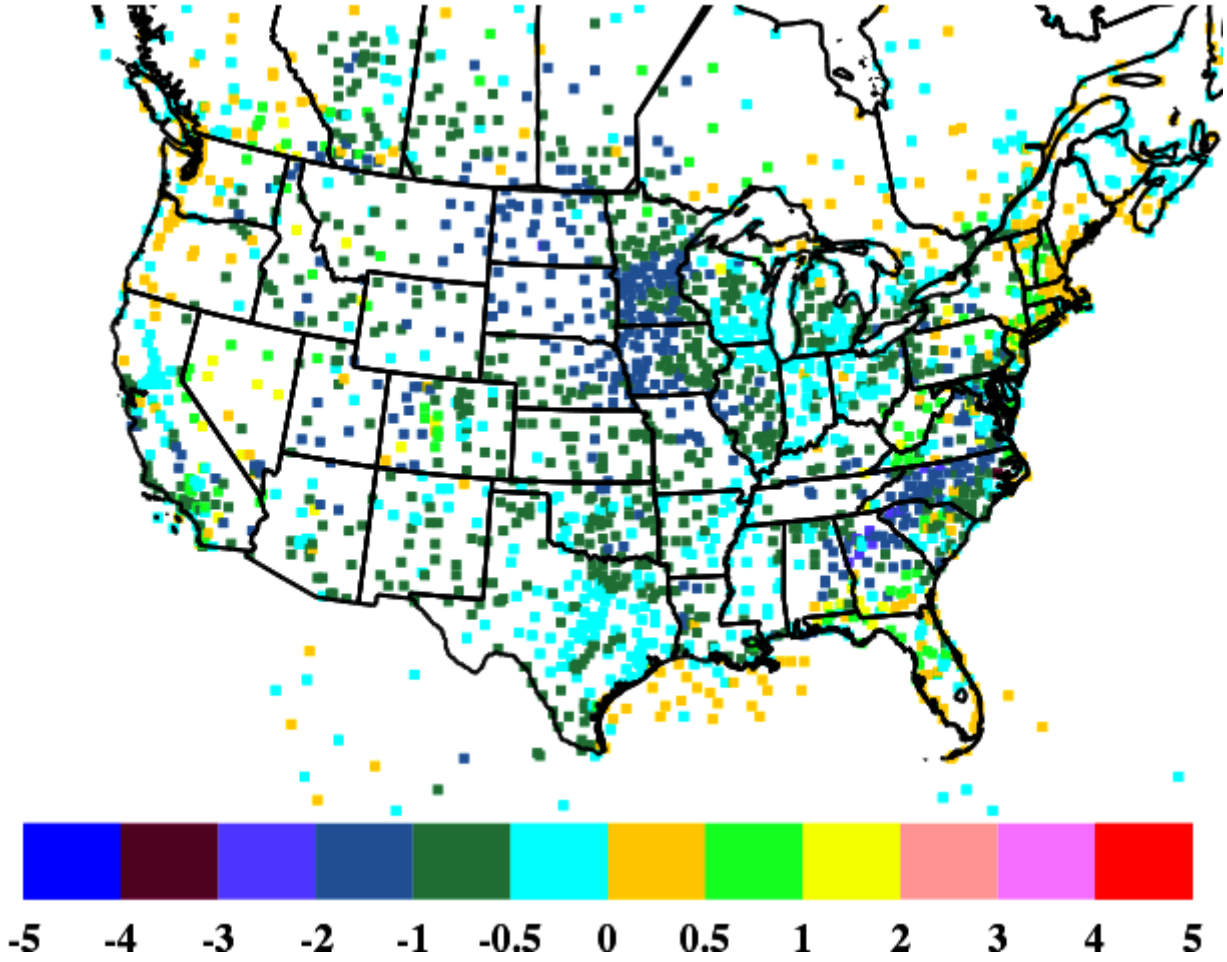

Figure 6-8 *Difference in the magnitudes of the respective bias values (units of degrees K) HC minus CNTRL of 2-m temperatures for the period 1-31 August 2012 for daytime conditions. Negative values indicate a decrease in the magnitude of the bias and vice versa*.

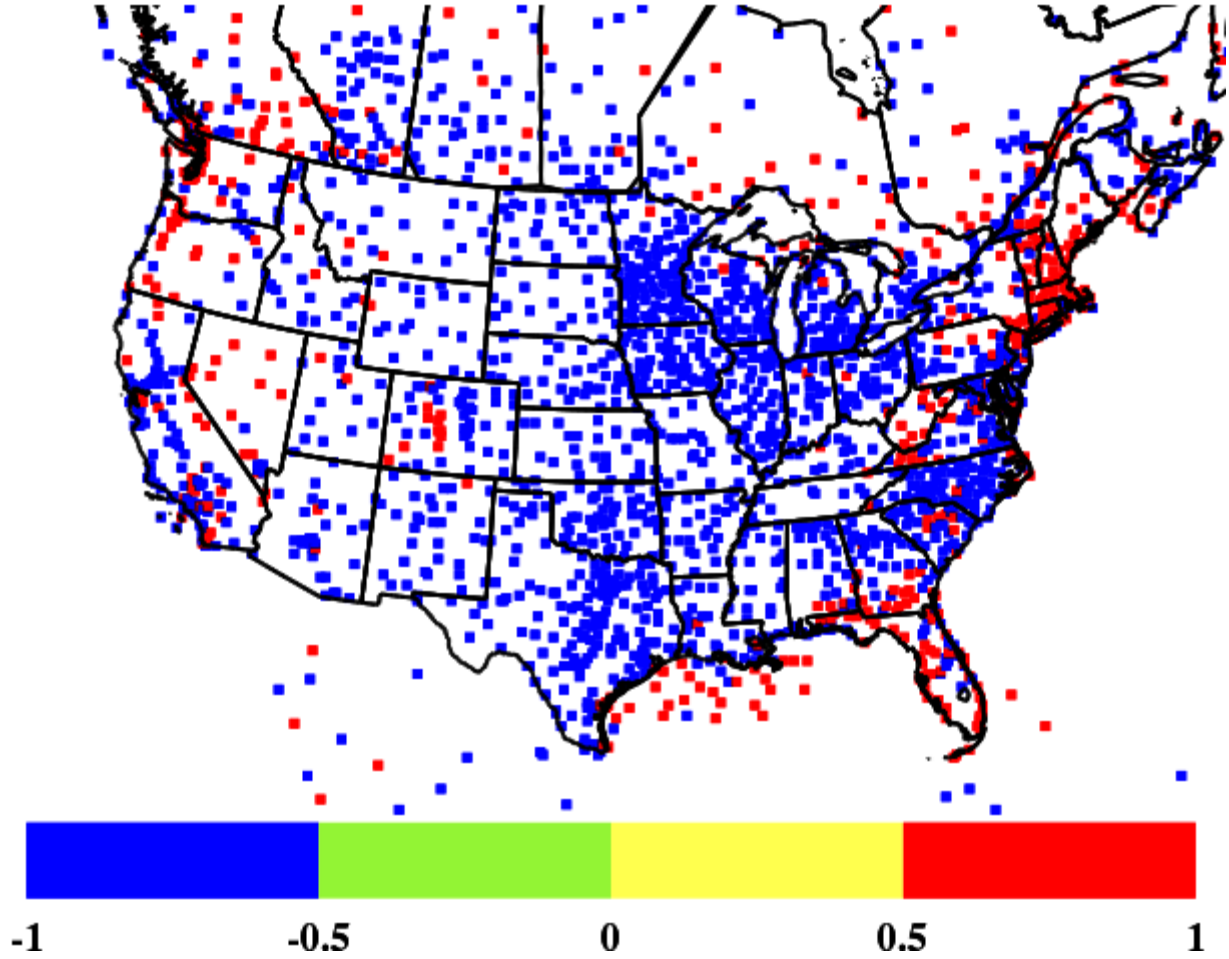

Figure 6-9 *The sign of the difference in the magnitude of bias values (HC – CONTRL) as shown in Figure 6-8. Blue (red) grid locations indicate a decrease (increase) in the magnitude of the bias.*

6.2 Evaluation with Respect to Satellite Skin Temperatures

The following compares the model performance and impact of satellite assimilation against GOES observed satellite skin temperatures. Figure 6-10 gives the bias for the U.S. It shows that the improvement for skin temperature is marginal. It further shows that impact of satellite insolation (INSOL-2) makes the largest impact with the skin temperature adjustments in moisture (SM-1) and HC-1 having minimal impact. The RMSE in Figure 6-11 shows only marginal impact of the assimilation. This seems curious in that the satellite skin temperature adjustment in moisture and heat capacity should perform best against skin temperatures. Yet, it appears that performance against NWS observations are more improved (see Figure 6-1 and Figure 6-4 above). As discussed below this is evidently due to large increase in bias due to the satellite assimilation in the West which overwhelms the domain in the skin temperature statistics. However in the East where the model improves statistics the existence of many more NWS stations make the NWS based improvement much better.

Figure 6-12 shows the spatial depiction of model magnitude of bias change between the final satellite assimilation run (HC-1) and the control run (CNTRL-1). It shows that over most of the East the skin temperature bias is decreased with some areas along the Atlantic coast and high plains showing relatively large improvements. However, in the West there are large consistent areas where the bias is increased by the satellite assimilation. This shows why the skin temperature domain NWS statistics in Figure 6-1 are much better in that they are largely reflecting the large number of NWS stations in the East where the model is reducing the bias.

So, what is the source of the deterioration in the West? For the 2013 period discussed (Chapter 5), in a series of plots (Figure 5-39 through Figure 5-43) it was shown that neither the satellite assimilation of insolation nor satellite vegetation was contributing to the increase in bias in the West. It appeared only after the skin temperature moisture nudging. It was speculated that perhaps satellite skin temperature errors were contributing to the increase in bias. Figure 6-12 shows that the western increase in bias appears in the final satellite assimilation. But which of the three products assimilated (insolation, vegetation and skin temperature moisture nudging) in this run is responsible?

Figure 6-13 provides the spatial depiction of model magnitude of bias change between the satellite solar assimilation run (INSOL-1) and the control run (CNTRL). It appears that this run is the source of the large western bias change. Note that in 2013 that the satellite insolation did not contribute an increased bias and in fact decreased the bias.

Figure 6-14 shows the spatial depiction of the change in magnitude of the bias after the skin temperature moisture nudging is carried out. It shows that the pattern of bias in the West is largely unchanged by this assimilation step.

Thus, it is concluded that for 2012 the insolation assimilation is the source of the increase in bias in the West. However, this bias may be an artifact of the original bias in the control simulation. Figure 6-15 shows the bias in the original control run compared to satellite skin temperature observations. Thus, it may be due to skin temperature errors in the West confounding the analysis.

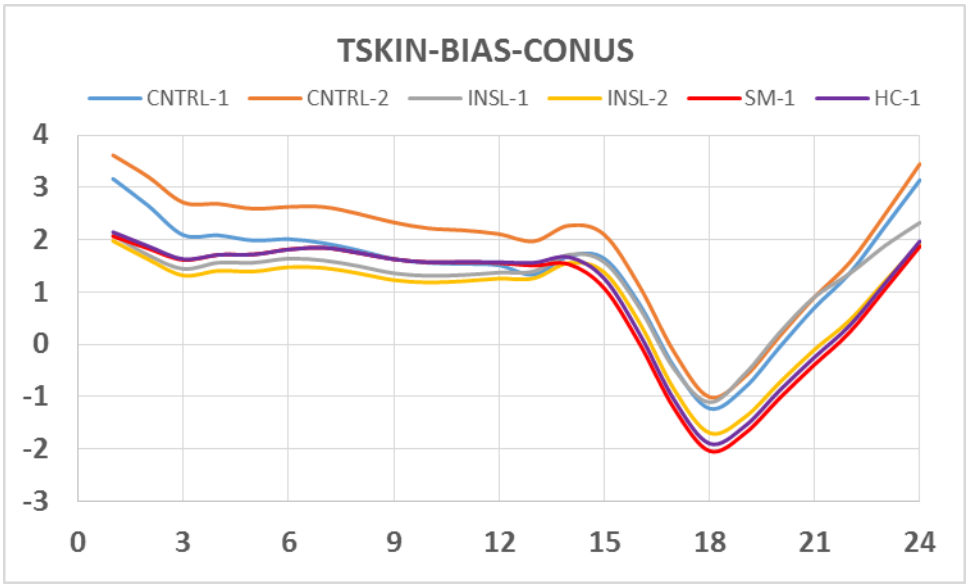

Figure 6-10 *Average hourly bias values (K) for skin temperature for various WRF simulations for the entire 12-km grid for 1-31 August 2012. Values calculated at all 12-km grid points. Values calculated at all 12-km grid points.*

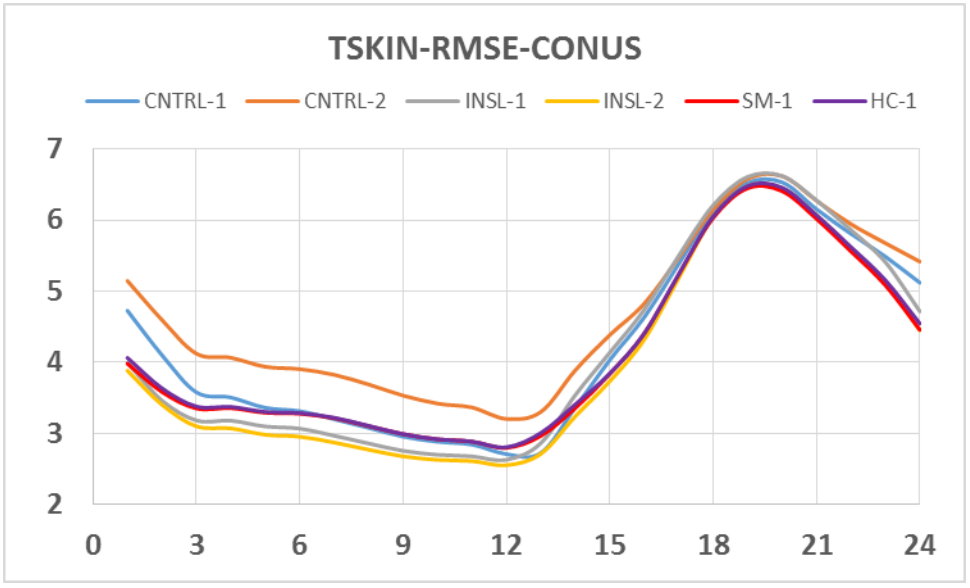

Figure 6-11 *Hourly root mean square error (RMSE) values (K) for skin temperature for various WRF simulations for the entire 12-km grid for 1-31 August 2012. Values calculated at all 12-km grid points.*

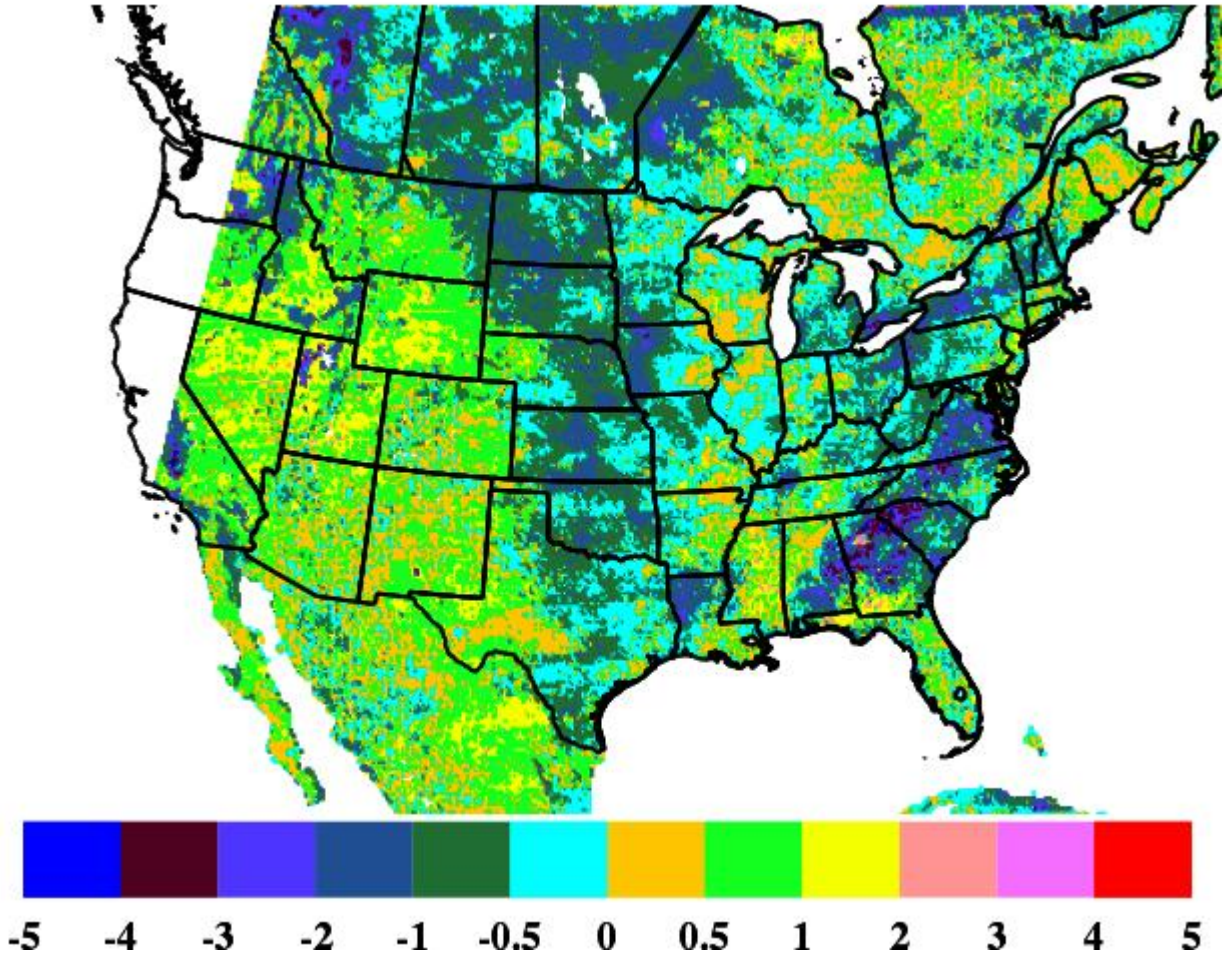

Figure 6-12 *Difference in the magnitudes of the respective bias values (units of degrees K) HC minus CNTRL of skin temperatures for the period 1-31 August 2012 for daytime conditions. Negative values indicate a decrease in the magnitude of the bias and vice versa*.

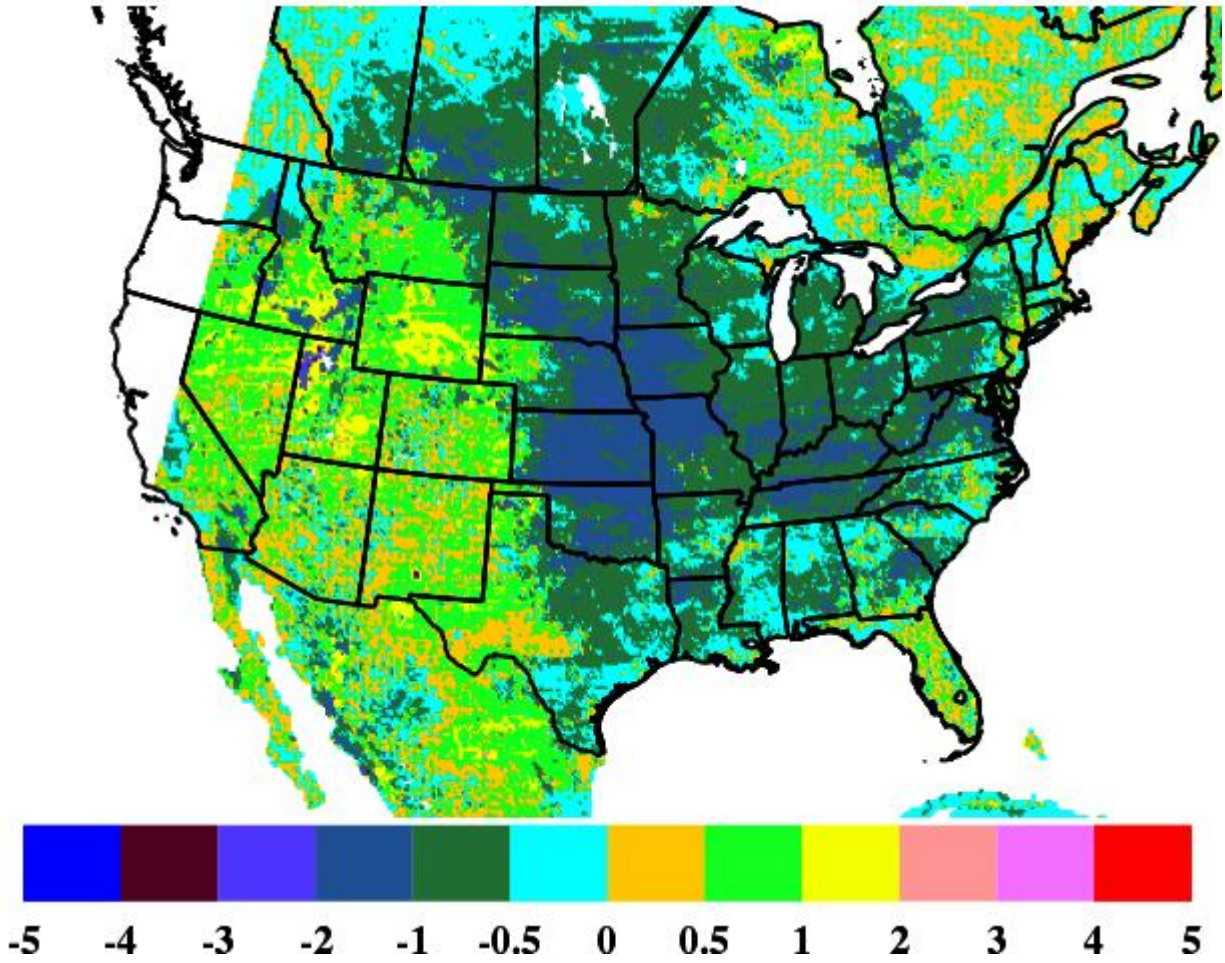

Figure 6-13 *Difference in the magnitudes of the respective bias values (units of degrees K) INSL-1 minus CNTRL of skin temperatures for the period 1-31 August 2012 for daytime conditions. Negative values indicate a decrease in the magnitude of the bias and vice versa*.

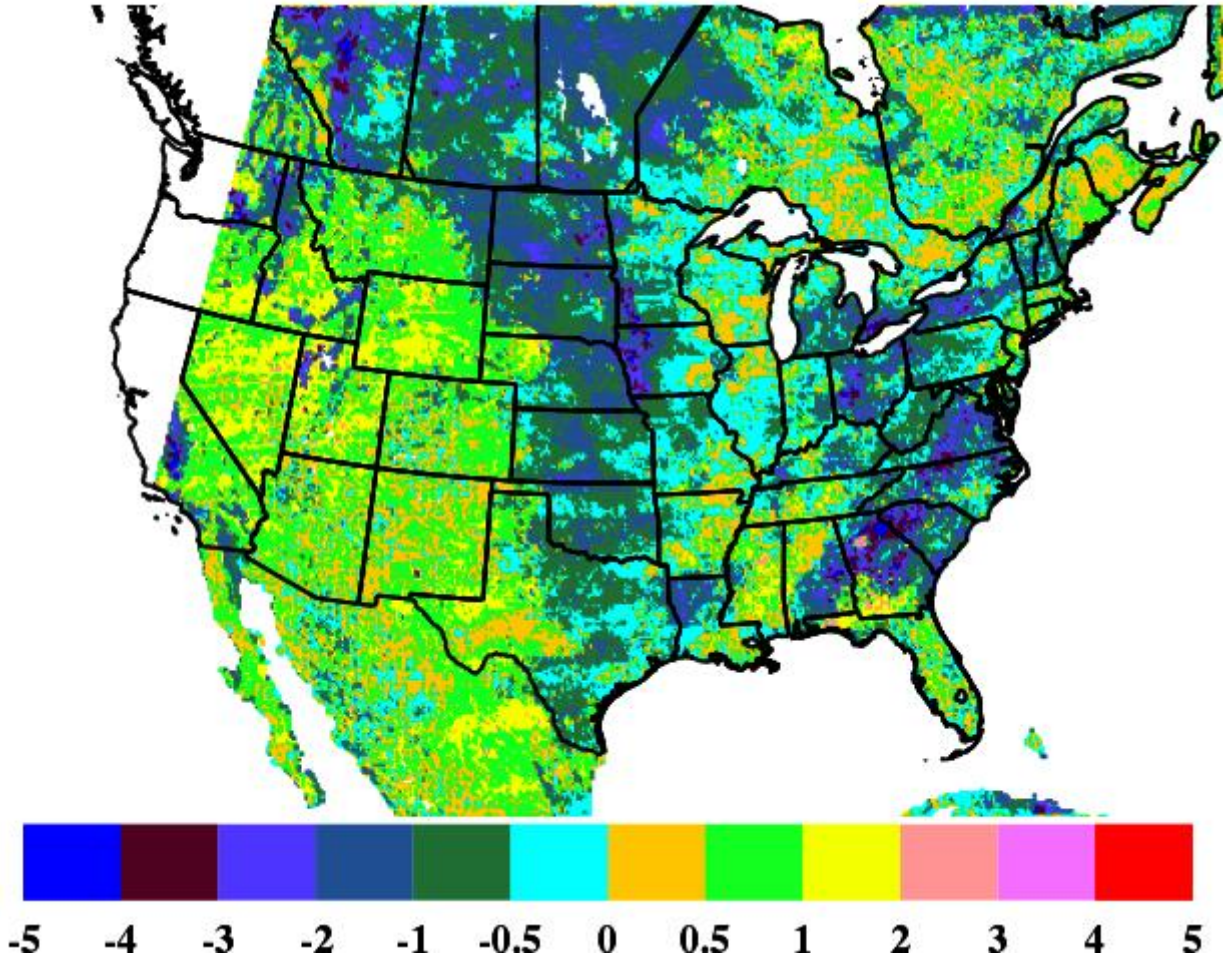

Figure 6-14 *Difference in the magnitudes of the respective bias values (units of degrees K) SM-1 minus CNTRL of skin temperatures for the period 1-31 August 2012 for daytime conditions. Negative values indicate a decrease in the magnitude of the bias and vice versa*.

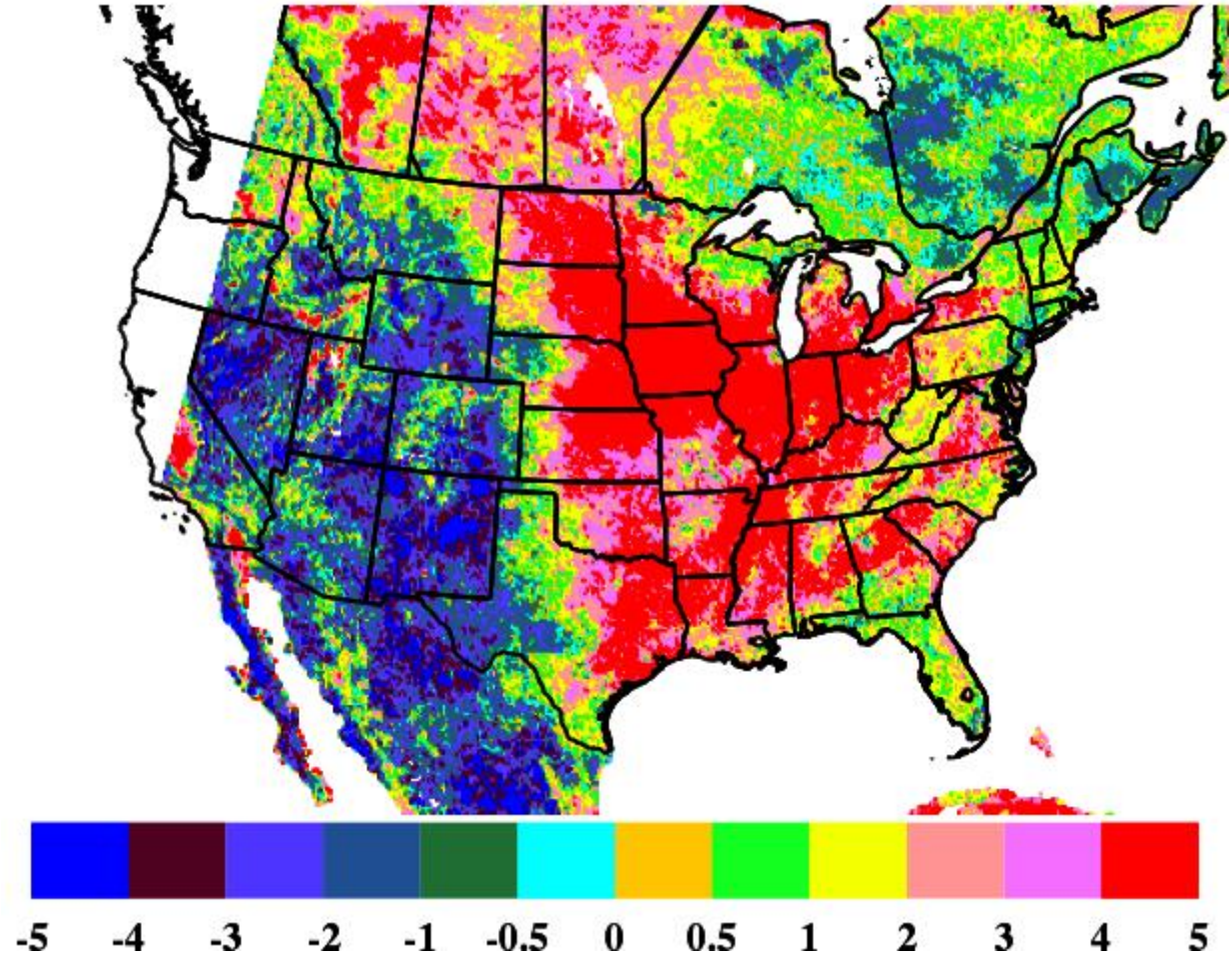

Figure 6-15 *Bias (model minus satellite) of skin temperature (units of degrees K) for the CNTRL simulation for the period 1-31 August 2012 for daytime conditions*.

7 Tendency Model Run

As discussed above in Chapter 4 Task 2, in the P-X scheme the original authors used absolute differences between observed 2m air temperatures and model 2m air temperatures to adjust ground moisture. In the present investigation differences between satellite observed 2m skin temperatures and model skin temperatures were used in a similar fashion to adjust ground moisture. However, satellite skin temperatures can sometimes have absolute errors due to atmospheric corrections or emissivity assumptions. Use of skin temperature tendencies avoids issues with such absolute offsets. In previous applications of adjustments in moisture parameters using satellite skin temperatures (McNider et al. 1994, Mackaro et al. 2011) skin temperature tendencies were used rather than absolute skin temperature differences.

The task will investigate whether differences in tendencies might perform better. That is the difference in rate of change in the model over time (the temperature tendency) will be compared to the temperature change in the satellite data used to adjust moisture. That is, schematically, moisture is adjusted by

$$\Delta w_G = \eta_1 (\partial T_s^{sat} / \partial t - \partial T_s^F / \partial t)_{Morning}$$

Here Δw_G represents the adjustment in soil moisture, $\partial T_s^{sat} / \partial t$ is the satellite skin temperature tendency, $\partial T_s^F / \partial t$ is the model skin temperature tendency, and η_1 represents a nudging time scale. Actual implementation requires a slight different form.

Figure 7-1 below illustrates the key components in nudging the soil moisture using the observed skin temperature tendencies as opposed to using the actual values directly. At each time step, the actual model diagnosed skin temperatures from the past 20 minutes are fitted to a simple linear regression equation. This gives a linear smoothed estimate of the model diagnosed skin temperature 20 minutes prior (Tsm,beg) and at the current time step (Tsm,end). The hourly observed skin temperatures which bracket the time step in question then give the observed skin temperature tendency as in (1), where Ts,obs,beg and Ts,obs,end are the hourly observed skin temperatures and the time scale Δtg is one hour for the observation frequency time. A so-called "quasi-observed" temperature Ts,qobs is then defined as in (2), which uses the observed skin temperature tendency, the temperature Tsm,beg, and the smoothing time scale Δt which is 20 minutes.

$$\frac{\partial T_{S,OBS}}{\partial t} = \frac{T_{S,OBS,END} - T_{S,OBS,BEG}}{\Delta tg} \qquad (1)$$

$$T_{S,QOBS} = T_{SM.BEG} + \frac{\partial T_{S,OBS}}{\partial t} \Delta t \qquad (2)$$

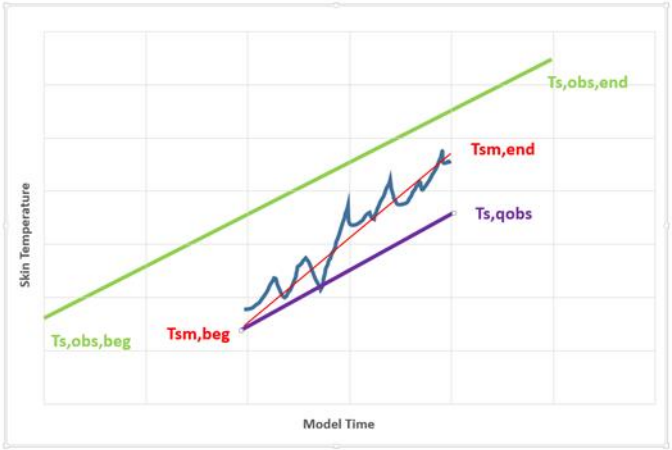

Figure 7-1 Hypothetical plot of various skin temperature variables versus time to illustrate the method of using the observed skin temperature tendency to nudge soil moisture. The blue jagged curve is the actual time step tendency for the WRF model diagnosed skin temperature for a 20 minute period. The red line is a linear regression fitted to the previous curve. The green line represents the hourly trend from the GOES observed skin temperature. See the text for further details.

Equation (3) illustrates, as discussed before in this report, how the soil moisture nudging in the top soil layer is accomplished when actual values of the observed and model skin temperature are utilized. In (3) Ts,obs is the observed skin temperature linearly interpolated to the model time step in question, and Ts,mod is the model skin temperature at the same time. The positive coefficient β1 contains, among other things, the inverse of the nudging time scale. It should be noted that in the equations reflecting the original P-X nudging using 2-m values of temperature and relative humidity the variable differences were of the opposite sign from what is used below, i.e. observed minus the model value. In those cases the coefficients which multiply the differences have negative signs which in reality brings the differences to model minus observed which is the convention shown below and what is used in the code. When skin temperatures are used for the nudging the coefficients are positive.

$$\Delta w_G = \beta_1 \left(T_{s,\mathrm{mod}} - T_{s,obs} \right)_{MORNING} \qquad (3)$$

Applying equation (3) to the hypothetical situation in Figure 7-1, it can be seen that Ts,obs is greater than Ts,mod so that (3) gives a negative value which possibly helps decrease evaporation which leads to warming and driving Ts,mod towards the warmer Ts,obs value.

For tendency nudging equation (3) is replaced with (4).

$$\Delta w_G = \beta_1 \left(T_{sm,end} - T_{s,qobs} \right)_{MORNING} \qquad (4)$$

Applying equation (4) to the hypothetical situation in Figure 7-1, it can be seen that Ts,qobs is less than Tsm,end so that (4) gives a positive value which possibly helps increase evaporation which leads to cooling and driving Tsm,end towards the cooler Ts,qobs value. So this simplistic example shows that you may not always get the same sign of correction between the two approaches.

Code was developed to calculate the tendencies (or quasi- observed temperature) in the P-X scheme to adjust moisture.

Model runs were made for 2013 with the tendency technique. The tendency run was made including the INSL-2 product, the VEG product and HC-1. The model tendency runs adjusting soil moisture are denoted as SM-2 and HC-2 for the accompanying heat capacity adjustment run. These are compared to the previous absolute difference runs described in Chapter 5 – SM-1 and HC-1.

Figure 7-2 shows the comparison between the runs for 2m temperature and Figure 7-3 for humidity. As can be seen for 2m temperature, the tendency adjustment (SM-2) did not perform significantly different during the daytime than the absolute temperature adjustment discussed in Chapter 5 (SM-1). However, the nighttime performance appears to be substantially degraded. It is not clear why this should occur. In fact may be an error in how the time tendency was introduced or in conflict with heat capacity adjustment. In any case, because the absolute difference technique showed dramatic improvement in the East and because the day time

tendency was little changed compared to the absolute difference run, further investigation was felt to be not warranted at the present time.

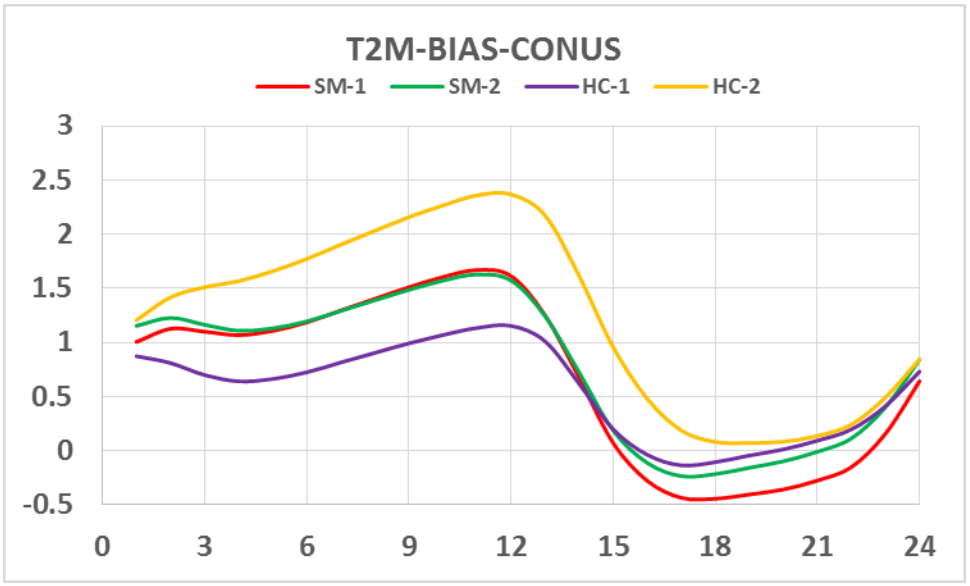

Figure 7-2 *Average hourly bias values (K) for temperature at 2-m for various WRF simulations for the entire 12-km grid for 1-30 September 2013. Values calculated at all surface observing stations.*

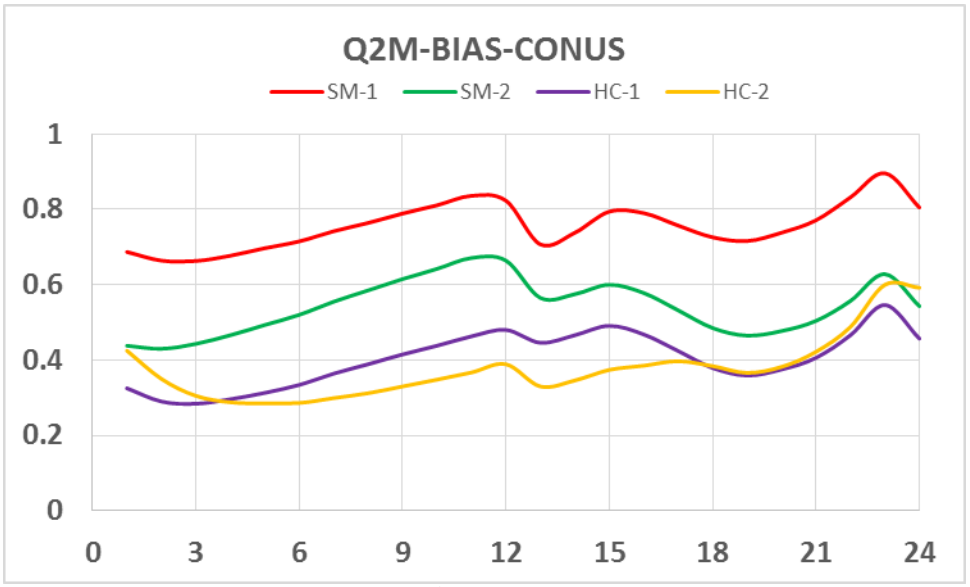

Figure 7-3 *Average hourly bias values (g kg^{-1}) for specific humidity at 2-m for various WRF simulations for the entire 12-km grid for 1-30 September 2013. Values calculated at all surface observing stations.*

8 Quality Assurance/Quality Control of Satellite Skin Temperature Data and Audits of Data Quality

8.1 Introduction

Most of the data used in the model are created and provided by dedicated data centers, such as the background meteorological re-analyses and land use data. These data are regularly used by other researchers and as such go through a set of QA/QC procedures overseen primarily by the National Weather Service and the U.S. Geological Survey (USGS). However, there are three datasets used in the present investigation that are not part of the standard model input. The three datasets include the vegetation fraction, the insolation data and satellite retrieved skin temperature. Previously, our team has evaluated the satellite retrieved insolation data against the ground based pyronameter data (see our last biennium project report). It was also found that the P-X model when run using the default set up altered the vegetation fraction which was an input from the USGS land use data base, and that the altered vegetation fraction appeared to be unreasonable especially in the West. The finding prompted us to use observation based vegetation fraction in the simulation. Derived vegetation fraction from MODIS observation is provided to us for the 2013 simulation period. The dataset has been used by other researchers (Case et al. 2014) with significant improvement in WRF simulations. Thus, only the skin temperature dataset is subjected to a QA/QC procedure which is described below.

The last biennium report (AQRP Project 14-022) stated the quality issues regarding the satellite observation of skin temperature and the rationale for the choice of using the NOAA ALEXI skin temperature product. The NOAA ALEXI single channel retrieval seems to inter-calibrate well with other IR products such as MODIS and with surface in situ data at flux sites around the country. Nevertheless, effective removal of cloud contamination is an important requirement for accurate satellite skin temperature measurement (Inamdar et al., 2008) as cloud contamination can be a critical factor in the usefulness of the skin temperature data. In the present investigation cloud contamination can produce bad data going into the soil moisture nudging and heat capacity adjustment. In the present investigation skin temperature is also used as a model evaluation metric. Here errors can lead to not only poor assessment of model performance, but can also mask improvements in model.

For these reasons, the present investigation has taken an aggressive approach to cloud screening of the surface skin temperature data. Note that the skin temperature data have gone through different screening processes for the 2012 simulation as compared to the 2013 simulation. The latter used the same skin temperature dataset for the simulation in the investigation of AQRP Project 14-022.

Percent of data audited: Since the QA/QC procedures here are different than the physical audit of instrumentation data, it is just as easy to QA/QC all the data. In this activity the technique for the QA/QC for cloud contamination described below was applied for 100% of the data taken from the satellite.

8.2 Skin Temperature Screening for 2013 Simulation

The ALEXI skin temperature product used for the 2013 simulation in this report is the same as that used for the simulation in the last biennium project. As stated in the previous report, the ALEXI product has undergone two different cloud screening algorithms. The ALEXI skin temperature product has used two different cloud screening algorithms. One is the same algorithm used in the GSIP skin temperature and the other involves further screening using established historical skin temperature range to filter out unrealistic values. The second algorithm has only been applied to the data for the 1015-2015 UTC time frames.

A second pass of skin temperature was developed by our team for the purpose of reducing the remaining cloud contaminated data, as well as removing unreasonably high values at the other daytime hours (2115-0315 UTC) in the model domain. The second pass was designed and tested by our team and the detailed description of the design and testing can be found in the report of AQRP Project 14-022. Here, give a brief summary is given of the second pass, which includes historical, spatial and temporal checks. Grid cells classified as water or within a distance of 36 km of a water point are excluded from the screening tests.

The historical check consisted of screening the data for the range of 2115-0315 UTC (late afternoon- evening) against the monthly maximum established from historical data. Any skin temperature which exceeded the maximum values was flagged as cloudy and set to missing.

The spatial check flags a target cell as cloudy and set the skin temperature to missing when the target cell's skin temperature is more than δT_S lower than any grid cell within a distance of R. The spatial check is done in two steps. In the first step, tighter criteria of $\delta Ts = 6$ K and R=40 km are used. After the first step check, the remaining non-missing data go through the second step test with loosened criteria $\delta T_S = 10$ K and R = 300 km. An elevation constraint is also utilized to waive data points with elevation difference of more than 500 m from the target cell.

The temporal check is done in three steps to flag a cloudy cell for the case of (1) the sudden steep decrease of skin temperature, (2) low value after being continuous cloudy for previous hours, and (3) lower value than surrounding cells after being continuous cloudy for previous hours.

On average, this second pass of screening (combination of historical, spatial and temporal checks) removes about 2-11% (depending on the hour) of the data for the 2115-0315 UTC time period.

8.3 Skin Temperature Screening for 2012 Simulation

The ALEXI skin temperature product obtained for the 2012 simulation has not gone through the same historical range screening as for the 2013 simulation by the ALEXI group. Therefore, the team conducted a cloud screening on the skin temperature data with a 2-pass algorithm. The first pass is a tendency test and the second pass is a spatial check.

In the first pass, the skin temperature data are divided into 4 regimens based on the solar zenith angle of the time.

1) The morning regimen that starts after sunrise until solar noon when the surface is warming. Only positive tendency of skin temperature is allowed in this regimen and a datum is flagged as cloudy and invalid if and when it makes the temperature tendency go zero or negative, i.e.

$$\text{For morning regimen } \begin{cases} if\ T_t - T_{t-1} > 0\ then\ T_t\ is\ valid \\ otherwise,\ T_t\ is\ invalid, \end{cases}$$

where T_t is the skin temperature at hourly time step *t*.

2) The afternoon regimen starts shortly after solar noon when skin temperature has reached the daily maximum and on the course of declining until sunset. Thus, only negative tendency is permitted as valid data trend, i.e.

$$\text{For afternoon regimen } \begin{cases} if\ T_t - T_{t+1} > 0\ then\ T_t\ is\ valid \\ otherwise,\ T_t\ is\ invalid; \end{cases}$$

3) The nighttime regimen starts after sunset and ends before sunrise. As the surface is cooling due to longwave radiation, only negative skin temperature tendency is valid in this regimen. The nighttime regimen test is similar to that for the afternoon regimen, but with an addition of a buffer of 0.5 K between the current time step and the nest time step the previous time step is added to account for nighttime turbulence effect, i.e.

$$\text{For nighttime regimen } \begin{cases} if\ T_t - T_{t+1} + 0.5K > 0,\ T_t\ is\ valid \\ otherwise,\ T_t\ is\ invalid; \end{cases}$$

4) The transition regimen includes the transition zone around the solar noon and the immediate hour after when the skin temperature tendency is going from positive to negative. As the direction of tendency around the transition zone is uncertain, a buffer of 2 K between the current time step and the previous or subsequent time step is used to allow for the uncertainty.

$$\text{For transition zone } \begin{cases} if\ T_t - T_{t-1} + 2K > 0\ and\ T_t - T_{t+1} + 2K > 0\ then\ T_t\ is\ valid \\ otherwise,\ T_t\ is\ invalid. \end{cases}$$

The second pass is a spatial check akin to that used in the second pass for the 2013 simulation that is designed to detect discontinuity of skin temperature among the surrounding cells. Unlike the 2-step spatial check for the 2013 simulation, the spatial check for 2012 simulation is only one-step, using a criterion for skin temperature difference (δTs=6K) between the target cell and the surrounding cells within the radius of R=40 km. When the target cell's skin temperature is more than δTs degrees lower than any of the surrounding cell, the target cell is flagged as cloudy and invalid. An elevation constraint is also utilized. Any grid point within the radius R which has an elevation difference of more than 500 m from the target cell is not considered. The second pass is only applied to data at 1015-2315 UTC and 0015 UTC. Figure 8-1 and Figure 8-2 show an example of the skin temperature data undergoing the screening checks. Most of the rejected data points that failed the checks are around the cloud edges.

As a result of the cloud screening, 7 to 43% of the data are flagged as cloudy and rejected depending on the hour and day (see Figure 8-3). In general, the hours with most rejected data are

1815-2215 UTC (afternoon) and the least are 1115-1215 UTC (around sunrise). Over all, the rejecting rate of Pass 1 is 17%, with an extra 5% rejected by Pass 2. The 2-pass cloud screening combined rejected 22% of the data points over the simulation month of August, 2012. Figure 8-4 shows that the ALEXI skin temperature after cloud screening is closely correlated with the MODIS LST product. The daytime correlation is 0.94 with standard deviation of 3.5 K. The nighttime correlation is even higher, at 0.98, with very narrow standard deviation of 1.2 K. The all-time correlation is 0.98 with standard deviation of 2.6 K.

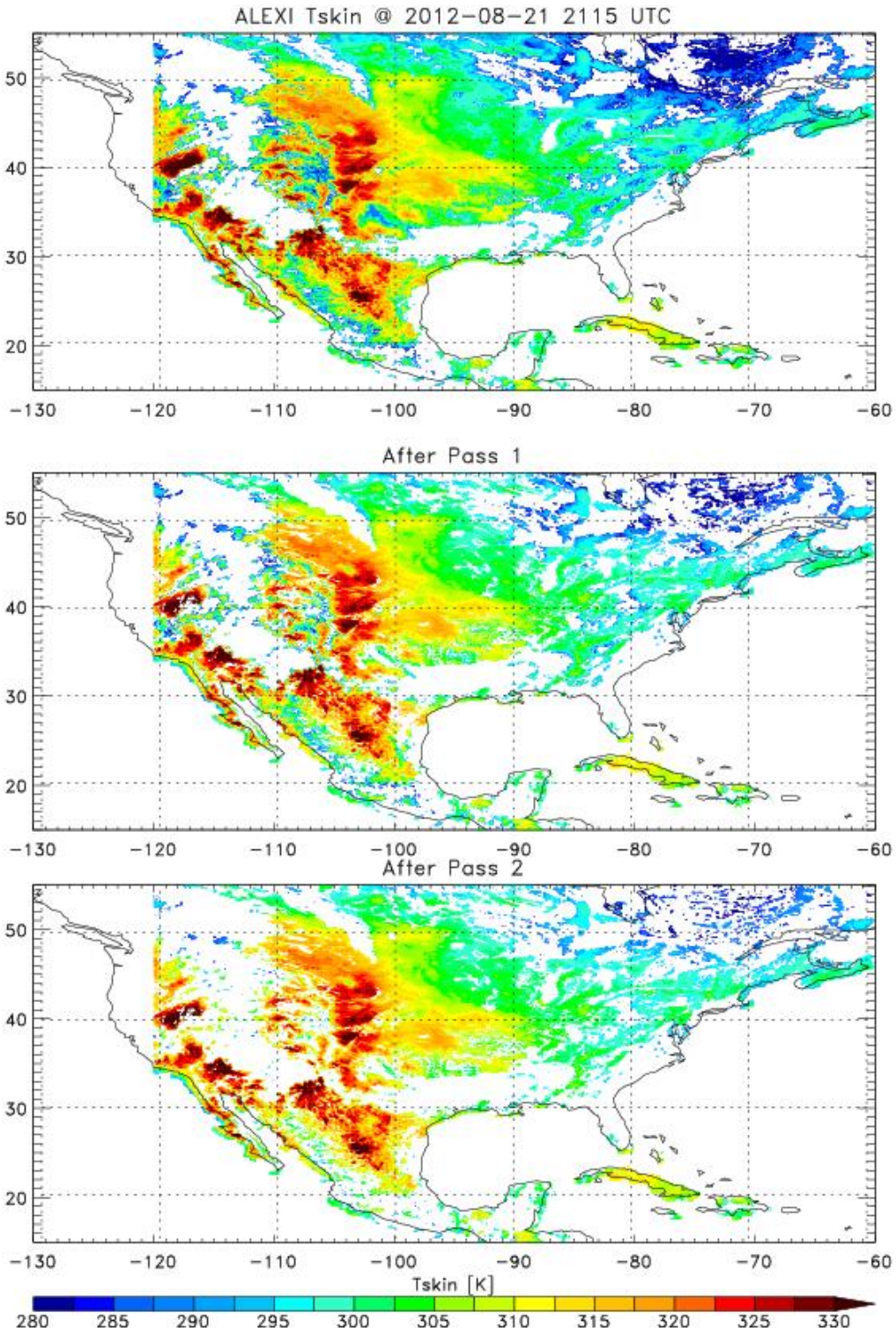

Figure 8-1 Skin temperature images at 2115 UTC August 21, 2012: original ALEXI product (top), after Pass 1 tendency check (middle), and after Pass 2 spatial check (bottom). Mostly, the rejected cells are the suspicious cloudy cells around the cloud edges.

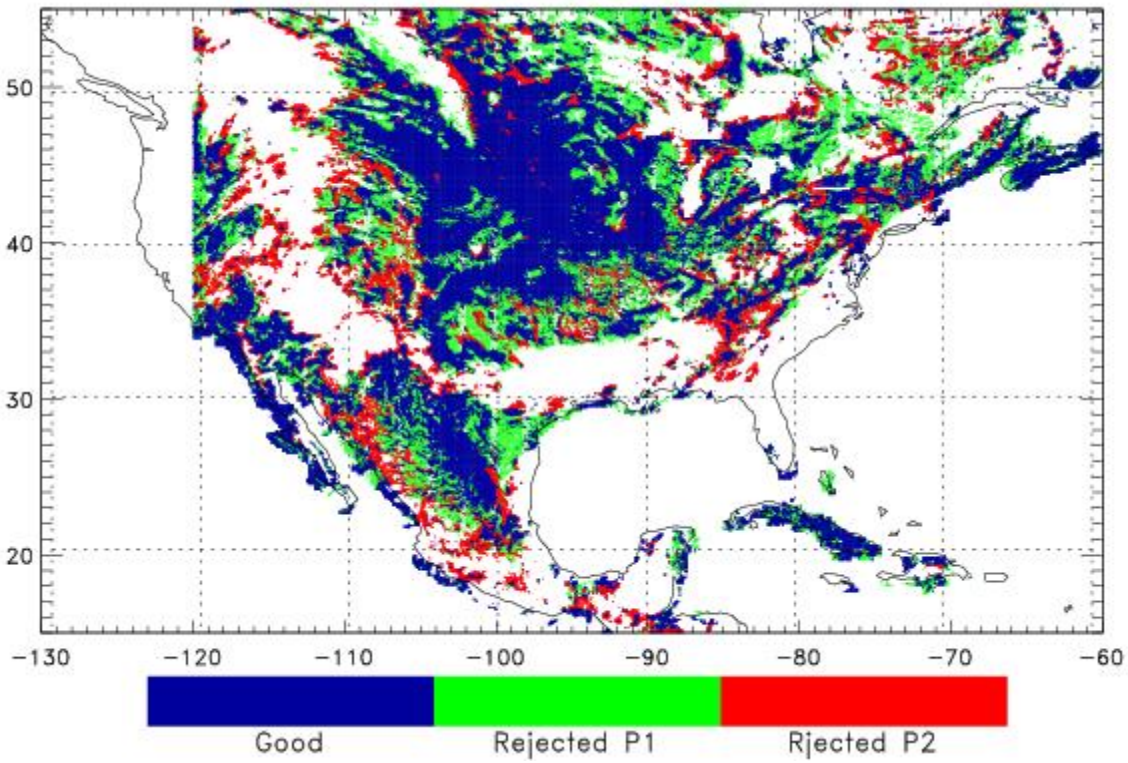

Figure 8-2 Illustration of data points being rejected by the two screening checks, for the same data frame shown in Figure 8-1. Blue indicates data points passed both checks, green shows the ones failed in the tendency check (Pass 1) and red indicates those failed in the spatial check (Pass 2). Note that the areas shown in the figure are only indicative of the data point locations, and not to be interpreted as the portion of points passed/failed the checks as the figure resolution is not fine enough to resolve that.

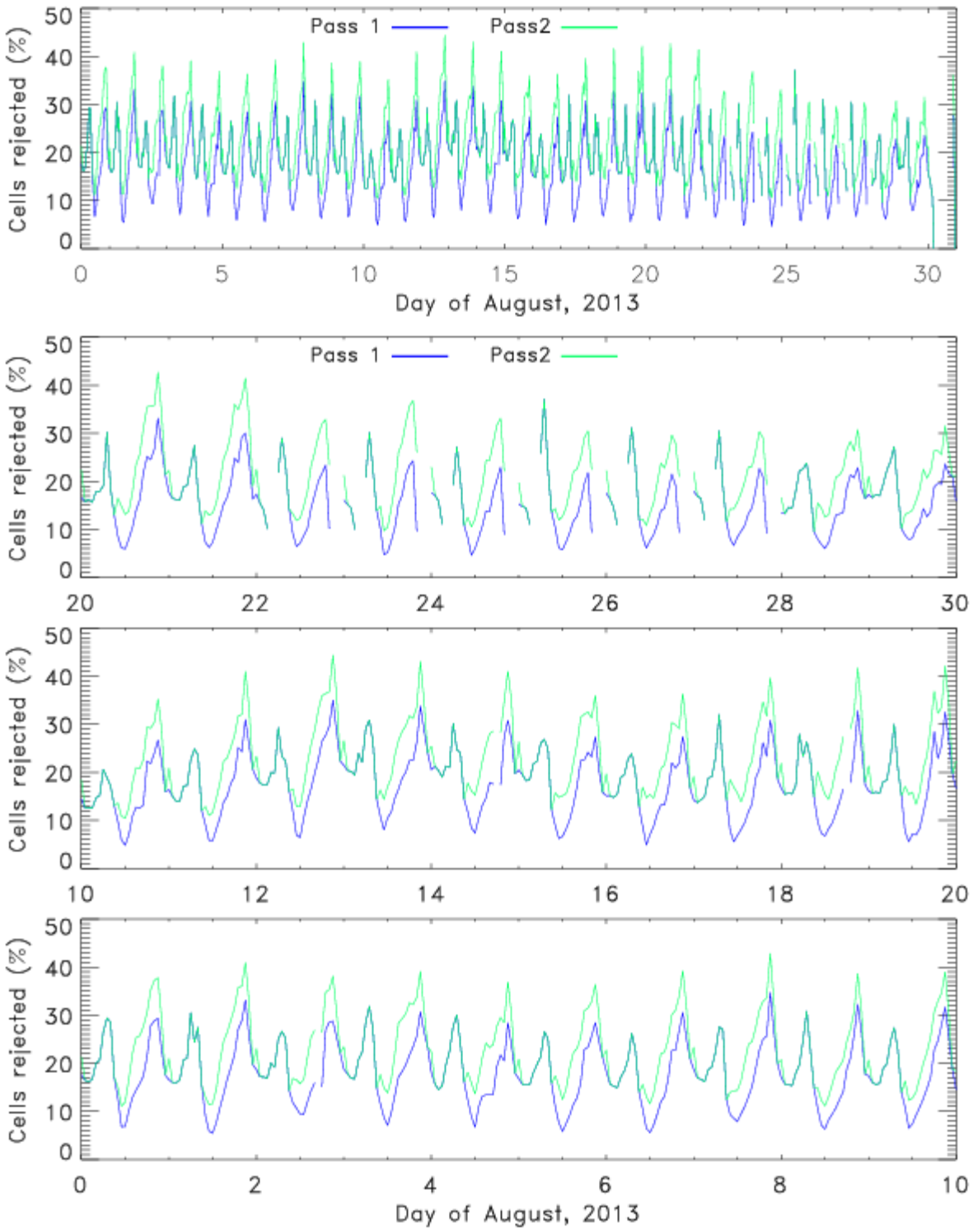

Figure 8-3 Percentage of cells rejected by each screening pass for the simulation month of August, 2012.

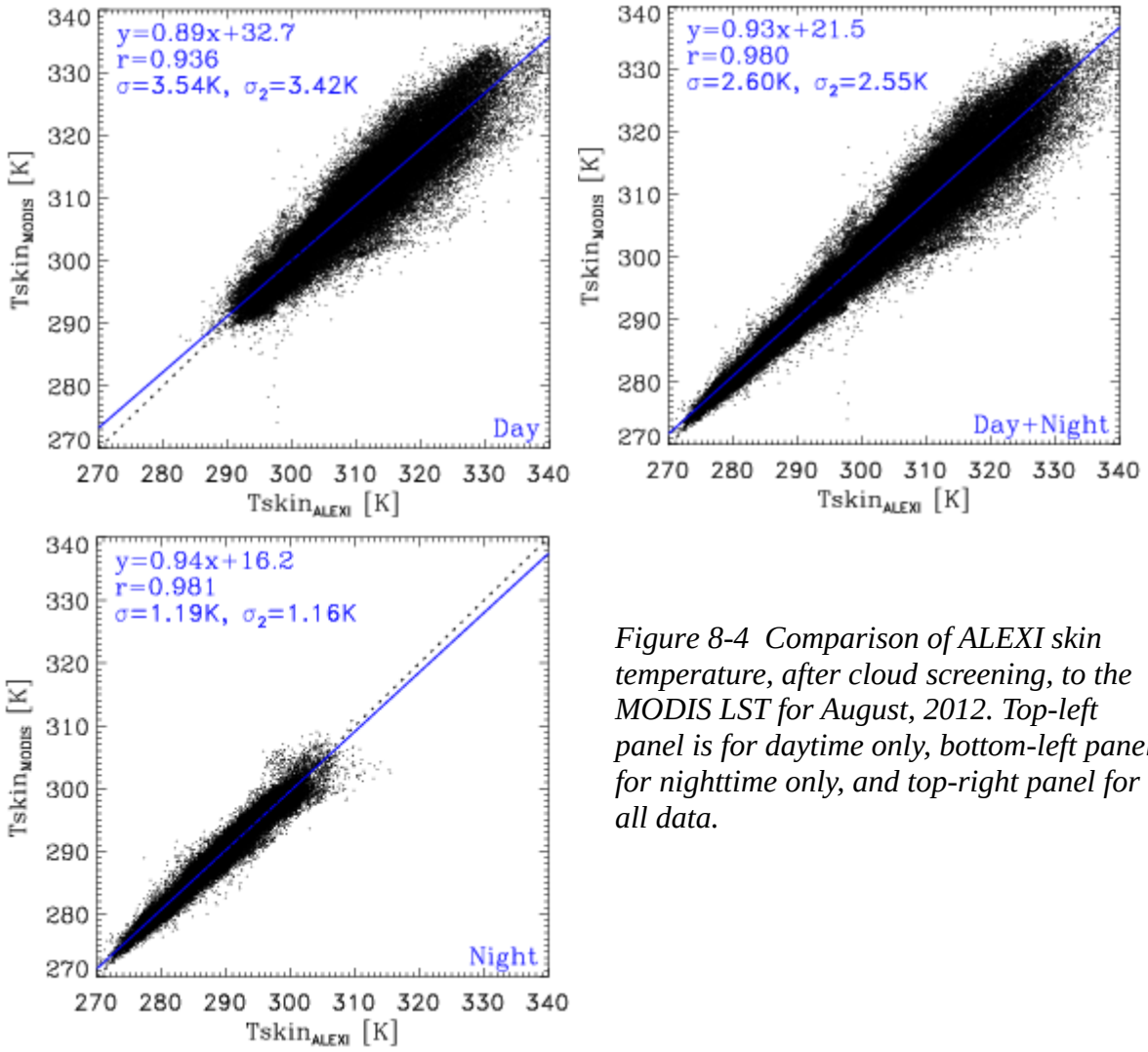

Figure 8-4 Comparison of ALEXI skin temperature, after cloud screening, to the MODIS LST for August, 2012. Top-left panel is for daytime only, bottom-left panel for nighttime only, and top-right panel for all data.

8.4 References

Case, J. L., F. J. LaFontaine, J. R. Bell, G. J. Jedlovec, S. V. Kumar, and C. D. Peters-Lidard, 2014: A Real-Time MODIS Vegetation Product for Land Surface and Numerical Weather Prediction Models, IEEE Transactions on Geoscience and Remote Sensing, 52(3), 1772-1786.

Inamdar, A. K., A. French, S. Hook, G. Vaughan, and W. Luckett (2008), Land surface temperature retrieval at high spatial and temporal resolutions over the southwestern United States, J. Geophys. Res., 113, D07107, doi:10.1029/2007JD009048.

9 Use of Regression Tool to Evaluate the Correlation of Variables/Parameters to Model Residual Errors

The 2012-17 AQRP call suggested that model analysis tools be developed to help understand over or under-prediction of ozone. In the meteorological model there is the same need to understand why 2-m air temperatures (or skin temperatures) are over or under-predicted. A model analysis tool based on forward stepwise regression (Efroymson 1960) to develop a linear regression equation for a selected dependent variable was constructed to be used in the model framework. At each step the variable with the highest correlation with the dependent variable is the candidate for inclusion if certain statistical measures are met. This tool can help determine what variables may be correlated with various surface energy budget errors or other model residual errors.

The following describes the application of the regression tool to understand those variables most correlated with the remaining error in the model.

Forward stepwise regression (Efroymson 1960) is one method of selecting independent variables to develop a linear regression equation for a selected dependent variable. At each step the variable with the highest correlation with the dependent variable is the candidate for inclusion if certain statistical measures are met. In addition, at each step, variables which have been selected previously are examined to see if they can be excluded. As mentioned by Miller (2002), this approach does not guarantee that the best subset will be chosen. F90 subroutines to implement this approach developed by Miller (2002) have been obtained from the web (http://jblevins.org/mirror/amiller/). After revisions the local code was tested against the Hald steam data in Draper and Smith (1998) with the results being verified in that example. The local version of the code is able to select subsets of a WRF simulation according to a wide range of criteria including region and time of day. The input data for the regression model consists of 85 two-dimensional variables related to the model surface.

In each of the tables below there are five columns. The first is the name of the independent variable. The second is the regression calculated coefficient for the respective independent variable. The third (R2) is the square of the multiple correlation coefficient and is a measure of how much of the variance of the independent variable is explained by the model including all the chosen independent variables up to the current variable. The fourth (AR2) is the adjusted square of the multiple correlation coefficient and accounts for the influence of the number of degrees of freedom in the regression model. The fifth (DIFF) is the difference between consecutive AR2 values and gives the contribution for that individual variable. R2, AR2, and DIFF are in units of percentages. These are preliminary results so not every chosen independent variable will be discussed.

Table 9-1 shows the results when the bias of 2-m temperature (model-control) is the dependent variable for land points and daytime conditions for the WRF VEG simulation. As mentioned elsewhere in the report, the VEG run has GOES insolation, model albedo, and MODIS greenness fraction but no soil moisture nudging and no heat capacity adjustment. The first variable chosen which explains about 15% of the variance is the 2-m specific humidity bias (model – observed). For dry conditions this bias is a negative number which when multiplied by the negative

coefficient (-0.27267) gives a positive contribution to the 2-m temperature bias. Horizontal plots of the 2-m temperature bias and the 2-m specific humidity bias (not shown) show clearly large areas with a positive 2-m temperature bias and a corresponding negative 2-m specific humidity bias. This is evidence that the regression model is giving results that are consistent with the horizontal features just mentioned.

Table 9-2 shows the results when the difference of skin temperature (model – observed) is the dependent variable for land points and daytime conditions for the WRF VEG simulation. The first variable chosen which explains about 13% of the variance is the terrain elevation (TERR). The second variable chosen which explains about 4% of the variance is the phase angle (PHASE), which is a

VARIABLE	COEFFICIENT	R2	AR2	DIFF
Q2_DIFF	-0.27267E+00	15.360	15.360	15.360
GFLUX	0.12089E-01	21.468	21.468	6.108
WSPEED_DIFF	0.29400E+00	24.481	24.481	3.013
PSFC	0.50567E-02	28.022	28.022	3.541
DEDX2	0.57958E-01	30.321	30.321	2.300
RATIOP	0.20819E+00	31.826	31.826	1.504
RATIO_OBSP	0.20243E+00	34.321	34.321	2.496
HFLUX	0.18472E-02	35.208	35.208	0.886
CONSTANT	0.55221E+01	0.000	0.000	0.000

Table 9-1 Multiple linear regression results for the bias of 2-m temperature (model – observed) for land points and daytime conditions for the WRF VEG simulation for 1-30 September 2013. "VARIABLE" is the name of the independent variable. "COEEFICIENT" is the regression calculated coefficient for the respective independent variable. "R2" is the square of the multiple correlation coefficient. "AR2" is the adjusted square of the multiple correlation coefficient "DIFF" is the difference between consecutive AR2 values. R2, AR2, and DIFF are in units of percentages. See the text for additional details.

VARIABLE	COEFFICIENT	R2	AR2	DIFF
TERR	-0.16307E-02	12.757	12.757	12.757
PHASE	0.28160E-01	17.234	17.234	4.477
SHRUBLAND	-0.26063E-01	20.718	20.718	3.484
WATER	0.53976E-01	21.404	21.404	0.686
CONSTANT	0.15093E+01	0.000	0.000	0.000

Table 9-2 *Multiple linear regression results for the difference of skin temperature (model – observed) for land points and daytime conditions for the WRF VEG simulation for 1-30 September 2013. Table headings same as in Table 9-1.*

function of the solar zenith angle, the GOES zenith angle, and the relative azimuth angle. The relative azimuth angle is the difference between the solar and GOES azimuth angles. The third variable chosen which explains about 3% of the variance is the percentage of landuse that is in

the category of shrubland (SHRUBLAND). This regression model is not impressive, but it did suggest the next experiment.

Table 9-3 shows the results when the difference of skin temperature (model – observed) is again the dependent variable for land points and daytime conditions for the WRF VEG simulation but restricted only to those model grid points where the shrubland percentage was greater than or equal to 20%. This landuse category is primarily in the western United States. The initial list of independent variables was restricted to mainly geophysical parameters as opposed to meteorological variables. The first variable chosen which

VARIABLE	COEFFICIENT	R2	AR2	DIFF
PHASE	0.13314E+01	7.611	7.611	7.611
GSW-KERNEL-1	0.27570E-02	16.506	16.506	8.895
PSFC	0.13712E-01	21.944	21.944	5.438
SHRUBLAND	-0.28752E-01	24.856	24.856	2.912
SCAT_ANG	-0.12502E+01	27.700	27.700	2.844
ZEN_GOES	-0.11518E+00	28.979	28.979	1.279
GSW-KERNEL-2	0.14106E-01	30.052	30.052	1.073
ZEN_DIFF	-0.37480E-01	30.605	30.605	0.554
CONSTANT	-0.83358E+01	0.000	0.000	0.000

Table 9-3 *Multiple linear regression results for the difference of skin temperature (model – observed) for land points and daytime conditions for the WRF VEG simulation for 1-30 September 2013 but restricted to model grid points having 20% or more of a landuse classification of shrub land. Table headings same as in Table 9-1.*

explains about 7% of the variance is the phase angle (PHASE), and the second one chosen which explains about 9% of the variance is the kernel function GSW-KERNEL-1. Minnus and Khayer (2000) gave evidence that the difference in skin temperatures observed by different GOES satellites closely followed land bidirectional reflectance distribution functions (BRDF). Using one of the BRDF models discussed in Maignanet et al. (2004) two so-called "kernel functions) KERNEL-1 and KERNAL-2 were calculated. These are complex trigonometric functions of various angles related to solar and satellite positions. The accompanying functions GSW-KERNEL-1 and GSW-KERNEL-2 are the previous kernel functions multiplied by the net downward shortwave radiation at the surface. The total variance explained by the regression model in Table 9-3 is about 30%. This suggests that at least for some regions and some landuse types the observed GOES skin temperatures may be influenced by BRDF issues.

References

Draper, N. R. and H. Smith, 1998: Applied Regression Analysis, Third Edition, John Wiley and Sons, Inc., 706 pp.

Efroymson, M.A., 1960: Multiple Regression Analysis, in Mathematical Methods for Digital Computers, Vol 1, wiley, pp 191-203.

Maignan, F., F.-M. Breon, abd R. Lacaze, 2004: Bidirectional reflectance of earth targets: Evaluation of analytical models using a large set of spaceborne measurements with an emphasis on the Hot Spot. *Remote Sensing of the Environment*, **90**. 210-220.

Miller, A, 2002: Subset Selection in Regression, Second Edition, CRC Press, 234 pp.

Minnus, P and M. M. Khayer, 2000: Anisotropy of land surface skin temperature derived from satellite data. *J. Appl. Meteor*., **39**, 1117-1129.

10 Summary and Conclusions

Under this activity a technique was developed which diagnoses a skin temperature consistent with the surface fluxes in the P-X model. This skin temperature is then used in a technique to nudge soil moisture (see equations (2-2) and (2-3)). Fundamentally, if the model temperatures are lower than the observed temperature, then soil moisture is decreased. If the model temperatures are greater than the observed temperature, then soil moisture is increased. This is consistent with that of P–X model since they argued that soil moisture is ill-observed and thus needs an indirect observational adjustment. Techniques have been implemented within the WRF framework which allow the nudging of soil moisture using satellite skin temperatures as opposed to the NWS soil moisture nudging in the original P-X model.

A base control run with no satellite assimilation was defined based on EPA model set-ups (see Chapter 3). This control run in general had a large daytime warm bias both day and night (see Chapter 5).

As part of this activity, a satellite derived insolation was used in place of the WRF modeled insolation for all runs except the control runs (see Chapter 5). The satellite derived insolation had better performance against pyranometer data.

The model case with satellite insolation and satellite albedo produced poorer performance and made the model further too warm. This was because the satellite albedo was too low giving extra energy into the surface of an already too warm model. The model case with satellite insolation and model albedo (INSOL-2) showed improved daytime performance and was used in subsequent satellite assimilation cases.

The addition of the satellite vegetation run (VEG) further improved the model performance. As was noted in the last biennium report, the standard vegetation field used by the P-X scheme had substantial errors especially in the West. It was replaced by the USGS vegetative fraction which performed much better. The improvement this year is against the USGS data.

The skin temperature nudging of moisture experiment (SM-1, SM-2 -which included the satellite insolation and satellite vegetation) further reduced the warm daytime bias in comparison with NWS observations.
The improvements were somewhat stronger in the Eastern U.S. with skin temperature as a metric. In fact in looking at the spatial plots for skin temperature there was a clear delineation

between improvement in the East and degradation in the West. Thus, while the domain average statistics showed improvement they were degraded by the performance in the West.

Comparisons for the Texas domain showed a similar pattern. Performance on the whole was better than for the domain in that Texas had smaller areas in the west suffering from degradation.

The source of this degradation in the West in the satellite moisture runs in 2013 is not fully clear. The original control case (CNTRL) did show a very strong cool bias in the west compared to satellite skin temperatures. But this initial model cool bias was not strongly evident in the NWS comparisons. Thus, it is tentatively concluded that the model cold bias in the West may be due to satellite skin temperature errors being too warm. It was noted that in the last biennium project that the NOAA GSIP operational product was found to be much too warm in the West. A switch was made to the NOAA ALEXI product for the last biennium project and for this year. However, it appears that the ALEXI product may also be too warm in the West.

While the warm bias in the skin temperature may explain the difference between the model control case and the skin temperature comparison, the actual degradation in performance against skin temperatures with the satellite assimilation is odd. Under the skin temperature assimilation technique both for soil moisture and heat capacity, even if the skin temperatures were in error the model should move toward the satellite skin temperature. However, the spatial results compared to the satellite assimilation runs show the model actually moving further from the satellite skin temperatures.

This could come from the morning skin temperature (when the moisture nudging is carried out) from the satellite not being representative of later times. The sign of the difference between the model and observations might change after the assimilation period. In this case the model in the morning assimilation would be driven to a moisture value that made it agree better with the satellite. For example if the model was too cool compared to a morning skin temperature then moisture would be reduced making the model warmer. But if the afternoon difference between the model and satellite were less than the model or even of opposite sign than in the morning this may cause over drying leading to temperatures that are too high compared to observations. This will require further analysis by comparing the magnitude and sign of the model bias through the day to see whether the bias changes.

The unrepresentativeness of the western morning skin temperatures may be consistent with studies (Minnish et al. 2000) that show that oblique viewing angles can lead to bidirectional effects on skin temperature. In the morning in the West a satellite to the east might see more sun exposed topography or sun exposed tall vegetation compared to what a satellite to the west might see. The regression tool used in Chapter 9 also appears to show that satellite view angles appear to have a possible influence on the remaining model error. This will be further investigated under some follow-on studies supported by the NASA AQAST program.

The degradation in the West should not detract from what appears to be a solid improvement in the model performance using the satellite assimilation over most of the domain. First the model skin temperature nudging of moisture worked well in reducing the warm bias in the model over much of the East. When the heat capacity adjustment is added the assimilation works as it

should. It decreases the nighttime over prediction and actually compensates for the increase in nighttime error introduced by increasing moisture which increases the heat capacity.

When only the Eastern domain is considered the improvement in performance is slightly better. This is especially true if the latter part of the assimilation is used where more grid points have been touched by the assimilation.

Thus, in conclusion, the satellite assimilation improves model performance compared to NWS observations especially in bias. The assimilation in general seems to improve model comparison to profiler wind data with substantial improvement in the low level jet at night. For some profilers there was also a degradation in daytime winds aloft. Performance against NWS surface winds were more mixed but for the Texas domain there was slight improvement in wind speed performance. While the RMSE statistic was improved the improvement was not large and there is considerable room for improvement.

In looking at the local performance the satellite assimilation model reduced the warm bias around Houston and the cool bias over the city center. But, in general it still left a warm bias around the region.

The application of the model to an additional evaluation period (August 2012) was also a success. The model showed improvement against NWS observations across the whole domain and for the Texas domain. The RMSE statistic was also improved though not as large as the improvement in bias. As for the 2013 case the comparison of model performance against satellite skin temperatures showed a much greater improvement in the East than West.

10.1 References

McNider, R.T., A.J. Song, D.M. Casey, P.J. Wetzel, W.L. Crosson, and R.M. Rabin, 1994: Toward a dynamic-thermodynamic assimilation of satellite surface temperature in numerical atmospheric models. *Mon. Wea. Rev.,* **122,** 2784-2803.

Minnish, P and M. M. Khayer, 2000: Anisotropy of land surface skin temperature derived from satellite data. *J. Appl. Meteor*., **39**, 1117-1129.

11 Recommendations Based on Project Results

In doing a final evaluation of the project there are several recommendations in the use of the products investigated.

(1) **Satellite Insolation**: Based on the 2012 and 2013 study periods use of satellite insolation improves model performance for both years. Thus, it is suggested that satellite insolation be used to replace model insolation in future retrospective modeling scenarios. However, there is caveat in that if the White et al. 2017 cloud assimilation provides nearly as good of performance then this would be a more physically consistent approach for clouds in the model.

(2) **Satellite Vegetation:** The results here for the use of satellite vegetation fraction also improved performance especially in the West. This is also consistent with the findings of

Ran et al. 2016. Thus, if the Pleim-Xiu scheme is used in future TCEQ simulations then satellite vegetation should be included.

(3) **Skin Temperature Nudging for Surface Moisture and Heat Capacity:** In the 2013 simulation, moisture nudging greatly improved the daytime 2m temperature performance over the Eastern U.S. However, it did deteriorate nighttime performance by making the soil too moist leading to nighttime temperatures that were too warm. When the heat capacity adjustment was carried out it compensated for this so that temperatures improved day and night compared to the control. Figures 5-17 and 5-23 for the Texas domain in 2013 show that 2m temperature was improved for the state as a whole when moisture and heat capacity were adjusted. The 2012 case did not provide as strong an advantage but still slightly improved results in the daytime. Thus, it is recommended that the satellite moisture and heat capacity adjustments should be tested in future modeling.

(4) **Analysis of the Large Scale Analyses:** As noted by Otte (2008), although FDDA nudging to large scale analyses is generally thought to improve model performance this may not be the case if the large scale analysis has substantial error. Furthermore, the effectiveness of satellite data assimilation will be reduced if the analysis is not consistent with the adjustments made based on satellite data assimilation. Essentially, in such cases, FDDA nudging will be constricting the impact of assimilation and forcing the model back to its original state. Late in this study it was found that the 2012 NAM-12 forecasts that used the same analysis for initialization also was too hot and too dry over most of the U.S., and produced much less cloud cover than observed (http://www.emc.ncep.noaa.gov/mmb/research/nearsfc/fvs_dir/AUG2012_diurnal_dir/T2M_00_diurnal_AUG2012_east_NAM.gif). This is the reason that the use of satellite insolation made such an improvement for 2012. It is recommended that before a decision on using large scale analysis for nudging in future modeling, an assessment of the large scale analysis should be carried out. It would be best for the air quality community to develop a standard analysis package that would provide diagnostics of several standard analyses that could guide analysis selection. This is consistent with conclusions stated in Otte (2008).

(5) **Special Caution for Extremely Dry Years:** While hot dry years favor ozone production and reduce surface loss by vegetation, it appears based on Figure 6-7 that the drought year 2012 had the largest errors. This also seems consistent with the large errors in the TEXAQS 2000 cases, where we had an extremely dry year. It appears that models of surface moisture perhaps do well in the East when precipitation dominates the moisture budget but do poorly when the moisture budget is controlled by non-observed parameters such as canopy resistance, soil moisture diffusion, etc. It is recommended that using PBL schemes, such as the P-X scheme, which have the ability to correct moisture and temperature levels using NWS observations, or the present technique using satellite data, have the best ability to overcome model errors.

References:

Otte, T.L., 2008. The impact of nudging in the meteorological model for retrospective air quality simulations. Part II: Evaluating collocated meteorological and air quality observations. *Journal of Applied Meteorology and Climatology*, *47*(7), pp.1868-1887.

Ran, L., Pleim, J., Gilliam, R., Binkowski, F.S., Hogrefe, C. and Band, L., 2016. Improved meteorology from an updated WRF/CMAQ modeling system with MODIS vegetation and albedo. *Journal of Geophysical Research: Atmospheres*, *121*(5), pp.2393-2415.

White, Andrew T., Arastoo Pour-Biazar, Richard T. McNider, Kevin Doty and Bright Dornblaser, 2017: Improving cloud simulation in retrospective meteorological modeling simulations through assimilation of GOES satellite observations for air quality studies. *Monthly. Weather Review.* In Press.

12 Acknowledgements and Disclaimer

This research was financed in part by a grant from the Texas Commission on Environmental Quality (TCEQ), administered by The University of Texas through the Air Quality Research Program and in part by NASA Air Quality Applied Sciences Team (AQAST) The contents, findings, opinions, and conclusions are the work of the author(s) and do not necessarily represent the findings, opinions, or conclusions of the TCEQ or NASA.

13 Appendix A: Acronyms

ALEXI	Atmosphere-Land Exchange Inverse
DISCOVER-AQ	Deriving Information on Surface conditions from Column and Vertically Resolved Observations Relevant to Air Quality
CLASS	Comprehensive Large Array-Data Stewardship System
FIFE	First International Satellite Land Surface Climatology Field Experiment
GEWEX	Global Energy and Water Cycle Experiment
GSIP	GOES Surface and Insolation Products
GOES	Geostationary Operational Environmental Satellite
IR	Infrared
LST	Land Surface Temperature
MODIS	The Moderate-resolution Imaging Spectroradiometer
MSFC	Marshall Space Flight Center
NASA	National Aeronautics and Space Administration
NCDC	National Climatic Data Center
NCEP	National Centers for Environmental Prediction
NOAA	National Oceanic and Atmospheric Administration
Noah	NCEP-Oregon State University-Air Force-Hydrologic Research Library
NWS	National Weather Service

PX	Pleim-Xiu
QA	Quality Assurance
RMSE	Root Mean Square Error
SCAN	Soil Climate Analysis Network
SIP	State Implementation Plan
SPoRT	Short-term Prediction Research and Transition Center (http://weather.msfc.nasa.gov/sport/)
SURFRAD	Surface Radiation budget network
TCEQ	Texas Commission on Environmental Quality
TOA	Top Of Atmosphere
UAH	University of Alabama in Huntsville
USDA	United States Department of Agriculture
USGS	United States Geological Survey
UTC	Coordinated Universal Time
WRF	Weather Research and Forecasting Model
WPS	WRF Preprocessing System

14 Appendix B: WRF Control Configuration

The following provides the raw Namelist configuration for the WRF control runs under this project. See Chapter 3 for explanation.

```
&time_control
 run_days                            = RUN_DAYS,
 run_hours                           = RUN_HOURS,
 run_minutes                         = RUN_MINUTES,
 run_seconds                         = RUN_SECONDS,
 start_year                          = START_YEAR,
 start_month                         = START_MONTH,
 start_day                           = START_DAY,
 start_hour                          = START_HOUR,
 start_minute                        = START_MINUTE,
 start_second                        = START_SECOND,
 end_year                            = END_YEAR,
 end_month                           = END_MONTH,
 end_day                             = END_DAY,
 end_hour                            = END_HOUR,
 end_minute                          = END_MINUTE,
 end_second                          = END_SECOND,
 interval_seconds                    = 3600,
 input_from_file                     = .true.,
 history_interval                    = 60,
 frames_per_outfile                  = 1,
 restart                             = .false.,
 restart_interval                    = 999999,
 io_form_history                     = 2
 io_form_restart                     = 2
```

```
io_form_input                       = 2
io_form_boundary                    = 2
io_form_auxinput4                   = 2
auxinput4_inname                    = 'wrflowinp_d<domain>'
auxinput4_interval                  = 60
debug_level                         = 1

auxinput7_inname             = "ALEXI_SPORT.d<domain>.<date>.nc"
auxinput7_interval_m               = 60
frames_per_auxinput7               = 24
io_form_auxinput7                  = 2

auxinput12_inname            = "GREENFRCT.d<domain>.<date>.nc"
auxinput12_interval_m              = 1440
frames_per_auxinput12              = 1
io_form_auxinput12                 = 2

/

&domains
time_step                           = 30,
time_step_fract_num                 = 0,
time_step_fract_den                 = 1,
max_dom                             = 1,
s_we                                = 1,
e_we                                = 472,
s_sn                                = 1,
e_sn                                = 312.
s_vert                              = 1,
e_vert                              = 42,
p_top_requested                     = 5000,
num_metgrid_levels                  = 40,
num_metgrid_soil_levels             = 4,

eta_levels       = 1.0000,0.9990,0.9980,0.9950,0.9900,0.9850,
                   0.9800,0.9700,0.9600,0.9500,0.9400,0.9200,
                   0.9000,0.8800,0.8600,0.8300,0.8000,0.7700,
                   0.7400,0.7000,0.6500,0.6000,0.5500,0.5000,
                   0.4500,0.4000,0.3500,0.3000,0.2600,0.2400,
                   0.2200,0.2000,0.1800,0.1600,0.1400,0.1200,
                   0.1000,0.0800,0.0600,0.0400,0.0200,0.0000

dx                                  = 12000,
dy                                  = 12000,
grid_id                             = 1,
parent_id                           = 0,
i_parent_start                      = 1,
```

```
j_parent_start                      = 1,
parent_grid_ratio                   = 1,
parent_time_step_ratio              = 1,
feedback                            = 0,
smooth_option                       = 0
/
&dfi_control
dfi_opt                             = 0,
dfi_nfilter                         = 0,
/
&physics
mp_physics                          = 10,
mp_zero_out                         = 2,
ra_lw_physics                       = 4,
ra_sw_physics                       = 4,
radt                                = 10,
sf_sfclay_physics                   = 7,
num_soil_layers                     = 2,
pxlsm_smois_init                    = 0,
sf_surface_physics                  = 7,
bl_pbl_physics                      = 7,
bldt                                = 0,
cu_physics                          = 1,
kfeta_trigger                       = 2,
cudt                                = 5,
prec_acc_dt                         = 60,
isfflx                              = 1,
ifsnow                              = 1,
icloud                              = 1,
cu_rad_feedback                     = .true.,
surface_input_source                = 1,
num_land_cat                        = 40,
num_soil_cat                        = 16,
sst_update                          = 1,
seaice_threshold                    = 0,
usemonalb                           = .true.,
rdmaxalb                            = .true.,
rdlai2d                             = .true.,
lagday                              = 1,
fractional_seaice                   = 0,
slope_rad                           = 1,
topo_shading                        = 1,
shadlen                             = 25000.,
do_radar_ref                        = 1,
sf_urban_physics                    = 0
/
&fdda
```

```
grid_fdda                           = 1,
grid_sfdda                          = 1,
pxlsm_soil_nudge                    = 1,
gfdda_inname                        = "wrffdda_d<domain>",
gfdda_interval_m                    = 60,
gfdda_end_h                         = 132,
fgdt                                = 0,

if_no_pbl_nudging_uv                = 1,
if_no_pbl_nudging_t                 = 1,
if_no_pbl_nudging_q                 = 1,
if_no_pbl_nudging_ph                = 1,
if_zfac_uv                          = 1,
 k_zfac_uv                          = 17,
if_zfac_t                           = 1,
 k_zfac_t                           = 17,
if_zfac_q                           = 1,
 k_zfac_q                           = 17,
if_zfac_ph                          = 1,
 k_zfac_ph                          = 17,
guv                                 = 0.0001,
gt                                  = 0.0001,
gq                                  = 0.00001,
gph                                 = 0.0000,

xwavenum                            = 2,
ywavenum                            = 2,
if_ramping                          = 0,
dtramp_min                          = 60.0,
io_form_gfdda                       = 2,
sgfdda_inname                       = "wrfsfdda_d<domain>",
sgfdda_interval_m                   = 60
sgfdda_end_h                        = 132
io_form_sgfdda                      = 2
guv_sfc                             = 0.000
gt_sfc                              = 0.000
gq_sfc                              = 0.000
rinblw                              = 250.0
/
&dynamics
w_damping                           = 1,
diff_opt                            = 1,
km_opt                              = 4,
diff_6th_opt                        = 2,
diff_6th_factor                     = 0.12,
base_temp                           = 290.,
damp_opt                            = 0,
```

```
zdamp                               = 5000.,
dampcoef                            = 0.01,
khdif                               = 0,
kvdif                               = 0,
non_hydrostatic                     = .true.,
moist_adv_opt                       = 1,
tke_adv_opt                         = 2,
scalar_adv_opt                      = 1,
fft_filter_lat                      = 91,
/
&bdy_control
spec_bdy_width                      = 5,
spec_zone                           = 1,
relax_zone                          = 4,
specified                           = .true.,
nested                              = .false.,
/
&grib2
/
&namelist_quilt
nio_tasks_per_group = 0,
nio_groups = 1
/
```